VERTICAL STRUCTURE OF DISK GALAXIES AND THEIR DARK MATTER HALOS

A Thesis
Submitted For the Degree of
Doctor of Philosophy
in the Faculty of Science

by

ARUNIMA BANERJEE

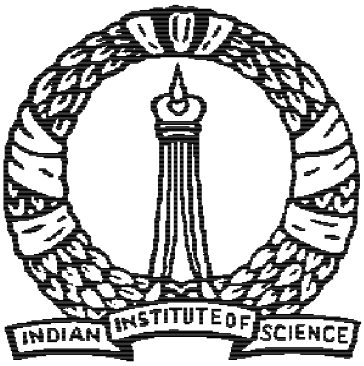

DEPARTMENT OF PHYSICS
Indian Institute of Science
BANGALORE – 560 012

JULY 2011

Declaration

I hereby declare that the work reported in this doctoral thesis titled "Vertical Structure of Disk Galaxies and their Dark Matter Halos" is entirely original and is the result of investigations carried out by me in the Department of Physics, Indian Institute of Science, Bangalore - 560012, under the supervision of Prof. Chanda J. Jog.

I further declare that this work has not formed the basis for the award of any degree, diploma, fellowship, associateship or similar title of any University or Institution.

Arunima Banerjee

January 2012
Department of Physics
Indian Institute of Science
Bangalore - 560012, India.

Dedication

to my family...

Acknowledgements

This is the most befitting occasion for me to convey my heartfelt thankfulness to my thesis supervisor Prof.Chanda J.Jog who introduced me to the exciting world of research in astrophysics and methodically guided me through its vicissitudes with lot of patience and care. I have greatly benefitted from her knowledge of Dynamics of Galaxies and Inter Stellar Medium. Under her able guidance, I have learnt the nuances and subtleties of research and appreciated the value of unrelenting persistence in this chosen vocation. I am grateful to her for her constant help, support and encouragement, without which this thesis could not have seen the light of the day.

I sincerely thank Dr.Victor Debattista (University of Central Lancashire, UK), meeting whom constituted another turning-point in my career as an astrophysicist. His valuable advice, feedback and criticism have greatly helped to improve the quality of my work and added a new dimension to my outlook of research in general.

Some of the research projects were collaborative in nature. I am thankful to Prof.Elias Brinks (University of Hertfordshire, UK), Dr.Lynn D. Matthews (MIT, Haystack Observatory, USA) and Mr.Ioannis Bagetakos (University of Hertfordshire, UK) for providing the observational data as well as for many stimulating discussions to clarify my doubts related to observational issues.

I would also like to thank Prof.Francois Combes (Observatory of Paris, France), Prof.Rajaram Nityananda (NCRA, Pune, India), Prof.John Kormendy (University of Texas, Austin, USA), Prof.Jayaram Chengalur (NCRA, Pune, India), Dr.Subhashis Roy (NCRA, Pune, India) and

Dr. Paola Di Matteo (Observatory of Paris, France) for showing interest in my research and providing useful suggestions all the while.

I acknowledge Prof.Andreas Burkert for inviting me to visit Munich University Observatory for a month in May 2009, which culminated in a useful learning experience in basic N-body simulations, a fruitful research collaboration and a favourable exposure to the research in astrophysics currently underway in Munich and Garching. I thank Dr.Paola Di Matteo again for inviting me to present a research seminar in Observatory of Paris, Meudon, France in May 2009, which helped me to gain useful suggestions and ideas for future research.

Thanks to Shashikant, Piyali, Sowjanya and Dr.Tarun Deep Saini for responding to my distress calls to help sorting out numerical and computational problems. Kshitij, Rajesh, Pratyush, Bidya, Indrani have been wonderful colleagues-thanks to all of them. Hats-off to my seniors Samriddhi, Shankha, Smarajit and Nandan for their tips, and thanks to Manas for providing this thesis template. Many thanks to my batchmates Bhupal, Nihal, Saroj, Sayak, Sayantan, Shaon, Shivaraj, Subhro and Vaibhav for their cooperation during the course work.

I thank the present and past Chairmen of the Department of Physics for their support. Thanks to all the faculty members of the Astronomy & Astrophysics Group for providing a friendly and congenial working environment.

My humblest regards to my high school teacher Mr.Manas Chakladar for kindling the love for Physics within me in the first place. I am fortunate to have come under the tutelage of excellent teachers like Mr.Anil Chandra, Mr.Srikumar Chowdhury, Dr.Sumit Ghosh, Dr.Shibaji Banerjee, Dr.Ananda Das Gupta, Prof.Albert Gomes and Dr.Mainak Gupta - regards to all of them. Thanks to Mr.Arup Bhattacharyya for teaching me the A-B-C of programming, without which I could not have succeeded in developing the code extensively used in this thesis. Thanks to Dr.Anindya Ghose Chowdhury and Dr.Arindam Ghosh for their guidance on academics and research in general.

Special thanks goes to my local guardians Mr.Biplab Majumder & Mrs.Paramita Majumder for providing me with a second home here in Bangalore, taking care of me and looking after my needs all this time. Thanks to my maternal uncle Mr. Joybrata Mukherjee

for his help in settling me down here in Bangalore during the initial years. I am indebted to Dadu, Chhordadu, Chhordida and Raghu Kaku for their constant support and encouragement. Thanks are due to my loving jethimas, Mrs.Ashoka Ghosh and Mrs.Monika Banerjee, for their kind and inspiring words which have enlivened me at dull moments.

Thanks to Ananya and my namesake, Arunima, for being fantastic friends and supporting me as and when required. Thanks to Sowjanya and Paramita, for their camaraderie which has enabled me to wade through tough times.

Finally I consider myself blessed to have extremely lovable, considerate and supportive family members, who have consistently shown immense confidence in me, boosted my morale all along and propelled me through crisis. It is the warmth of their affection that has sustained me through the hardships and difficult phases all these years. Regards ...

Preface

The topic of this thesis is the study of the vertical structure of the disk galaxies and their dark matter halos through theoretical modeling and numerical calculations. The basic theoretical model of the galactic disk used involves gravitationally-coupled stars and gas under the force-field of a dark matter halo; the disk is rotationally-supported in the plane and pressure-supported perpendicular to the plane of the galaxy. The first part of the thesis involves evaluating the vertical structure of stars and gas in normal as well as dwarf spiral galaxies. The second part of the thesis deals with probing the dark matter halo density profiles of disk galaxies using both the observed rotation curve and the H I scale height data. Following is the layout of the thesis.

Chapter 1 gives a general introduction to the topic of vertical structure of spiral galaxies and their dark matter halos, followed by a broad overview of the theoretical development of the topic and ends with highlighting the motivation and challenges met in this thesis. Chapters 2 & 3 deal with the vertical structure of stars and gas in galaxies, Chapters 4-6 focus on obtaining the dark matter halo density profiles of disk galaxies from the observed rotation curve and the H I scale height data whereas Chapter 7 is devoted to the summary of results and future research plans.

Vertical structure of stars and gas in galaxies

The vertical thickness of the stars and the gas, namely atomic hydrogen (H I) and molecular hydrogen (H_2) in a spiral galaxy, is crucial in regulating the disk dynamics close to the

mid-plane, especially in the inner galaxy. However, measuring it observationally is not in general practicable due to the limitations of astronomical observations, and often impossible as in the case of face-on galaxies. Therefore, it is imperative to develop a theoretical model of the galaxy which can predict the thickness of the disk components by using as input parameters the physical quantities, which are more observationally-amenable compared to the disk thickness. The vertical thickness of the disk components is determined by a trade-off between the upward kinetic pressure and the net downward gravitational pull of the galaxy. The fraction of the disk mass due to the stars is an order of magnitude higher than that of the gas in ordinary spiral galaxies, and therefore the gas contribution to the disk gravity is ignored in general. We have developed a multi-component model of gravitationally-coupled stars, H I and H_2 subjected to the force-field of an external dark matter halo, and conclusively demonstrated the importance of the inclusion of gas gravity in explaining the steep vertical stellar distribution observed in galaxies. These apart, this model does not implicitly assume a flat rotation curve for the galaxy and therefore is applicable in general to obtain the thickness of stars and gas in dwarfs (with linearly rising rotation curves) as well as in ordinary spirals.

In **Chapter 2**, we investigate the origin of the steep vertical stellar distribution in the Galactic disk. One of the direct fall outs of our above model of the galaxy, which incorporates the self-gravity of the gas unlike the earlier theoretical models, lies in explaining the long-standing puzzle of the steep vertical stellar density distribution of the disk galaxies near the mid-plane. Over the past two decades, observations revealed that the vertical density distribution of stars in galaxies near the mid-plane is substantially steeper than the sech^2 function that is expected for a self-gravitating system of stars under isothermal approximation. However, the physical origin for this has not been explained so far. We have clearly demonstrated that the inclusion of the self-gravity of the gas in the dynamical model of the Galaxy solves the problem even under the purview of isothermal approximation for the disk components. Being a low dispersion component, the gas resides closer to the mid-plane compared to the stars, and forms a thin, compact layer near the mid-plane, thereby strongly governing the local disk dynamics. This novel idea, highlighting the significance of gas gravity has produced substantial impact on the field and triggered research activities by

other groups in related areas of disk dynamics. The strong effect of the gas gravity on the vertical density profile of the stellar disk indicates that it should also bear its imprint on the Milky way thick disk, as the epoch of its formation 10^9 years ago is marked by a value of gas fraction, almost an order of magnitude higher than its present day value. Interestingly, the findings of the upcoming **Gaia** mission can be harnessed to verify this theoretical prediction. It may also hold the clue as to the reason behind the absence of thick disk in superthin galaxies.

In **Chapter 3**, we use the same model to theoretically determine the H I vertical scale heights in the dwarf galaxies: DDO 154, Ho II, IC 2574 & NGC 2366 for which most of the necessary input parameters are available from observations. We stress the fact that the observational determination of the gas thickness in these dwarf irregulars is not viable. Nevertheless, it is important to estimate it theoretically as it plays a crucial role in calculating the star-formation activities and other related phenomena. However, two vital aspects have to be taken care of while modeling these dwarf galaxies. Firstly, the mass fraction in gas in these galaxies is comparable to that of the stars, and hence the gas gravity cannot be ignored on any account unlike in the case of large spirals. Secondly, dwarf galaxies have a rising rotation curve over most of the disk unlike the flat rotation curves of ordinary spirals. Both these factors have been considered in developing our model of the dwarf galaxies. We find that three out of the four galaxies studied show a flaring of their H I disks with increasing radius, by a factor of a few within several disk scale lengths. The fourth galaxy (Ho II) has a thick H I disk throughout. A comparison of the size distribution of H I holes in the four sample galaxies reveals that of the 20 type 3 holes, all have radii that are in agreement with them being still fully contained within the gas layer.

Probing the dark matter halo profiles of disk galaxies

The next part of the thesis involves the dynamical study of the shapes and density profiles of galactic dark matter halos using observational constraints on our theoretical model of a spiral galaxy. The density distribution of the dark matter halo is generally modeled using the observed rotation curve of the spiral galaxies. The rotational velocity at any radius

is determined by the radial component of the net gravitational force of the galaxy, which, however, is weakly dependent on the shape of the dark matter halo. Therefore, one cannot trace the dark matter halo shape by the observed rotation curve alone. The vertical thickness of the stars and gas, on the other hand, is strongly dependent on the flattening of the dark matter halo, and therefore the observed gas thickness can be used as a diagnostic to probe the halo shape. In this thesis, we have used the double constraints of the rotation curve and the H I thickness data to obtain the best-fit values of the core density, core radius and the vertical-to-planar axis ratio (or flattening) of the dark matter halos of our largest nearby galaxy Andromeda (or M31), a low-surface brightness (LSB) superthin galaxy UGC 7321 and to study the dark matter halo shape of our Galaxy.

In **Chapter 4**, we study the dark matter halo of M31 or Andromeda, the largest nearby galaxy to the Milky Way. We find that M31 has a highly flattened isothermal dark matter halo with the vertical-to-horizontal axis ratio equal to 0.4, which interestingly lies at the most oblate end of the halo shapes found in cosmological simulations. This indicates that either M31 is a unusual galaxy, or the simulations need to include additional physics, such as the effect of the baryons, that can affect the shape of the halo. This is quite a remarkable result as it challenges the popular practice of assuming a spherical dark matter halo in the dynamical modeling of the galaxy

In **Chapter 5**, we have applied this technique to the superthin galaxy UGC 7321. Superthins are somewhat the "extreme" objects in the local Universe because of their high gas fraction and absence of a thick disk component. It is interesting to analyze their so-called extreme characteristics in the light of the physical mechanisms which determined them to understand better the properties of ordinary spirals. We find that UGC 7321 has a spherical isothermal halo, with a core radius almost equal to the disk scale length. This reveals that the dark matter dominates the dynamics of this galaxy at all radii, including the inner parts of the galaxy. This is unlike the case for the large spiral galaxies, where the core radius is typically about 3-4 disk scale lengths. Interestingly, the best-fit halo core density and the core radius are consistent, with deviations of a few percent, with the dark matter fundamental plane correlations, which depict the systematic properties of the dark matter

halo in late-type and dwarf spheroidal galaxies. This apart, a high value of the gas velocity dispersion is required to get a better fit to the H I scale height data, although the superthin nature of the stellar disk implies a dynamically cold dynamic galactic disk. However, it explains the low star-formation rates in these galaxies since the Toomre Q criterion ($Q < 1$) for instability is less likely to be satisfied, and hence the disk is liable to be more stable to star formation.

In **Chapter 6**, we investigate the shape of the dark matter halo in the outer Galaxy. We find that the halo is prolate, with the vertical-to-planar axis ratio monotonically increasing to 2.0 at 24 kpc, or 8 radial disk scale lengths. The resulting prolate-shaped halo can explain several long-standing puzzles in galactic dynamics, for example, it permits long-lived warps thus explaining their ubiquitous nature. It also imposes novel constraints on the galaxy formation models.

Finally, in **Chapter 7**, the thesis is concluded with a summary of the main results and a brief discussion of the scope for future work.

List of Publications

1. **Banerjee A.**, & Jog, C. J. 2011, *Progressively More Prolate Dark Matter Halo in the Outer Galaxy as Traced by Flaring H I Gas*, **Astrophysical Journal Letters, 732**, L8

2. **Banerjee A.**, Jog, C. J., Brinks, E., & Bagetakos, I. 2011, *Theoretical determination of HI vertical scale heights in the dwarf galaxies DDO 154, Ho II, IC 2574 and NGC 2366*, **Monthly Notices of the Royal Astronomical Society, 415**, 687

3. **Banerjee, A.**, Matthews, L.D. & Jog, C. J. 2010, *Dark matter dominance at all radii in the superthin galaxy UGC 7321*, **New Astronomy, 15**, 89

4. **Banerjee, A.**, Jog, C. J., & Matthews, L.D. 2009, *Dark Matter Halo Properties as Deduced from the Observed H I Scale Height Data*, **Astronomical Society of the Pacific Conference Series, 407**, 99

5. **Banerjee A.**, & Jog, C. J. 2008, *The Flattened Dark Matter Halo of M31 as Deduced from the Observed H I Scale Heights*, **Astrophysical Journal, 685**, 254

6. **Banerjee A.**, & Jog, C. J. 2007, *The Origin of Steep Vertical Stellar Distribution in the Galactic Disk*, **Astrophysical Journal, 662**, 335

Contents

1

Introduction

1.1 Spiral Galaxies

The topic of this thesis is vertical structure of disk galaxies and their dark matter halos. As the very name suggests, these galaxies exhibit a disk-like morphology and are accommodated on the right hand side of the Hubble's Tuning Fork diagram. Popularly, these are also referred to as spiral galaxies as most of them exhibit distinctive spiral features in their outer regions. Also, spirals or disk galaxies have substantial gas content, which is yet to be exhausted to fuel up further star-formation activities.

A spiral galaxy consists of a luminous disk of stars and gas (mainly atomic and molecular hydrogen) with a diameter between 10 kpc to 30 kpc, embedded in a huge envelope of dark

matter halo, the existence of which is indicated by the dynamical requirements of the observed kinematics. The observed rotation curve, i.e, a plot depicting the observed azimuthal velocity as a function of Galactocentric radius, remains flat out to several optical radii in the outer galaxy. This feature hinted at the presence of an unseen source of gravitating matter (dark matter) as the rotation curve due to the luminous disk alone should have been Keplerian in nature. In general, the mass fraction due to the stars is an order of magnitude higher than that due to the gas. However, the total dynamical mass of the galaxy is primarily attributed to its dark matter halo, which is typically required to be ten times more massive than the stellar and the gaseous disks taken together. Magnetic fields pervade the system and cosmic ray particles spiral along the field lines. But the largest forces governing both shape and velocity field of the system are gravitational.

Spiral galaxies are effectively rotationally-supported in the plane with the rotational velocity varying with distance from the centre of the disk. In the vertical direction, the galaxy is pressure-supported. This highly-flattened mass distribution in the form of a disk culminates in a strong vertical constraining force, resulting in a well-defined vertical structure. The vertical structure of the disk galaxy constitutes an exciting field of galactic dynamics by itself apart from providing valuable insights into the process of formation and evolution of the galaxy. With the breakthrough in modern astronomical observations in the past few decades (surveys like SDSS, for instance) and in the upcoming era (GAIA, for example), the galactic disks can now be viewed in unprecedented detail revealing a plethora of interesting features and characteristics, and thereby posing novel challenges to the next generation of astrophysicists. A careful theoretical modeling of the galaxy at par with N-body simulation studies is necessary for understanding the physics behind these observed structural features.

Superimposed on this background distribution of the disk and the dark matter halo is the spiral structure. These spiral arms are visible mainly due to the young, luminous objects concentrated there. Although they do not contain large fraction of total mass density, they exhibit a high rate of massive star formation, at least in the outer parts of the galaxy.

So this is the scenario that a successful theory of galactic dynamics has to enlarge on, and we require that this theory should be mainly gravitational in character.

1.2 Disk Vertical Structure

1.2.1 Theoretical Development

In this section, the formulation of the basic equations of stellar dynamics and subsequently those governing the vertical structure of the galactic disk, which is one of the topics of interest of this thesis, is discussed (Rohlfs 1977, Binney & Tremaine 1987).

Equilibrium of Collisionless Systems: The inverse square nature of the gravitational force ensures that the net gravitational force acting on a star in a galaxy is determined by the large-scale density distribution of the galaxy rather than the proximity of the test star to its neighbouring stars. The net force on a star does not vary rapidly and the star in question accelerates smoothly through the force field generated by the galaxy as a whole. It can be shown that it is possible to understand the dynamics of the galaxies by investigating the orbits of the stars in a suitable mean potential, and that the underlying dynamics is that of a collisionless system.

The Collisionless Boltzmann Equation: Let us consider a large number of stars moving under a smooth external potential $\Phi(\mathbf{x}, t)$. At a given time t, the complete description of the state of a collisionless system is given by its phase-space density or distribution function (DF) $f(\mathbf{x}, \mathbf{v}, t)$. The number of stars present in a small volume $d^3\mathbf{x}d^3\mathbf{v}$ around the phase space vector ($\mathbf{x}$,$\mathbf{v}$) is given by $f(\mathbf{x}, \mathbf{v}, t)d^3\mathbf{x}d^3\mathbf{v}$.

According to Newton's Laws, if the positions and velocities of all the stars at a given initial time is known, one can calculate the positions and velocities at any later time t. In other words, if $f(\mathbf{x}, \mathbf{v}, t_0)$ is known, Newton's Laws say, one can calculate $f(\mathbf{x}, \mathbf{v}, t)$ using the information in $f(\mathbf{x}, \mathbf{v}, t_0)$. With the above idea in mind, let us consider the flow of points in phase space that arises as the stars move along their orbits.

The co-ordinates in phase space are $(\mathbf{x}, \mathbf{v}) = \mathbf{w} = (w_1, ..., w_6)$. So the velocity of the flow may be written as $\dot{\mathbf{w}} = (\dot{\mathbf{x}}, \dot{\mathbf{v}}) = (\mathbf{v}, -\nabla\Phi)$. Here $\dot{\mathbf{w}}$ is a six-dimensional vector that bears the same relationship with $\mathbf{w}$ as the three dimensional fluid flow velocity $\dot{\mathbf{x}}$ has to the

position vector $\mathbf{x}$ in an ordinary fluid flow. A characteristic of the flow described by $\dot{\mathbf{w}}$ is that it conserves stars i.e stars donot jump from one point in phase to another in the absence of encounters. Therefore $f(\mathbf{w}, t)$ obeys a continuity equation analogous to the density $\rho(\mathbf{x}, t)$ in ordinary fluid flow.

$$\frac{\partial f}{\partial t} + \sum_{\alpha=1}^{6} \frac{\partial (f \dot{w_\alpha})}{\partial w_\alpha} = 0 \tag{1.1}$$

The physical meaning of this equation can be envisaged by integrating over volume space. The first term then gives the rate of increase in the number of stars within this volume. Application of the divergence theorem to the second term shows that it is the rate at which the stars flow out of this volume. Now the flow described by $\dot{\mathbf{w}}$ has the property

$$\sum_{\alpha=1}^{6} \frac{\partial \dot{w_\alpha}}{\partial w_\alpha} = \sum_{i=1}^{3} \left(\frac{\partial v_i}{\partial x_i} + \frac{\partial \dot{v_i}}{\partial vi} \right) = \sum_{i=1}^{3} - \frac{\partial}{\partial v_i} \left(\frac{\partial \Phi}{\partial x_i} \right) = 0 \tag{1.2}$$

Here $\frac{\partial v_i}{\partial x_i} = 0$ as v_i and x_i are the independent co-ordinates of the phase space. Substituting equation (1.2) in equation (1.1) we obtain

$$\frac{\partial f}{\partial t} + \sum_{\alpha=1}^{6} \dot{w_\alpha} \frac{\partial f}{\partial w_\alpha} = 0 \tag{1.3}$$

i.e

$$\frac{\partial f}{\partial t} + \sum_{i=1}^{3} \left(v_i \frac{\partial f}{\partial x_i} - \frac{\partial \Phi}{\partial x_i} \frac{\partial f}{\partial v_i} \right) = 0 \tag{1.4}$$

In vector notation,

$$\frac{\partial f}{\partial t} + \mathbf{v}.\nabla f - \nabla \Phi . \frac{\partial f}{\partial \mathbf{v}} = 0 \tag{1.5}$$

Equation (1.5) is known as the **collisionless Boltzmann Equation**, a special case of Liouville's theorem, which is the fundamental equation of stellar dynamics.

Now

$$\frac{df}{dt} = \frac{\partial f}{\partial t} + \sum_{\alpha=1}^{6} \dot{w_\alpha} \frac{\partial f}{\partial w_\alpha} = 0 \tag{1.6}$$

$\frac{df}{dt}$ represents the rate of change of density of phase points to an observer who moves through phase space with a star with velocity $\dot{\mathbf{w}}$. Therefore the collisionless Boltzmann equation is simply

$$\frac{df}{dt} = 0 \tag{1.7}$$

This shows that the flow of stellar phase points through phase space is incompressible. In other words, phase space density f around the phase-point of a given star remains constant.

Jeans Equations: The collisionless Boltzmann Equation in galactic cylindrical co-ordinates R, ϕ, z read

$$\frac{\partial f}{\partial t}+v_R\frac{\partial f}{\partial R}+\frac{v_\phi}{R}\frac{\partial f}{\partial \phi}+v_z\frac{\partial f}{\partial z}+\left(\frac{{v_\phi}^2}{R}-\frac{\partial \Phi}{\partial R}\right)\frac{\partial f}{\partial v_R}-\frac{1}{R}\left(v_R v_\phi+\frac{\partial \Phi}{\partial \phi}\right)\frac{\partial f}{\partial v_\phi}-\frac{\partial \Phi}{\partial z}\frac{\partial f}{\partial v_z}=0 \quad (1.8)$$

The distribution function f is a function of seven variables and therefore the complete solution of the collisionless Boltzmann equation is a cumbersome task in general. However one can gain valuable insights by taking moments of this equation. Integrating the above equation over velocity we get

$$\frac{\partial \nu}{\partial t}+\frac{1}{R}\frac{\partial (R\nu\overline{v_R})}{\partial R}+\frac{\partial (\nu\overline{v_z})}{\partial z}=0 \quad (1.9)$$

where $\nu=\int f\, d^3\mathbf{v}$ is the spatial density of stars and $\overline{v_i}=\int f v_i\, d^3\mathbf{v}$ is the mean of the i^{th} component of the stellar velocity.

Then we multiply equation (1.8) with v_R or v_z, and then integrate over velocity space to obtain respectively

$$\frac{\partial (\nu\overline{v_R})}{\partial t}+\frac{\partial (\nu\overline{{v_R}^2})}{\partial R}+\frac{\partial (\nu\overline{v_R v_z})}{\partial z}+\nu\left(\frac{\overline{{v_R}^2}-\overline{{v_\phi}^2}}{R}+\frac{\partial \Phi}{\partial R}\right)=0 \quad (1.10)$$

$$\frac{\partial (\nu\overline{v_\phi})}{\partial t}+\frac{\partial (\nu\overline{v_R v_\phi})}{\partial R}+\frac{\partial (\nu\overline{v_\phi v_z})}{\partial z}+\frac{2\nu}{R}\overline{v_\phi v_R}=0 \quad (1.11)$$

and

$$\frac{\partial (\nu\overline{v_z})}{\partial t}+\frac{\partial (\nu\overline{v_R v_z})}{\partial R}+\frac{\partial (\nu\overline{{v_z}^2})}{\partial z}+\frac{(\nu\overline{v_R v_z})}{R}+\nu\frac{\partial \Phi}{\partial z}=0 \quad (1.12)$$

Since the last three equations were first applied to stellar dynamics by Sir James Jeans, this set of equations is popularly known as the **Jeans equations**.

Vertical density distribution of the stars & gas at a given radius: Equation (1.12) can be simplified further. For instance, under the steady state condition, the first term on

the left hand side of the equation vanishes. Also, it can be shown (Binney & Tremaine 1987) that $\overline{v_R v_z} = \frac{1}{2}(\overline{{v_R}^2} - \overline{{v_z}^2})\frac{z}{R}$ and therefore the second and the fourth terms are not larger than $(\overline{{v_R}^2} - \overline{{v_z}^2})\frac{z}{RR_d}$, which is a factor of $\frac{z^2}{RR_d}$ times smaller than the third and the fifth terms and hence can be neglected. With these assumptions, equation (1.12) can be written as

$$\frac{1}{\nu}\frac{\partial(\nu\overline{{v_z}^2})}{\partial z} = -\frac{\partial\Phi}{\partial z} \tag{1.13}$$

Further assuming that the stellar mass is conserved (which is a good enough assumption for low mass stars which dominate the stellar mass function), equation (1.13) can be written as

$$\frac{1}{\rho}\frac{\partial(\rho\overline{{v_z}^2})}{\partial z} = -\frac{\partial\Phi}{\partial z} \tag{1.14}$$

where $\rho(z)$ denotes the mass density of the stars as a function of z.

Equation (1.14) is the governing equation to study the vertical structure of the stellar disks in spiral galaxies. Since the underlying governing dynamics in this case is Newtonian gravitation, solution of the above equation jointly with the Poisson Equation will determine the vertical density distribution and hence the thickness of the stellar layer at any Galactocentric radius R.

One may note here that the gas component of the disk also obeys an equation similar to equation (1.14). However, in case of the gas, the equation follows from the Euler Equation of Fluid Dynamics (instead of the collisionless Boltzmann Equation) in conjunction with the isothermal equation of state for the gas namely $P = \rho {v_z}^2$, where P is the pressure, ρ the density and v_z the vertical velocity dispersion for the gas (Dyson & Williams 1997).

1.2.2 The Stellar Disk

The Stellar Surface Density Profiles: Observations of external spiral galaxies suggest that the surface brightness and hence the surface density of the galactic disk falls exponentially with radius and is given by

$$\Sigma(R) = \Sigma_0 \exp(-R/R_d) \tag{1.15}$$

where Σ_0 is the central surface density and R_d is the disk scale length (Freeman 1970). For our Milky way, $\Sigma_0 = 641 M_\odot pc^{-2}$ and $R_d = 3.2$kpc (Binney & Tremaine 1987).

Thin disk & Thick Disk: The stellar disk can be subdivided into two parts, namely the thin disk and the thick disk. The major mass fraction of the stars is concentrated in a thin disk centered on the mid-plane of the galaxy (for our Galaxy the thin disk scale height is around $300pc$ at the solar neighborhood). The existence of a low density thick disk (1 kpc) was pointed by stellar luminosity distribution studies of external and early-type galaxies (Burstein 1979, Tsikoudi 1979) and star counts in the Milky Way (Gilmore & Reid 1983). This thick disk constitutes an older population of stars, is substantially thicker than the thin disk, and has a radial scale length that appears to be uncorrelated with that of the embedded thin disk (Dalcanton & Bernstein 2002). Formation of the thick disk is a nearly universal feature of disk formation. Both internal and external processes have been invoked to explain the formation of this component. A monolithic collapse, vertical heating of an earlier thin disk, accretion from infalling satellites or a merger are the various possibilities suggested for the origin of a thick disk (For details, see Qu et al. 2011).

The Isothermal Approximation: The velocity dispersion of the stellar disk generally falls off with radius, sometimes exponentially with a scale length equal to twice the disk scale length of the stars (Lewis & Freeman 1989). However, the dependence of the stellar velocity dispersion on the distance from the mid-plane (z) is not very clear (Korchagin et al. 2003). In this thesis, we have assumed that the velocity dispersion of the stars remains constant with z, which is usually referred to as the isothermal approximation. This is routinely done in the study of the disk vertical structure (Spitzer 1942). For a galaxy like our Milky Way, the typical value of the stellar velocity dispersion is $18 kms^{-1}$. In fact, the velocity dispersion is closely related to the age of the stellar disk and bears the fingerprint of heating by several agents like the molecular clouds (Spitzer & Schwarzschild 1951, Spitzer & Schwarzschild 1953, Lacey 1984), spiral arms (Barbanis & Woltjer 1967), bars (Sellwood & Merritt 1994), black holes (Lacey & Ostriker 1985) among others.

1.2.3 The Gaseous Disk

The Different Phases of the Gas & their Tracers: The Inter Stellar Medium (ISM) contains gas over a wide range of temperatures, densities and ionization states. In fact, the interstellar gas can be broadly categorized into neutral atomic gas (mainly atomic hydrogen HI), ionized gas (mainly ionized atomic hydrogen HII) and molecular gas (mainly molecular hydrogen H_2 (See for example, Kulkarni & Heiles 1988, Tielens 2005). Each gas component is marked by its characteristic properties and can be probed by different tracers, which are discussed below.

1. Neutral Atomic Gas: The neutral atomic gas can be studied in two distinct regimes based on the temperature: Cold Neutral Medium (CNM) and the Warm Neutral Medium (WNM). The CNM (100 K) is present in cold diffuse HI clouds. The WNM (8000 K) constitutes the intercloud gas. A standard HI cloud (often called a Spitzer-type cloud) has a typical density of 50cm^{-3} and a size of 10 pc. The density of the WNM is much less (0.5cm^{-3}). Between 4 and 8 kpc from the galactic center, 80 percent of the HI mass in the plane of the Galaxy is in diffuse clouds in a layer with a (Gaussian) scale height of about 100 pc. At higher latitudes, however, much of the HI mass is in the intercloud medium with a larger scale height of 220 pc but with an exponential tail extending well into the lower halo. These two neutral phases have, on average, similar surface densities. The 21 cm line of atomic hydrogen traces the neutral gas of the ISM.

2. Ionized Gas: The ionized gas, often referred to as the warm ionized medium (WIM), has a low density (0.1cm^{-3}), a temperature of 8000 K and a scale height of 1 kpc. The WIM shows a complex spatial structure including thin filaments sticking 1 kpc out of the plane of the Galaxy. The WIM can be traced through dispersion of pulsar signals, through optical and UV ionic absorption lines against background sources, and through emission in the Hα recombination line.

3. Molecular Gas: In a galaxy like our Milky Way, the molecular gas is localized in discrete giant molecular clouds with typical sizes of 40 pc, masses of $4 \cdot 10^5 \text{M}\odot$, densities of 200cm^{-3} , and temperatures of 10 K. However, molecular clouds show a large variation in range in each of these properties. They are characterized by high turbulent pressures as

indicated by the large linewidths of emission lines. Also, they are self-gravitating rather than in pressure equilibrium with other phases in the ISM. While they are stable over time scales of $3 \cdot 10^7$ years, presumably because of a balance of magnetic and turbulent pressure and gravity, molecular clouds are the sites of active star formation. Observations of molecular clouds in the rotational transitions of a variety of species allow a detailed study of their physical and chemical properties. While CO is commonly used to trace interstellar molecular gas, H_2 is thought to be the dominant molecular species, with a H_2/CO ratio of 10^4 to 10^5. Table 1.1 lists the surface densities and the scale heights of the different phases of the gas.

TABLE 1.1: Surface densities and vertical scaleheights of the different gas phases at the solar neighbourhood *(Tielens 2005)*

Phase	Σ ($M_\odot pc^{-2}$)	H^a (kpc)
Warm neutral medium	1.5	0.220
Warm ionized medium	1.1	0.900
Cold neutral medium	2.3	0.094
Molecular clouds	1.0	0.075

[a]Gaussian scale height

1.2.4 Our galactic disk model of gravitationally-coupled stars & gas

In an ordinary spiral, the disk generally dominates the net galactic potential over dark matter in the inner parts of the galaxy whereas their respective roles are reversed in the outer parts. Typically, the total mass present in the stellar disk is an order of magnitude higher than that present in the gaseous disk, and hence the contribution of the self-gravity of the gas is neglected in obtaining the net gravitational potential. As a result, traditionally, only the stars and the dark matter are considered to be the sole contributors to the galactic potential. In this thesis, we argue in favour of the inclusion of gas gravity in the dynamical model of a

galaxy. Being a low dispersion component, the gas lies closer to the mid-plane compared to the stars and strongly governs the disk dynamics there. We therefore use a three-component model of gravitationally-coupled stars and gas in the force-field of an external dark matter halo (Narayan & Jog 2002) to study the effect of gas gravity on the disk vertical structure.

1.3 Dark Matter Halos in Spiral Galaxies

It will not be exaggerating to state that the quest for dark matter constitutes the most prolific field of research in astrophysics today. Most interestingly, this unseen or dark component of the universe is highly elusive and has stubbornly defied all human attempts to track it till date. However, on the sly, it lets its presence felt by its strong dynamical effect on the luminous universe, provided our current understanding of the dynamics governing the universe is correct. The term dark matter therefore veritably evokes a feeling of enigma, and unravelling its mystery is one of the greatest challenges of modern physics. It may be stressed here that the success of this study lies in an effective synergy among ongoing research spanning various disciplines like astronomy, astrophysics, cosmology and particle-physics. This not only indicates the scale and immensity of the problem, but also highlights its tremendous potential to unleash newer avenues of physics, apart from nurturing the prospect of revolutionizing our current understanding of the universe altogether.

1.3.1 Historical Development

The first concrete evidence for the presence of dark matter on galactic scales was given by Oort (1932) while analyzing Milky Way local stars. Later the presence of dark matter was also indicated by the study of the optical rotation curves of external galaxies (Rubin et al. 1970). Theoretically the luminous disk of the galaxy, being finite in size, is expected to give rise to a rotation curve, which initially rises with radius and then falls off in a Keplerian fashion. Surprisingly the observed rotation curves were found to remain flat with radius in sharp contrast to theoretical prediction. This necessitated the presence of unseen gravitating matter in the outer parts of the galaxy to reconcile theory with observations.

However, optical probes could trace only a few kiloparsecs from the centre of the galaxy, which corresponded either to the rising part of the rotation curve or the part where it just started to flatten out. Therefore the optical rotation curves could not be considered to be the conclusive evidence for the presence of dark matter in galaxies. The final breakthrough came with the pioneering work of Bosma (1978), who obtained the rotation curves of twenty spirals, extending up to several stellar disk scale lengths in the outer galaxy, using the 21-cm line of the atomic hydrogen (HI) as a tracer. This firmly established the authenticity of the prevailing conjecture about the presence of dark matter in the outer galaxy, and finally convinced the scientific community about the feasibilty of the existence of dark matter in galaxies.

Clusters of galaxies have provided the best evidence for DM ever since Zwicky's (1933) seminal work in, which, in fact, also provided the first evidence about the presence of dark matter. Applying the virial theorem on the observed radial velocity dispersions of the galaxies in the Coma Cluster, he obtained the underlying gravitational potential of the cluster, which was much larger than the visible part of the cluster could account for. The Coma cluster of galaxies provides perhaps the single strongest piece of evidence for DM because of the dramatic difference in its mass-to-light ratio (M/L = 400) from that of the Solar neighbourhood (M/L = 2 - 3).

1.3.2 Role of Dark Matter in Galaxy Formation & Evolution

The necessity for the presence of dark matter is warranted not only by the observed flatness of the galactic rotation curves. In fact, the presence of these huge masses of unseen gravitating matter is essential for the formation of galaxies and large scale structures seen in the universe today. Interestingly, the observable universe comprises of a reasonably uniform, foam-like structure on large scales (a few hundred million light years), but marked by inhomogeneities on smaller scales. On more precise terms, colossal voids containing relatively few galaxies are surrounded by immense filaments spanning hundred million light years. It may be noted here that although filaments host the major mass fraction of the universe, they can be effectively fitted into only a few percent of its total volume. The structure-formation

in the universe is believed to have taken place due to the presence of seeds of irregularities superimposed on the smooth background potential of the universe. With time, these tiny, relatively dense regions accrete more and more mass, and grow bigger and bigger in size. Parallely the surrounding rarefied regions become thinner and thinner. Now the estimated baryonic content of the universe is inadequate to have produced gravitational wells to sustain the structure-formation seen in the universe today, and this is exactly where the dark matter has to step in salvage the situation (Freeman & McNamara 2006).

Cold, Hot & Warm Dark Matter: In currently popular cosmologies the universe is usually considered to be consisting of three main components. In addition to the baryonic matter that make up the visible universe, astronomers have found various indications for the presence of dark matter and dark energy. Although the nature of both dark matter and dark energy is still unknown, it is believed that they are responsible for more than 95 percent of the energy density of the universe. Different cosmological models differ mainly in (i) the relative contributions of baryonic matter, dark matter, and dark energy, and (ii) the nature of dark matter and dark energy. The most popular model is the so-called Λ-CDM model, a flat universe in which about 75 percent of the energy density is due to a cosmological constant (Λ), 21 percent is due to cold dark matter (CDM), and the remaining 4 percent is due to the baryonic matter out of which stars and galaxies are made. Lambda is interpreted as the fraction of the total mass-energy density of a flat universe that is attributed to dark energy that explains the current accelerating expansion of space against the gravitational collapse. CDM is described as being cold (its velocity is non-relativistic at the epoch of radiation-matter equality), possibly non-baryonic, dissipationless (cannot cool by radiating photons) and collisionless (the dark matter particles interact with each other and other particles only through gravity). Besides there are Hot Dark Matter (HDM) and Warm Dark Matter (WDM) models as well. HDM is a hypothetical form of dark matter which consists of particles that travel with ultra-relativistic velocities. The best candidate for the identity of HDM is the neutrino. This implies thermal motions sufficient to smooth out all structures on scales smaller than a few tens of Mpc. The first non-linear structures should be a few tens

of Mpc in size, which must fragment to form smaller structures such as the galaxies, thus supporting a top-down scenario of galaxy formation. However such a picture is at conflict with observations. Simulations of structure formation in a neutrino-dominated universe by White et al. (1984) demonstrated they could not produce galaxies without at the same time producing much stronger galaxy clustering than is observed. Warm dark matter (WDM) is a hypothesized form of dark matter that has properties intermediate between those of hot dark matter and cold dark matter, causing structure formation to occur bottom-up from above their free-streaming scale, and top-down below their free streaming scale (Mo, van de Bosch & White 2010).

Dark Matter in Cosmological simulations: Over the last few decades, cosmological simulations have been aimed at modeling the structure formation of the universe. The basic process of structure formation involves gravitational collapse of dark matter dominated material, with the assumption that this mass comprises gravitationally-interacting non-relativistic cold dark matter (CDM). Aided by the recent breakthrough in high performance computations, large computer simulations can now probe the formation and properties of individual galaxies in unprecedented detail in CDM cosmology. This has culminated into robust predictions about the density distribution of dark matter on galactic scales, which interestingly, has been found to have a central power law cusp, $\rho \propto r^{-\gamma}$ with γ lying between 1 and 1.5 (Merrifield 2004). However, observational methods still favour a cored density distribution in ordinary spirals (de Blok et al. 2003), in dwarfs (Flores & Primack 1994, Marchesini et al. 2002, Gentile et al. 2005) as well as in low surface brightness galaxies (de Blok et al. 2001, McGaugh et al. 2001, Marchesini et al. 2002, Kuzio de Naray et al. 2006, 2008). This cusp-core problem continues to be a debatable issue till date and attempts are made being made to resolve the issue (Pontzen & Governato 2011).

The simulations also predict the overall shapes of dark matter halos, which are typically oblate, with the shortest-to-longest axis ratios being 0.5 ± 0.2. Besides, these studies have also allowed us to gain valuable insight into the dependence of halo shapes on various other parameters like mass and redshift. While massive halos are found to be more spherical, halos of a given mass have been found to become flatter with redshift. These apart, the shape

of halos seems to be highly correlated with the merger history. In fact, halos which have experienced a recent merger are found to be prolate in shape, with the major axis showing the direction along which the merging event occured (Bailin & Steinmetz 2005, Houjon et al. 2010).

1.3.3 Modified Newtonian Dynamics: Alternative to Dark Matter

A plausible alternative to dark matter to comply with the observations at galactic scales is the Modified Newtonian Dynamics (MOND) theory. According to theory, flat rotation curves reflect a failure of General Relativity rather than the existence of dark matter (Milgrom 1983). The theory is based on the assertion that there is a characteristic acceleration $a \sim cH_0/2\pi$ below which Newtonian gravity fails; when Newtonian dynamics predict the gravitational attraction to be $g_N \leq a_0$, then the actual acceleration is $g_M = \sqrt{g_N a_0}$. Several studies have demonstrated that MOND can predict the rotation curves of galaxies from their light profiles. In fact, the mass-to-light ratios that are assigned to each galaxy vary with waveband and galaxy type very much as is expected from the point of view of astrophysics. This in turn has confirmed that a characteristic acceleration a_0 is involved between galaxy photometry and dynamics. However, the main problem with MOND lies in the non-universality of a_0. The value of a_0 required if dark matter is not to be invoked in galaxy clusters is about a factor of two larger than that fitted to data for disk galaxies (Binney 2004).

1.3.4 Dark Matter Halo Density Profiles

A range of profiles have been suggested to describe the spatial density distribution of the dark matter halos in the galaxies. Some of them are based on simulation results of cosmological models of galaxy formation. Others have been proposed to comply with observations. Following are some of the dark matter density profiles which are commonly used in the literature.

Pseudo-isothermal Profile: The pseudo-isothermal density profile of the dark matter halo is routinely used by astronomers (de Blok et al. 2008, Oh et al. 2008) to fit the observed

rotation curves. It is simple and physically-motivated, and is given by

$$\rho_{DM}(R,z) = \frac{\rho_0}{1+\frac{r^2}{{r_c}^2}} \tag{1.16}$$

where ρ_0 is the core density and r_c is the core radius.

NFW Profile: The NFW profile was proposed by Navarro et al. (1996) using high-resolution N-body simulations of structure formation in a CDM cosmology. They found that the density profiles of the dark matter halos are well-described by

$$\rho_{DM}(r) = \rho_{crit}\frac{\delta_{char}}{(r/r_s)(1+r/r_s)^2} \tag{1.17}$$

Here r_s is the scale radius and δ_{char} the characteristic overdensity.

Einasto Profile: The Einasto profile (See for example, Merritt et al. 2006) was suggested to account for the small but systematic deviations from the spherically-averaged dark matter halos as was seen in numerical simulations of higher resolution (Navarro et al. 2004, Hayashi & White 2008, Gao et al. 2008, Springel et al. 2008). It is given by

$$\rho_{DM}(r) = \rho_{-2}\exp\left[\frac{-2}{\alpha}\left(\frac{r}{r_{-2}}\right)^{\alpha}-1\right] \tag{1.18}$$

Here r_{-2} is the radius at which the logarithmic slope of the density distribution is -2 and $\rho_{-2} = \rho(r_{-2})$. Einasto profile has 3 free parameters compared to 2 of the NFW profile. Therefore, it is not surprising that it fits the simulation results better than the NFW profile.

Burkert Profile: Another viable alternative is the phenomenological model proposed by Burkert (1995) which is given by

$$\rho_{DM}(r) = \frac{\rho_0 {r_0}^3}{(r+r_0)(r^2+{r_0}^2)} \tag{1.19}$$

Here ρ_0 and r_0 are the central density and the scale radius respectively. This density profile resembles an isothermal profile in the inner regions($r < r_0$) and has a finite central density ρ_0.

de Zeeuw & Pfenniger profile: The above density profiles assume the halo to be spherical in shape, and therefore does not allow one to probe the shape or flattening (i.e vertical-to-planar axis ratio) of the halos, which is often the parameter of interest. The 4-parameter model proposed by de Zeeuw & Pfenniger (1988) allows one to investigate the shape of the halo, and is given by

$$\rho(R,z) = \frac{\rho_0}{\left[1+\frac{m^2}{{R_c}^2}\right]^p} \tag{1.20}$$

where ρ_0 is the core density, R_c is the core radius, p is the density index, and q is the vertical-to-planar axis ratio. For $p = 1$ and $q = 1$, this profile reduces to the pseudo-isothermal profile described above. In this thesis, the de Zeeuw & Pfenniger density profile has been used to study the dark matter halos in spiral galaxies.

1.3.5 The Issue of the Maximal/Minimal Disk

The total amount of dark matter present within a given radius is ill-constrained by the observed rotation curve. This is due to uncertainties both in the geometry of the dark mass, and in the fraction of the total mass contained in the stellar disk itself. Maximal disks are disks where the total mass is assumed to be maximum that is consistent with the observed rotational velocity, while minimal disks are those in which the total mass is assumed to be the minimum that is consistent with the observed rotational velocity. In general, models of dissipationless dark matter predict that spiral disks should not be maximal. For the Milky Way as well as the external spirals, evidence has been presented both for and against maximal disks, with most of the controversy centered on the uncertainty in the stellar disk mass (Sackett 1997; Bershady et al. 2011).

1.3.6 Probes of the Dark Matter Halos in Galaxies

There has been persistent efforts to study the galactic dark matter halos and their shapes ever since their discovery. One may reiterate the fact that the dark matter constitutes the bulk of the total mass of the galaxy, and therefore it is essential to know their structure, mass and density distribution to understand the dynamics of galaxies better, apart from the history

of the formation and evolution of the galaxy as a whole. More specifically, determination the dark matter halo concentration near the galactic midplane is vital in order to gauge its effect on the disk dynamics, which is one of the prime objectives of this thesis. Also, the relevance of measuring the dark matter halo shapes lies in the fact that they are sensitive to the nature of the dark matter particles (Helmi 2004).

The determination of the dynamical mass, however, is not a trivial task. This is because we always observe projected positions on the plane of the sky and line-of-sight velocities at a given instant rather than complete three-dimensional orbits over an extended period of time (Tremaine & Mok Lee 2004). In the following sections, the common probes for studying the dark matter halo profiles are briefly discussed .

Rotation Curve Constraint: An array of observational probes is used as diagnostics to trace the density distribution of the dark matter halos. Primarily the observed rotation curve of a galaxy is used to estimate its dark matter halo content, the rotational velocity being determined employing the Doppler Shift Method. In the beginning, however, such studies were limited to the inner parts of galaxies as astronomers had only optical probes at their disposal to measure rotational velocity. In general, the inferred mass was consistent with the luminous components at these small radii. However, the discovery that spiral galaxies are surrounded by huge disks of atomic hydrogen, aided by the emergence of radio astronomy, completely altered the picture. The $21cm$ radio emission line traced the rotational velocity of the galaxies at larger and larger radii. Surprisingly, the rotational velocity was found to remain constant instead of falling off with radius in a Keplerian fashion, as was predicted based on the gravitational field of the luminous components only. This discovery caused a huge shift of paradigm, and established the fact that dark matter dominates the Universe at all scales. Currently, rotation curves are extensively used to measure the dark matter properties of spiral galaxies (de Blok et al. 2008, Oh et al. 2008). However, a word of caution needs to be borne in mind: As rotation curve itself played a key role in the development of the dark matter paradigm, it will be surprising if the theory failed to reproduce those properties that strongly motivated it in the first place. Instead, one should employ alternative probes for some independent confirmation or refutation of the theory.

Flaring of HI gas layer of spirals: The flaring HI gas layer traces the dark matter halo distribution near the mid-plane in the outer part of the galaxy. The thickness of the HI gas layer at any galactocentric radius is determined by a balance between the upward kinetic pressure and the net downward gravitational pull of the galaxy. Since the magnitude of turbulent gas pressure is generally known a priori, the observed gas thickness can be used to determine the net underlying gravitational potential of the galaxy, and hence that of the dark matter halo, by subtracting the contribution of the disk which can be estimated from the modeling of observational data. Since the HI disk in spiral galaxies extends radially outward over several stellar disk scalelengths, the thickness of the HI gas layer in the outer galaxy can be used to trace the dark matter halo properties directly, as the gravitational potential in this region is practically due to the dark matter halo only (Olling & Merrifield 2001, Narayan et al. 2005). However, obtaining the HI scale height data for galaxies is a challenging task, and therefore has been measured only for a handful of galaxies. This is because the observed width of the HI layer in the direction perpendicular to the major axis is the combined result of the beam broadening, inclination and disk thickness. The determination of the z distribution of the neutral hydrogen is further complicated by optical depth effects which are probably the greatest across the major axis and therefore tend to make the z distribution appear somewhat broader (Sancisi & Allen 1979).

Population II Kinematics: The underlying gravitational potential and hence the DM of the Galaxy can be determined from the dynamics of the Population II objects such as stars, globuler clusters and satellite galaxies, which have large random velocities. Application of virial theorem yields the underlying potential from which the contribution of the dark matter can be estimated. The velocity dispersion tensor of the Population II stars in the solar neighbourhood is anisotropic and this feature is used to obtain the local mass distribution of the Galaxy. However, due to uncertainties in the Galactic parameters and particularly the orbital structures of the tracer stars, these studies have remained largely inconclusive (Binney et al. 1987, van der Marel 1991, Amendt & Cuddeford 1994). Because globular clusters and satellite galaxies are found out to large distances, they can be used to constrain the force field at large distances, where the rotation curve cannot be measured directly. The

Population II tracers appear to confirm that, the Galaxy contains substantial amounts of dark mass, but the results are not yet reliable enough to constrain the distribution of dark mass or accurately measure its extent.

Kinematics of Polar Rings: A galaxy which hosts a gas ring, the plane of which is almost orthogonal to the plane of the galaxy, is referred to as a Polar Ring Galaxy (PRG). The fact that the accreted gas has settled into orbits that are near the polar planes of the galaxies suggests that the underlying the potential in these galaxies is not spherical. As the gas ring lies on a plane perpendicular to the symmetry plane of the light distribution, the velocity field can be mapped on two different planes and hence these galaxies provide the unique oppotunity to study the 3-D distribution of the underlying mass distribution, and specially its shape (Arnaboldi et al. 1993, Sackett et al. 1994, Sackett & Pogge 1995, Combes & Arnaboldi 1996).

Tidal Streams: The stellar tidal streams constitute a powerful probe of the shape of dark matter halo. In general, the probes used are sensitive to the density profile of the halo only. Satellite galaxies are tidally disrupted as they orbit the Milky Way. Stars infalling towards the Galactic center orbit the Galaxy faster than the satellite itself. Conversely, stars stripped from the side of the satellite further from the Galactic center orbit more slowly and trail behind the satellite. As they spread out, these stars form leading and trailing tidal streams respectively, which serves as a sensitive probe of average properties of the dark matter halo (Helmi 2004, Law & Majewski 2010, Varghese et al. 2011).

Weak Lensing: One of the consequences of Einstein's theory of general relativity theory was that massive bodies could bend the path of light rays. This effect is called gravitational lensing. In some cases the bending of light is so extreme (when the lens galaxy is very massive and the source galaxy is close enough to it), that the light travels along two different paths to the observer, multiple images of one single source appear on the sky and arcs of light are created which are aligned tangentially with respect to the center of the lens. This is

known as strong gravitational lensing where usually a rich galaxy cluster acts as the lensing system. However, in most cases the lens is not strong enough to form multiple images or giant arcs. The background galaxies, however, are still distorted, stretched and magnified but by a smaller degree. This is called weak gravitational lensing. In recent years weak lensing has emerged as a probe of the dark matter distribution. The tangential distortion of the background galaxies due to weak lensing by foreground galaxies is statistically measurable for large samples of source-lens pairs and high quality data, which gives an idea of the mass distribution of the foreground galaxies (Bartelmann & Schneider 2001).

Other Tracers: Apart from the above methods, the evolution of gaseous warps, the precession of accreted dusty gas disks, strong radio lensing of spirals and geometry of X-ray isophotes are the other tracers used to study the dark matter halos of galaxies. For detailed discussion, see Sackett (1999).

1.3.7 Our method of probing the Galactic Dark Matter Halos

This thesis focusses on constraining the density distribution along with the shape of the underlying dark matter distribution, using the both the observed rotation curve and the HI scale height data on an equal footing. Neither the rotation curve nor the HI scale height data is sufficient on its own to constrain the dark matter halo profile. While the rotation curve determines the radial derivative of the net galactic potential, the HI scale height data fixes its vertical derivative. In a way, the rotation curve grossly determines the halo mass within a certain radius, whereas the HI scale height data acts as a finer constraint determining the shape of the halo. However, the major challenge in using the above method lies in obtaining the HI scale height data as discussed earlier.

It may be noted here that in the first part of the thesis, namely "Vertical Structure of Spiral Galaxies", the vertical density distributions of the stars and/or the gas for a known dark matter halo is predicted. In the second part, which concerns the "Dark Matter Halos of Spiral Galaxies", the complementary approach is adopted. The dark matter halo is not known a priori and is constrained using the observed HI scale height data.

References

Amendt, P. & Cudderford, P. 1994, ApJ, 435, 93

Arnaboldi, M., Capaccioli, M., Cappellaro, E., Held, E. V. & Sparke, L. 1993, A&A, 267, 21

Bailin, J., & Steinmetz, M. 2005, ApJ, 627, 647

Barbanis, B., & Woltjer, L. 1967, ApJ, 150, 461

Bartelmann, M. & Schneider, P. 2001, Physics Reports, 340, 291

Bershady, M. A., Martinsson, T. P. K., Verheijen, M. A. W., Westfall, K. B., Andersen, D. R., Swaters, R. A. 2011, ApJ, 739L, 47

Binney, J., May, A. & Ostriker, J. P. 1987, MNRAS, 226, 149

Binney, J. & Tremaine, S. 1987, Galactic Dynamics (Princeton: Princeton University Press)

Binney, J. 2004. IAUS, 220, 3

Bosma, A. 1978, PhD Thesis, University of Groningen

Burkert, A. 1995, ApJ, 447, L25

Burstein, D. 1979, ApJ, 234, 829

Combes, F. & Arnaboldi, M. 1996, A&A, 305, 763

Combes, F. & Tiret, O. 2010, in the "Invisible Universe": AIP Conference Proceedings, Volume 1241, 154

Dalcanton, J. J. & Bernstein, R. A. 2002, AJ, 124, 1328

de Blok, W. J. G., Bosma, A. & McGaugh, S. 2003, MNRAS, 340, 657

de Blok, W. J. G., McGaugh, S. S., Bosma, A. & Rubin, V. C. 2001, ApJ, 552, L23

de Blok, W. J. G., Walter, F., Brinks, E., Trachternach, C., Oh, S.-H., & Kennicutt, R. C., Jr. 2008, AJ, 136, 2648

de Zeeuw, T., & Pfenniger, D. 1988, MNRAS, 235, 949

Dyson, J. E. & Williams, D. A. 1997, "The Physics of the Interstellar Medium", (Bristol & Philadelphia: Institute of Physics Publishing)

Flores, R. A. & Primack, J. R. 1994, ApJ, 427, L1

Freeman, K. & McNamara, G. 2006, "In Search of Dark Matter" (Chichester, UK: Springer)

Freeman, K. C. 1970, ApJ, 160, 811

Gao, L., Navarro, J. F., Cole, S., Frenk, C. S., White, S. D. M., Springel, V., Jenkins, A., & Neto, A. F. 2008, MNRAS, 387, 536

Gentile, G., Burkert, A., Salucci, P., Klein, U. & Walter, F. 2005, ApJ, 634, L145

Hayashi E. & White S. D. M. 2008, MNRAS, 388, 2

Helmi, A. 2004, ApJ, 610, L97

Korchagin, V. I., Girard, T. M., Borkova, T. V., Dinescu, D. I., & van Altena, W. F. 2003, AJ, 126, 2896

Houjun, M., van den Bosch, F., & White, S. 2010, "Galaxy Formation & Evolution", (Cambridge: Cambridge University Press)

Kulkarni, S. R. & Heiles, C. 1988, "Neutral hydrogen and the diffuse interstellar medium" in "Galactic and Exragalactic radio astronomy", Eds: Varschuur, G. I. & Kellerman, K. I.

Kuzio de Naray, R., McGaugh, S. S., de Blok, W. J. G. & Bosma, A. 2006, ApJS, 165, 461

Kuzio de Naray, R., McGaugh, S. S. & de Blok, W. J. G. 2008, ApJ, 676, 920

Lacey, C. G. 1984, MNRAS, 208, 687

Lacey, C. G. & Ostriker, J. P. 1985, ApJ, 299, 633

Law, D. R. & Majewski, S. R. 2010, ApJ, 714, 229

Lewis, J. R. & Freeman, K. C. 1989, AJ, 97, 139

Marchesini, D., D'Onghia, E., Chincarini, G., Firmani, C., Conconi, P., Molinari, E., & Zacchei, A. 2002, ApJ, 575, 801

McGaugh, S. S., Rubin, V. C. & de Blok, W. J. G. 2001, AJ, 122, 2381

Milgrom, M. 1983, ApJ, 270, 365

Merrifield, M. R. 2004, "Dark Matter on Galactic Scales (or the Lack Thereof)", arxiv:astro-ph/0412059v1

Merritt, D., Graham, A. W., Moore, B., Diemand, J. & Terzic, B. 2006, AJ, 132, 2685

Mo, van de Bosch & White 2010, Galaxy Formation and Evolution (Cambridge: Cambridge Univ. Press)

Navarro, J. F., Frenk, C. S. & White, S. D. M. 1996, ApJ, 462, 563

Navarro, J. F., Hayashi, E., Power, C., Jenkins, A. R., Frenk, C. S., White, S. D. M., Springel, V., Stadel, J. & Quinn, T. R. 2004, MNRAS, 349, 1039

Narayan, C. A. & Jog, C. J. 2002, A&A, 390, L35

Narayan, C. A., Saha, K. & Jog, C. J. 2005, A&A, 440, 523

Oh, S.H., de Blok, W. J. G., Walter, F., Brinks, E. & Kennicutt, R. C., Jr. 2008, AJ, 136, 2761

Olling, R. P. & Merrifield, M. R. 2001, MNRAS, 326, 164

Oort, J. H. 1932, BAN, 6, 249

Pontzen, A. & Governato, F. 2011, arXiv:1106.0499

Qu, Y., Di Matteo, P., Lehnert, M. D. & van Driel, W. 2011, A&A, 530, 10

Rohlfs, K. 1977, Lectures on Density Wave Theory (Berlin: Springer)

Rubin, V. C. & Ford, W. K., Jr. 1970, ApJ, 159, 379

Sancisi, R., & Allen, R.J. 1979, A&A, 74, 73

Sackett, P. D. 1997, ApJ, 483, 103

Sackett, P. D. 1999, "The Shape of Dark Matter Halos" in "Galaxy Dynamics: ASP Conference Series, Vol.182, 1999", Eds: Merrit, D., Sellwood, J. A. & Valluri, M

Sackett, P. D. & Pogge, R. W. 1995, in "Dark Matter", eds. S. S. Holt & C. S. Bennet (New York: AIP press), pg.141

Sackett, P. D., Rix, H-W., Jarvis, B. J. & Freeman, K. C. 1994, ApJ, 436, 629

Sellwood, J. A. & Merritt, D. 1994, ApJ, 425, 530

Spitzer, L. 1942, ApJ, 95, 329

Spitzer, L, Jr., & Schwarzschild, M. 1951, ApJ, 114, 385

Spitzer, L, Jr., & Schwarzschild, M. 1953, ApJ, 118, 106

Springel, V., Wang, J., Vogelsberger, M., Ludlow, A., Jenkins, A., Helmi, A., Navarro, J. F., Frenk, C. S. & White, S. D. M. 2008, MNRAS, 391, 1685

Tielens, A. G. G. M. 2005, "The Physics and Chemistry of the Interstellar Medium", (Cambridge: Cambridge University Press)

Tremaine, S., & Mok Lee, H. 2004, in "Dark Matter in Galaxies & Galaxy systems" in Dark Matter in the Universe:, ed. John Bahcall, Tsir Piran & Steven Weinberg (Hackensack, NJ: World Scientific), 71

Tsikoudi, V. 1979, ApJ, 234, 842

van der Marel, R. P. 1991, MNRAS, 248, 515

Varghese, A., Ibata, R. A., & Lewis, G. F. 2011, arXiv:1106.1765

Zwicky, F. 1933, AcHPh, 6, 110

2

The origin of steep vertical stellar distribution in the Galactic disk [1]

Abstract

Over the past two decades observations have revealed that the vertical density distribution of stars in galaxies near the mid-plane is substantially steeper than the sech^2 function that is expected from an isothermal approximation. However, the physical origin for this has not been explained so far. Here we show that such steep profiles result naturally even within the isothermal regime, on taking into account the gravitational force due to the gas. Due to its low velocity dispersion the gas is concentrated closer to the galactic mid-plane

[1] Banerjee & Jog 2007, ApJ, 662, 335

than the stars, and hence it strongly affects the vertical stellar distribution even though its contribution to the total surface density is small. We apply a three-component galactic disk model consisting of gravitationally coupled stars and the HI and H_2 gas, embedded in the dark matter halo, and calculate the vertical density distribution of stars for the Galaxy. The resulting vertical density distribution of stars is shown to be steeper than the sech^2 function, and lies between the sech and an exponential function, in good agreement with observations of galaxies. We also show that a multi-component stellar disk consisting of coupled dwarfs and two populations of giants does not explain the observed steep stellar profiles.

2.1 Introduction

It is well-known that a gravitating, isothermal stellar disk in a galaxy can be represented by a self-consistent vertical distribution that obeys a sech^2 profile as was shown theoretically (Spitzer 1942); and confirmed by observations (van der Kruit & Searle 1981 (a,b)). However, recent studies have shown that the observed vertical distribution in galaxies is steeper, and is well-approximated by an exponential or a sech function, especially close to the galactic mid-plane, as shown for the Galaxy (Gilmore & Reid 1983; Pritchet 1983; Kent, Dame & Fazio 1991; Gould, Bahcall & Flynn 1996) and also for external galaxies (Wainscoat et al. 1989; Aoki et al. 1991; Barnaby & Thronson 1992; van Dokkum et al. 1994; Rice et al. 1996). These later, near-infrared observations, which are free from the errors due to dust extinction, allow one to probe regions closer to the mid-plane. These show an excess over the isothermal case near the mid-plane, which is better-fitted by an exponential or a sech profile.

The sech^2 profile results under the isothermal assumption for the equation of state so that the pressure p can be written as density ρ times the square of the sound velocity or the random velocity dispersion, and the additional assumption that the velocity dispersion is independent of vertical distance (Spitzer 1942, Bahcall 1984). An exponential distribution as observed in some cases was argued to be unphysical when extended all the way to the mid-plane, and a fit intermediate between an exponential and an isothermal was suggested in terms a family of curves denoted by a parameter n (van der Kruit 1988). Subsequent

observational papers analyze the data and give their results in terms of this parameter n - see e.g., de Grijs & van der Kruit (1996); de Grijs, Peletiers & van der Kruit (1997). However, the set of models proposed by van der Kruit (1988) is somewhat ad-hoc since it is not obtained as a solution to the basic equations relevant in this context.

The physical origin of the steeper-than-isothermal vertical profile has not been fully explained so far. An exponential profile is shown to result if the gas settles in a protogalaxy into isothermal equilibrium and if the star formation rate is equal to the cooling rate of the gas (Burkert & Yoshii 1996). However, this model requires a specific set of initial conditions, and does not take account of the secular heating (e.g., Binney & Tremaine 1987) that stars undergo, and also it cannot explain the sech behaviour seen in many galaxies.

In this paper, we show that the steep vertical profile occurs naturally on taking account of the strong constraining effect of the gravitational force due to gas. Because of its lower velocity dispersion the gas forms a thin layer and thus lies closer to the galactic mid-plane than the stars, hence despite its small mass-fraction the inclusion of gas is shown to significantly affect the stellar vertical distribution. We apply a three-component model of a galactic disk consisting of gravitationally coupled stars, HI and H_2 gas, in the field of a dark matter halo, developed earlier by Narayan & Jog (2002 b). The resulting thickness was defined as the HWHM of the vertical distribution for each component and it showed a good agreement with observations for the inner Galaxy (Narayan & Jog 2002 b), and also the moderate stellar flaring predicted agreed well with observations of external galaxies (Narayan & Jog 2002 a). In the current paper, we concentrate on the density distribution close to the mid-plane. There is no discrepancy in these two approaches since at higher vertical distances, the various functional forms have the same (sech^2) behaviour. We treat the stellar disk to be a single component for simplicity, this assumption is justified later.

The results obtained in this paper show that the inclusion of gas gravity can account for the observed steepness in the stellar profiles closer to the mid-plane. Also, we predict the surface brightness distribution in the K-band at different galactocentric radii within the Galaxy, considering it as an edge-on system as it would appear to an external observer.

In Section 2.2, we discuss the model used and the method for solving the equations, and

give the parameters used. Section 2.3 contains the results obtained, Sections 2.4 and 2.5 give the discussion and the conclusions respectively.

2.2 Formulation of Equations and Solutions

We have used the three-component, galactic disk model of Narayan & Jog (2002 b) to obtain the vertical density distribution of stars in the Galaxy, as discussed in Section 2.1. In this model, the response of each component to the joint potential determines the net vertical density distribution in a self-consistent manner. The atomic and molecular hydrogen gas are distributed in two thin disks, embedded within the stellar disk, and are also axisymmetric and coplanar with it. We use the galactic cylindrical co-ordinates (R, ϕ, z). The equation of hydrostatic equilibrium in the vertical direction is given by (Rohlfs 1977):

$$\frac{\langle (v_z)_i^2 \rangle}{\rho_i} \frac{d\rho_i}{dz} = (K_z)_s + (K_z)_{HI} + (K_z)_{H_2} + (K_z)_{DM} \tag{2.1}$$

where i = 1,2,3, and DM denotes these quantities for stars, HI and H_2 gas, and the dark matter halo respectively. Here $K_z = -\partial\psi/\partial z$ is the force per unit mass along the z, and ψ_i is the corresponding potential, and $< (v_z)_i^2 >^{1/2}$ is the random velocity dispersion along z. We have assumed the equation of state to be isothermal and the dispersion to be constant with z.

Under the assumption of a thin disk, the joint Possion equation simpifies to

$$\frac{d^2\psi_s}{dz^2} + \frac{d^2\psi_{HI}}{dz^2} + \frac{d^2\psi_{H_2}}{dz^2} = 4\pi G(\rho_s + \rho_{HI} + \rho_{H_2}) \tag{2.2}$$

On combining equations (2.1) & (2.2), the density distribution of a component i at any radius is given by

$$\frac{d^2\rho_i}{dz^2} = \frac{\rho_i}{\langle (v_z)_i^2 \rangle} \times [-4\pi G(\rho_s + \rho_{HI} + \rho_{H_2}) + \frac{d(K_z)_{DM}}{dz}] + \frac{1}{\rho_i}\left(\frac{d\rho_i}{dz}\right)^2 \tag{2.3}$$

From the above equation, it is evident that though there is a common gravitational potential, the response of each component will be different due to the difference in their random velocity dispersions.

2.2.1 Solution of the equations

The above equation represents a set of three coupled, second order ordinary differential equations which is solved numerically by the Fourth order Runge-Kutta method in an iterative fashion (Narayan & Jog 2002 b) with the following two boundary conditions at the mid-plane i.e z=0 for each component:

$$\rho_i = (\rho_0)_i \qquad \frac{d\rho_i}{dz} = 0 \tag{2.4}$$

However, the modified mid-plane density $(\rho_0)_i$ for each component is not known a priori. Instead the net surface density $\Sigma_i(R)$, given by twice the area under curve of $\rho_i(z)$ versus z, is used as the second boundary condition, since this is known observationally. Hence the required value of $(\rho_i)_0$ can be determined by trial and error method, which eventually fixes the $\rho_i(z)$ distribution.

2.2.2 Parameters used

We require surface density and the velocity dispersion for each component to solve the coupled set of equations at each radius, these parameters have been taken as in Narayan and Jog (2002 b). The observed values were used for the gas surface densities (Scoville & Sanders 1987), see Table 2.1. The stellar surface density, and the density profile of the dark matter halo, were taken from the standard mass model for the Galaxy by Mera et al (1998): here the stellar disk has an exponential distribution with a disk scale length of 3.2 kpc and the local stellar density of 45 $M_\odot$ pc^{-2}, which gives the central stellar surface density of 641 $M_\odot$ pc^{-2}, and the dark matter halo is taken as an isothermal sphere with a core radius of 5 kpc and the rotation velocity of 220 km s $^{-1}$. Table 2.1 also lists the values of the ratio $\Sigma_{\rm HI+H_2}/\Sigma_s$, the total gas to stellar surface mass density.

The observed gas velocity dispersion values are taken, with 8 km s $^{-1}$ for HI (Spitzer 1978) and 5 km s $^{-1}$ for H_2 gas (Stark 1984, Clemens 1985). The observed planar stellar velocity dispersion values from Lewis & Freeman (1989) were used to obtain the vertical dispersion values assuming the same ratio, namely 1/2, of the velocity dispersions as seen in the solar neighborhood (Binney & Merrifield 1998). This gives an exponential velocity

TABLE 2.1: Best-fitting $2/n$ values at different radii

Radius (kpc)	Σ_{HI} $M_\odot pc^{-2}$	Σ_{H_2} $M_\odot pc^{-2}$	$\frac{\Sigma_{HI+H_2}}{\Sigma_s}$	n	2/n
2	1.8	4.0	0.02	3.33	0.6
3	3.8	4.9	0.04	5.4	0.37
4	4.6	13.1	0.10	7.32	0.27
4.5	4.6	19.7	0.16	9.12	0.22
5	4.6	14.2	0.14	7.91	0.25
6	4.6	10.8	0.16	6.89	0.29
7	4.7	4.9	0.13	4.86	0.41
8	5.3	3.6	0.17	4.5	0.44
8.5	5.6	2.1	0.17	4.26	0.47
9	5.6	1.4	0.18	4.22	0.47
10	5.6	0.8	0.23	2.93	0.68
11	5.6	0.6	0.30	2.88	0.69
12	5.6	0.4	0.40	2.83	0.71

distribution with a scale length of 8.7 kpc and the local value of 18 km s $^{-1}$ (Lewis & Freeman 1989, Narayan & Jog 2002 b).

2.3 Results

2.3.1 Effect of gas on stellar vertical distribution

We first illustrate the dynamical effect of the inclusion of the low-dispersion component, namely the gas, on the vertical distribution of stars. First compare the gravitational force due to stars and gas taken separately. The strength of the force per unit mass $|K_z|$ for an isothermal single component is obtained by solving the force equation and the Poisson equation (eqs. 2.1-2.2) together. These can be solved analytically and give (Spitzer 1944,

Rohlfs 1977):

$$\left|K_z\right| \;=\; 2\frac{\langle v^2\rangle}{z_0}\;\tanh z/z_0 \tag{2.5}$$

where $< v^2 >$ is the mean square of the velocity. The vertical density distribution is given by

$$\rho(z) \;=\; \rho_0\,\mathrm{sech}^2(z/z_0) \tag{2.6}$$

where the constant z_0 is given in terms of the mid-plane density, ρ_0, as:

$$z_0 \;=\; \left[\frac{\langle v^2\rangle}{2\pi G\rho_0}\right]^{1/2} \tag{2.7}$$

We treat the stars-alone case first and use the total observed stellar surface density Σ_s at a given radius as a boundary condition, and integrating eq. (2.6), we constrain both ρ_0 and z_0 simultaneously. The procedure is then repeated for the gas-alone HI and H_2 components taken separately. The resulting values for the $|K_z|$ the strength of the force per unit mass due to stars-alone and that due to HI and H_2 alone (drawn on a log scale) vs. z are shown in Fig. 2.1, as calculated at R=6 kpc. It is clear that up to $|\,z\,| <$ 150 pc, the force due to gas is significant $\sim$ 30% of that due to stars. This is the spatial region over which we have fitted the n(z) profiles to obtain the parameter n (Section 2.3.2). Thus we expect to see steepening of the density profile of stars on taking account of the gas gravity.

A similar plot for the coupled case cannot be given since the three disk components (stars, HI and H_2) are coupled, hence the individual terms on the r.h.s. of equation (2.1) are not known. However, a gradient of $|K_z|$ with z can be given in terms of the mass density, ρ, for each component using the Poisson equation. The resulting values of mass densities for the three coupled components as obtained from our model at R=6 kpc are plotted in Figure 2.2. This is another indicator of the importance of gas in the dynamics close to the mid-plane. The mid-plane density of the gas and the stars are comparable, hence the gas gravity affects the stellar dynamics significantly.

The dynamical effect of gas gravity on the net vertical density distribution of stars is clearly shown in Figure 2.3, where we plot and compare the stellar density distribution vs.

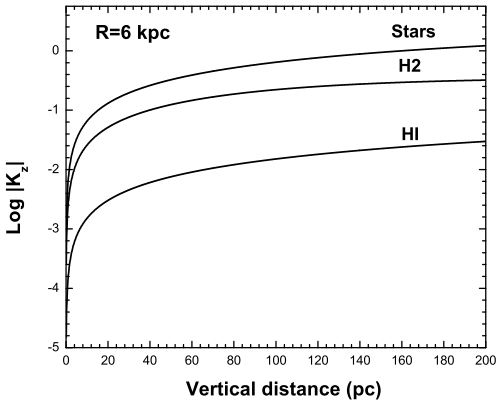

FIGURE 2.1: Plot of force per unit mass $|K_z|$ for the star-alone case and the H_2-alone and HI-alone cases on a log scale vs. z , calculated at R= 6 kpc. The force due to the gas is a significant fraction $\sim 30\%$ of the stars-alone case for the z values close to the galactic mid-plane ($|z| \leq 150$ pc).

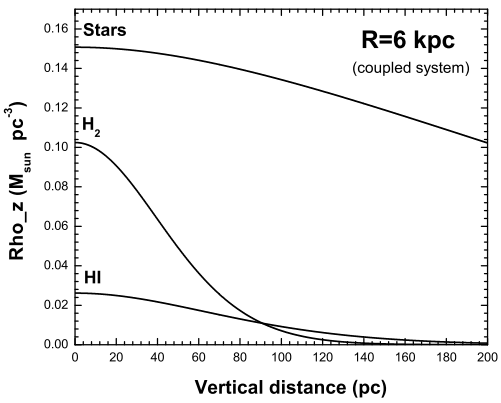

FIGURE 2.2: The density distribution vs. z for the gravitationally coupled three-component system obtained at R= 6 kpc, plotted for the stars, H_2, and HI gas components. The gas density is a significant fraction of the stellar density close to mid-plane, hence the force due to gas has a strong effect on the stellar distribution despite the fact that the gas surface density is a small fraction of the total disk surface density.

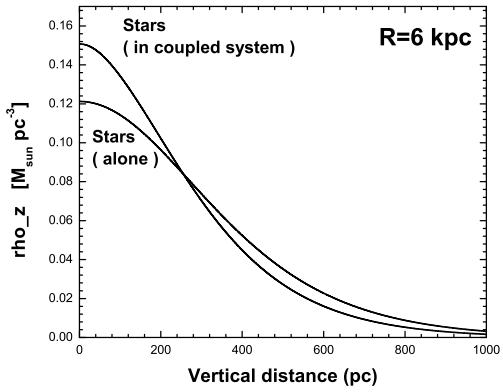

FIGURE 2.3: The density distribution vs. z for the star-alone case and for the stars in a gravitationally coupled three-component system obtained at R = 6 kpc. Because of the gravitational force due to gas, the stellar distribution in the coupled case has a higher central value, the profile is steeper, and the thickness (HWHM) is smaller.

z for the stars-alone case and also as obtained in the coupled system. First, the central or the mid-plane peak in density is increased, and the shape of the central profile becomes sharper which is studied quantitatively in terms of the parameter "n" in the rest of the paper. Further, the scale height (HWHM) of the stellar distribution is lower in the coupled system due to the inclusion of gas gravity - this aspect was studied in detail in our earlier work (Narayan & Jog 2002 b). Thus the inclusion of gas affects the central peak density of the stellar distribution, and the shape of the profile, and also it decreases the stellar vertical scale height.

Thus we have shown that due to its lower velocity dispersion, the gas forms a thinner layer and is concentrated closer to the galactic mid-plane than the stars. Hence, despite the fact that the gas contains a small fraction of the total disk surface density, it has a significant effect on the vertical density distribution of the main mass component, namely the stars.

A study highlighting a similar constraining effect of a molecular cloud complex was done by Jog & Narayan (2001). The cloud complex is massive ($\sim 10^7$ $M_\odot$) and extended ($\sim$ 200 pc in size), with an average density much higher than the mid-plane stellar density, hence in that case the $|K_z|$ due to the complex dominates over the $|K_z|$ due to stars-alone case (Fig. 1 in that paper), and the resulting changes in the vertical density distribution of stars and

the HWHM (Figs. 3 and 4 respectively in that paper) are much stronger. Figures 1 and 3 in that paper are the analogs of Figures 2.1 and 2.3 given above.

2.3.2 Model Stellar Vertical Profiles

The self-consistent vertical density distribution of stars was determined for the radial range of 2-12 kpc in the Galaxy, following the method discussed in Section 2.1. In order to compare our results with the observational papers in the literature which have fitted their data to the van der Kruit (1988) curves, we also fit our numerical solution for $\rho(z)$, the stellar mass density, to the family of curves suggested by van der Kruit (1988):

$$\rho(z) = 2^{-2/n}\, \rho_e\, \mathrm{sech}^{2/n}(nz/2z_e) \tag{2.8}$$

which is characterized by three parameters ρ_e, z_e and n. Here ρ_e is the extrapolated outer mass density away from the galaxy plane which is the same for all values of n at large z , and z_e is the vertical scale parameter. For a given ρ_e, the effective scale heights and the amplitudes at z=0 are obtained as a function of the parameter n.

In the limiting cases of n=1 and n=∞, eq. (2.8) reduces to the usual isothermal (or the sech^2 function), and an exponential function respectively, while n=2 denotes an intermediate case of the sech profile.

In Figures 2.4 and 2.5, we compare the vertical stellar-density profiles for n=∞(exp), n=2(sech) and n=1(sech^2) cases with our model curves obtained at R=6 kpc and 8.5 kpc respectively. The values of the parameters ρ_e and z_e in these cases are the best-fitting values obtained from fitting our model curves to within $|z| \leq 150$ pc of the galactic mid-plane. The model curve in Figs. 2.4 and 2.5 is best-fitted by n = 6.9 and n = 4.3 respectively, thus it lies between the sech and an exponential profile. In the region of the molecular ring, which includes R= 6 kpc, the influence of gas is higher and hence the resulting vertical profile is steeper than in the solar neighbourhood region of 8.5 kpc. This underlines the crucial effect of gas in causing a steepening of the vertical stellar density profile in the galactic disk. The best-fit values for z_e are 368 pc and 362 pc respectively. From these figures, it is clear that the best-fitting value of n depends on the range of z used, and at large enough z-range all

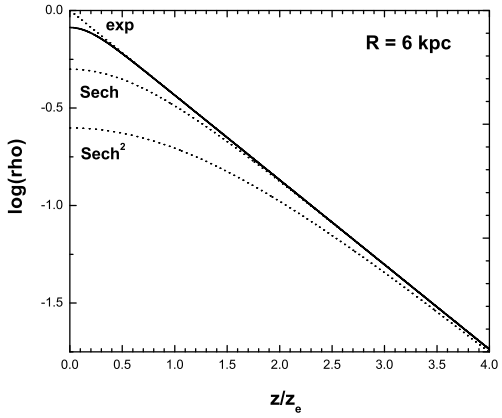

FIGURE 2.4: Plot of vertical density distribution versus z/z_e, at R = 6 kpc. The model profile (solid line) is best-fitted by the n = 6.9 case from van der Kruit (1988), and is steeper than the stars-alone isothermal or the sech^2 case (n=1), and lies between the sech z (n=2) and an exponential (n=∞) cases (shown as dotted lines). This region lies within the molecular ring of high gas density , hence it results in a steep vertical profile.

curves go over to the usual sech^2 profile.

The effect of gas gravity is further illustrated by plotting the best-fitting $2/n$ values versus radius for the Galaxy obtained from our analysis in Figure 2.6. Also, Table 2.1 gives the best-fitting $2/n$ values obtained at different radii along with the total gas-fraction at each radius. It shows that $2/n$ lies between 0 and 1 in general, or that n lies between ∞ and 2. Thus, *our model vertical distribution is steeper than the one-component isothermal case (n=1) at all radii*, and lies between an exponential and a sech profile. This is in direct conformity with the results obtained by Peletiers et al (1997) for a complete sample of external, edge-on galaxies.

Interestingly, the best-fitting steepness index n is more directly dependent on the total absolute gas surface density than on the gas fraction (see Table 2.1). This needs to be studied for other galaxy types and gas mass ranges in a future paper.

2.3.3 Luminosity profile of a multi-component stellar disk

So far we have treated the stars to consist of a single, isothermal component and our dynamical model gives the steep vertical density profile for this single stellar component when

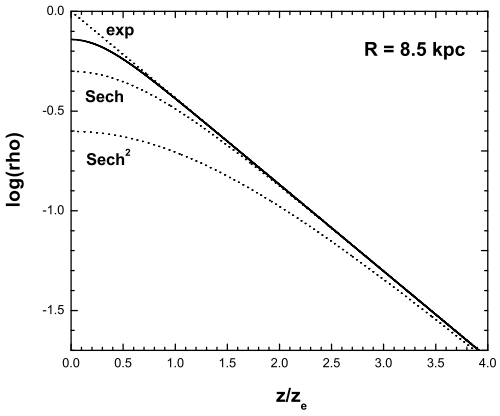

FIGURE 2.5: Plot of vertical density distribution versus z/z_0, at R = 8.5 kpc. The vertical model profile is best-fitted by n=4.3 case from van der Kruit (1988), which is closer to the sech case and is less sharp than at R = 6 kpc, but is still sharper than the stars-alone, isothermal case (sech^2 z).

coupled to the HI and H_2 gas components. We confirm the validity of this assumption next.

Alternatively, a steepening of stellar vertical luminosity profile could also occur if a superposition of stellar components with different velocity dispersions is considered, as has been suggested qualitatively (de Grijs et al. 1997). We check and refute this idea by considering a coupling of the G-K-M dwarfs which contain the main mass fraction in the stellar disk, and giants which contain a much smaller disk mass fraction but dominate the disk luminosity. This latter feature is well-known, namely that the luminosity of the disk is dominated by giants which may not determine its dynamics as cautioned by Mihalas & Binney (1981). The giants span a large range of velocities covering a factor of 2, and at a first glance it may seem that that would result in a non-isothermal stellar luminosity profile, or a profile steeper than sech^2. However, as we show next, the net dynamics in a disk consisting of coupled dwarfs and giants is largely determined by the dwarfs because they constitute the main disk mass component and the two have comparable dispersions.

We treat the giants to consist of two separate components or populations characterized by vertical dispersions of 14 km s^{-1} and 28 km s^{-1} respectively, with 23 % of the mass surface density of giants in the higher velocity component, as was shown in a recent study based on the *Hipparcos* data by Holmberg & Flynn (2004). We then apply our coupled,

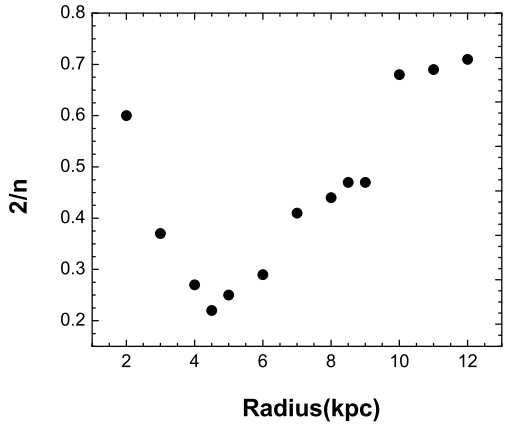

FIGURE 2.6: Plot of vertical density distribution versus z/z_0, at R = 8.5 kpc. The vertical model profile is best-fitted by n=4.3 case from van der Kruit (1988), which is closer to the sech case and is less sharp than at R = 6 kpc, but is still sharper than the stars-alone, isothermal case (sech^2 z).

three-component disk model to the G-K-M dwarfs (treated as a single component) and the above two giant components. The total surface densities of dwarfs and giants are taken to be 13.5 and 0.19 $M_\odot pc^{-2}$ respectively as observed, see Table 4-16 in Mihalas & Binney (1981).

The resulting net stellar density distribution from our model is fitted by the van der Kruit (1988) function to obtain the "n" parameter. Our dynamical model gives the n value for dwarfs in this case to be 1.01, which is almost identical to a one-component sech^2 profile (which is given by n=1). For each of the two populations of giants, the best-fit n value is also 1.01. Next, we add the density profiles for these two giant populations, and the best-fit value for n in this case is found to be 1.07, which is still close to the isothermal case, although it is very slightly steeper than the profile for the individual components. The net luminosity profile, as set by the sum of the giant populations, will thus be nearly a sech^2 or close to an isothermal. This is a somewhat surprising result and physically this can be explained by the fact that the high-velocity giant population has a much lower surface density, hence in the coupled three-component system treated here, its density contribution within 150 pc (this is the z-range over which the fitting for n is done) is much smaller than the other giant component. This is why despite the two giant populations having such different vertical velocity dispersions, the net density profile of the giants is close to that of a single isothermal.

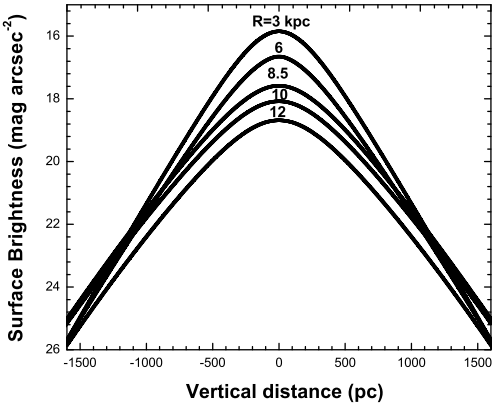

FIGURE 2.7: A plot showing the model surface brightness curves in the K-band versus the distance z from the mid-plane, calculated at different galactocentric radii, treating the Galaxy as an edge-on system as seen by an external observer.

The n for the combined giants is thus very similar to the n for the main mass component namely the dwarfs.

Note that the observed stellar luminosity profile is much steeper with n=2 or higher, that is, it lies between a sech and an exponential (Section 2.3.2). Thus, a multi-component stellar disk with observed parameters for the dwarfs and the giants cannot explain the steep light distribution seen in galaxies. In contrast, the inclusion of gas in our model despite its small mass fraction naturally results in the steep stellar profile as observed, as shown in Section 2.3.2.

This calculation also confirms that our assumption of a single-component stellar disk is valid for the dynamical study, since the giants do not affect the dynamics of dwarfs.

Similarly, even in the coupled stars-gas case treated in our paper, the luminosity profile of the giants at low z can be taken to trace that of main stellar-mass component, namely the dwarfs.

2.3.4 Model Surface Brightness vs. Height, z

The luminosity density of stars in a particular colour-band is the directly observed quantity in astronomy rather than mass density itself. But as the luminosity density in any colour-band is taken to be a constant multiple of the stellar density function, we conclude that the vertical luminosity distribution follows the same functional form as the corresponding mass density distribution, and hence is characterized by the same value of the steepness index n.

We next obtain the surface brightness distribution of a typical edge-on galaxy like our Milky Way as seen by an external observer by integrating the luminosity density function along a line of sight. If the luminosity density at a galactocentric radius R, and vertical distance z above the mid-plane is given by (see van der Kruit & Searle 1981 a)

$$L(R,z) = L_0 \mathrm{sech}^{2/n}(nz/2z_e)\exp(-R/h) \tag{2.9}$$

where 'h' is the disk scale length, then the surface brightness is given by:

$$I(R,z) = I(0,0)(R/h)K_1(R/h)\mathrm{sech}^{2/n}(nz/2z_e) \tag{2.10}$$

where I(0,0)=$2L_0$h and K_1 is the modified Bessel function. If I(R,z) is in units of $\mathrm{L}_\odot$ pc^{-2}, the surface brightness in units of magnitude arcsec^{-2} is (Binney & Merrifield 1998):

$$\mu(R,z) = -2.5\log_{10}(I/L_\odot pc^{-2}) + M_\odot + 21.572 \tag{2.11}$$

Here $M_\odot$ denotes the absolute solar magnitude in the chosen colour-band. For the K-band, $M_\odot$= 3.33 (Cox 2000), and the above formula reduces to

$$\mu(R,z) = -2.5\log_{10}(I/L_\odot pc^{-2}) + 24.902 \tag{2.12}$$

Our Galaxy is known to have an exponential disk (e.g., Mera et al. 1998) with an exponential luminosity profile as given in equation (2.9), from this we obtain the surface-brightness profiles in K-band at a given radius as follows. The stellar density value at each z (in units of $\mathrm{M}_\odot\mathrm{pc}^{-3}$) at a given R obtained from our numerical analysis is divided by $\mathrm{M}_\odot$/ $\mathrm{L}_\odot$ of 1 to obtain the corresponding luminosity density in the K-band in units of $\mathrm{L}_\odot\mathrm{pc}^{-3}$. This ratio

of mass-to-luminosity is obtained using the K-band disk luminosity from Kent et al. (1991) and the disk mass from Binney & Tremaine (1987), and is in agreement with the study based on a large number of galaxies (Bell & de Jong 2001) which has shown the typical value of this ratio to be ~ 0.5 with a scatter of a few around it. Then using eqs. (2.10) and (2.11), we obtain the surface-brightness distribution at a given radius. In Fig. 2.7, we plot the model surface-brightness distribution in the K-band calculated at different radii, treating the Milky Way Galaxy as an edge-on system as seen by an external observer. These curves are strikingly similar to the observed profiles for external edge-on galaxies (see Fig. 3 from Barteldrees & Dettmar 1994; and Fig. 5 from de Grijs et al. 1997).

2.4 Discussion

1. We have assumed the stellar disk to be isothermal for simplicity as is the standard practice in the study of the vertical structure of galactic disks (e.g., Spitzer 1942, Bahcall 1984). The stellar velocity dispersion increases due to secular heating by tidal interactions and molecular clouds (e.g., Binney & Tremaine 1987). Despite this the resulting stellar vertical velocity dispersion is shown to be constant with height (Jenkins & Binney 1990, Jenkins 1992), hence the isothermal assumption made is robust.

2. The model developed here is general, and since the gas velocity dispersion in external galaxies is universally much smaller than the stellar dispersion (see e.g., Lewis 1984, Wilson & Scoville 1990), the analysis in this paper can be applied to other galaxies as well. We predict that the late-type galaxies being gas-rich will show steeper stellar profiles (higher n or lower $2/n$ values) than the early type galaxies, for the same range of radial range. This could be checked with future observations.

2.5 Conclusions

It is well-established that the vertical distribution of stars in galactic disks is observed to be steeper than the sech^2 profile expected from a one-component, isothermal case, especially closer to the galactic mid-plane. In this paper, we provide a simple, physical origin for this:

we show that on taking account of the gas gravity, the resulting stellar vertical profile even under the isothermal assumption, is steeper than the sech^2 function. The resulting profile is calculated for our Galaxy using a three-component model of a galactic disk consisting of gravitationally coupled stars and gas, and is shown to be steeper than sech^2 and lies between the sech profile and an exponential profile, in agreement with observations of galaxies. The higher the gas surface density, the steeper is the resulting stellar vertical profile, asymptotically approaching the exponential curve. Due to the lower velocity of gas it is concentrated close to the mid-plane, this crucial feature results in the steepening of the stellar profile. We also show that the observed steep stellar profiles cannot be explained by a superposition of several stellar components, as has sometimes been proposed qualitatively in the literature.

References

Aoki, T.E., Hiromoto, N., Takami, H., Okamura, S. 1991, PASJ, 43, 755

Bahcall, J.N. 1984, ApJ, 276, 169

Barnaby, D., Thronson, H. A., Jr.,1992, AJ, 103, 41

Barteldrees, A., Dettmar, R.-J., 1994, A & A S, 103, 475

Bell, E.F., de Jong, R.S. 2001, ApJ, 550, 212

Binney, J., Merrifield, M., 1998, Galactic Astronomy. Princeton Univ. Press, Princeton, NJ

Binney, J., Tremaine, S., 1987, Galactic Dynamics. Princeton Univ. Press, Princeton, NJ

Burkert, A., Yoshii, Y., 1996, MNRAS, 282, 1349

Clemens, D.P., 1985, ApJ, 295, 422

Cox, A.N., Ed. 2000, Astrophysical Quantities, Springer, New York

de Grijs, R., Peletier, R.F., van der Kruit,P.C., 1997, A&A, 327, 966

de Grijs, R., van der Kruit, P.C., 1996, A&A S, 117, 19

Gilmore, G., Reid, N., 1983, MNRAS, 202, 1025

Gould, A., Bahcall, J.N., Flynn, C., 1996, ApJ, 465, 759

Holmberg, J., Flynn, C. 2004, MNRAS, 352, 440

Jenkins, A., 1992, MNRAS, 257, 620

Jenkins, A., Binney, J.J., 1990, MNRAS, 245, 305

Jog, C.J., Narayan, C.A. 2001, MNRAS, 327, 1021

Kent, S.M., Dame, T.M., Fazio, G., 1991, ApJ, 378, 131

Lewis, B.M. 1984, ApJ, 285, L453

Lewis, J.R., Freeman, K.C., 1989, AJ, 97, 139

Mera, D., Chabrier, G., Schaeffer, R., 1998, A&A, 330, 953

Mihalas, D., & Binney, J. 1981, Galactic Astronomy. Freeman, San Fransisco

Narayan, C.A., Jog, C.J., 2002 a, A&A, 390, L35

Narayan, C.A., Jog, C.J., 2002 b, A&A, 394, 89

Pritchet, C., 1983, AJ, 88, 1476

Rice, W., Merrill, K.A., Gatley, I., Gillett, F.C., 1996, AJ, 112, 114

Rohlfs, K. 1977, Lectures on Density Wave Theory. Springer-Verlag, Berlin

Scoville, N.Z., Sanders, D.B., 1987, in Interstellar Processes, eds. D.J.Hollenbach,H.A.Thronson. Reidel, Dordrecht, p. 21

Spitzer, L., 1942, ApJ, 95, 329

Spitzer, L., 1978, Physical processes in the Interstellar Medium. John Wiley, New York

Stark, A.A., 1984, ApJ, 281, 624

van der Kruit, P.C., 1988, A&A, 192, 117

van der Kruit, P.C., Searle, L., 1981a, A&A, 95, 105

van der Kruit, P.C., Searle, L., 1981b, A&A, 95, 116

van Dokkum, P.G, Peletier, R.F, de Grijis, R., Balcells, M. 1994, A&A, 286, 415

Wainscoat, R.J., Freeman, K.C., Hyland, A.R., 1989, ApJ, 337, 163

Wilson, C.D., & Scoville, N.Z. 1990, ApJ, 363, 435

3

Theoretical determination of HI vertical scale heights in the dwarf galaxies: DDO 154, Ho II, IC 2574 & NGC 2366 [2]

Abstract

In this paper, we model dwarf galaxies as a two–component system of gravitationally coupled stars and atomic hydrogen gas in the external force field of a pseudo–isothermal dark matter halo, and numerically obtain the radial distribution of HI vertical scale heights. This is done for a group of four dwarf galaxies (DDO 154, Ho II, IC 2574 and NGC 2366) for which

[2]Banerjee et al. 2011, MNRAS, 415, 687

most necessary input parameters are available from observations. The formulation of the equations takes into account the rising rotation curves generally observed in dwarf galaxies. The inclusion of self–gravity of the gas into the model at par with that of the stars results in scale heights that are smaller than what was obtained by previous authors. This is important as the gas scale height is often used for deriving other physical quantities. The inclusion of gas self–gravity is particularly relevant in the case of dwarf galaxies where the gas cannot be considered a minor perturbation to the mass distribution of the stars. We find that three out of four galaxies studied show a flaring of their HI disks with increasing radius, by a factor of a few within several disk scale lengths. The fourth galaxy has a thick HI disk throughout. This flaring arises as a result of the gas velocity dispersion remaining constant or decreasing only slightly while the disk mass distribution declines exponentially as a function of radius.

3.1 Introduction

In this paper we address the vertical distribution of neutral atomic hydrogen HI in four dwarf irregular (dIrr) galaxies that are part of THINGS (The HI Nearby Galaxy Survey; (Walter et al. 2008)). These objects occupy the low mass, low luminosity tail of the galaxy luminosity function. They have accordingly low metallicities, in agreement with the finding that star formation in these systems occurs episodically, in bursts, with long periods during which apparently little star formation is taking place. Contrary to larger spiral galaxies, where stars dominate, in dwarf galaxies stars and HI make up the baryonic mass content on an equal footing, with little or no H_2 being traced through CO observations (Tacconi & Young 1997; Taylor, Kobulnicky, & Skillman 1998). The jury is still out on the relation of CO to H_2 in low–metallicity, low–mass environments encountered in dwarf galaxies, although it seems clear that a low CO signal does not necessarily mean a correspondingly low H_2 mass (Wilson 1995, Bolatto et al. 2008, Leroy et al. 2009). Their low metallicity and the fact that a large fraction of their gas has not yet been turned into stars is often used to argue that dwarf galaxies, within the paradigm of hierarchical galaxy formation, then must be broadly similar to the building blocks at high redshift that eventually formed today's larger galaxies. In accordance with models of hierarchical structure formation dwarf galaxies are

dark matter dominated, something which is borne out by observations (Carignan & Freeman 1988; Ashman 1992; Oh et al. 2010). They constitute the largest number of galaxies in the present day observable universe (Mateo 1998).

Brinks, Walter, & Ott (2002) postulated that the gas scale height in dIrrs was larger, both in absolute as well as relative sense, than in larger, spiral galaxies. This has several implications, especially if indeed nearby dIrrs are broadly similar to those found at large look–back times. For example, their cross section for intercepting distant QSOs, giving rise to damped Lyman–α signatures, will be much larger. Also, a thicker gas layer will tend to allow HI shells and bubbles to grow to larger diameters, preventing early break–out and thus reducing the likelihood that metals pollute the intergalactic medium.

The vertical stellar distribution has been extensively studied observationally (see for a review, van der Kruit 1988). The fact that the stellar distribution shows a moderate flaring at large radii was shown observationally by de Grijs, Peletier & van der Kruit (1997), and predicted from a general self-consistent model by Narayan & Jog (2002a). In broad terms, the observed constant velocity dispersion of the gas combined with a decreasing mass surface density (as traced by the exponential decline of the stellar light distribution) predicts a flaring HI layer. Early direct observations of this flaring were made in the Milky Way (Henderson, Jackson, & Kerr 1982) and M 31 (Brinks & Burton 1984).

Observing the HI gas scale height directly is difficult, even for a perfectly edge–on galaxy, due to effects such as line–of–sight integration, beam smearing and optical depth effects as was already pointed out by Sancisi & Allen (1979). More recent observations of the Milky Way are given by Wouterloot et al. (1990) and Levine, Blitz, & Heiles (2006), (see also Kalberla & Kerp 2009), and for M31 by Braun (1991). Some other systems whose scale heights have been measured are NGC 3198 and NGC 2403 (Sicking 1997). No serious attempt has been made to date to investigate the vertical stellar and gas distributions in dIrrs. As discussed by Brinks, Walter, & Ott (2002), because their observed HI velocity dispersion is not very different from that observed in spirals, but their mass surface density is considerably lower, dIrrs must have a larger scale height in HI as compared to spiral galaxies in an absolute sense.

The origin of flaring of the gas layer in spiral galaxies has been treated recently in a self–consistently manner by Narayan & Jog (2002b), who produced a numerical model of the vertical scale heights of the gas and stars in a gravitationally–coupled, three–component Galactic disk. In this paper, we extend this earlier work on the vertical stellar and gas distribution in spirals to dwarf galaxies, and determine the scale height of the gas as a function of radius analytically. We model the galaxy as a gravitationally coupled system of stars and gas subjected to the external force field of a dark matter halo, and use the model to obtain the HI vertical scale height as a function of galactocentric radius for four dwarf galaxies. In earlier papers we had assumed a flat rotation curve (Narayan & Jog 2002b, Narayan, Saha & Jog 2005). This approximation is not warranted for dwarf galaxies which show a steadily rising rotation curve throughout most of their disk. Instead we explicitly take account here of a rising rotation curve, and show that the originally two–dimensional partial differential equations can still be written as one–dimensional or ordinary differential equations, as in the case for the giant spiral galaxies which have flat rotation curves.

We will concentrate in this paper on the properties of the bulk of the gas and therefore ignore the contribution by the $\sim$ 10 percent of extra–planar gas found by Fraternali and collaborators (Fraternali & Binney 2008, Marasco & Fraternali 2011), most of which seems to be related to energy input from supernovae into the interstellar medium. We describe our methodology in Sections 3.2 and 3.3, justify the values for the input parameters to the model for the four galaxies studied here in Section 3.4, and present our results and discussion in Section 3.5.

3.2 Model

3.2.1 Gravitationally–coupled, two–component, galactic disk model

We use a two–component galactic disk model of gravitationally–coupled stars and HI gas subjected to the external force–field of a dark matter halo with a pseudo–isothermal density profile. In this model, the stars and gas are assumed to be present in the form of concentric, thin, axisymmetric disks embedded within each other (See Narayan & Jog 2002b, Banerjee

& Jog 2007).

The joint Poisson equation in cylindrical co-ordinates for an axisymmetric system of stars and gas is given by:

$$\frac{1}{R}\frac{\partial}{\partial R}\left(R\frac{\partial \phi_{total}}{\partial R}\right) + \frac{\partial^2 \phi_{total}}{\partial z^2} = 4\pi G(\sum_{i=1}^{2} \rho_i + \rho_h) \tag{3.1}$$

where ϕ_{total} is the net potential of the disk due to the stars, the HI gas and the dark matter halo, ρ_i with $i = 1$ to 2 denotes the mass volume density for each of the disk components (stars, gas) while ρ_h denotes the same for the halo, and is given by de Zeeuw & Pfenniger (1988):

$$\rho_h(R, z) = \frac{\rho_0}{1 + \frac{R^2+z^2}{R_c^2}} \tag{3.2}$$

where ρ_0 is the central core density of the halo, and R_c is the core radius, as applicable for a pseudo–isothermal density distribution. One may note here that since dwarf galaxies have rotation curves that are generally rising out to the last measured point (Salucci et al. 2007), the radial term in equation (3.1) cannot be ignored as in the case for large spirals with almost flat rotation curves (Narayan et al. 2005, Banerjee & Jog 2008).

The equation of hydrostatic equilibrium for the i^{th} disk component in the z direction is given by Rohlfs (1977):

$$\frac{\partial}{\partial z}(\rho_i \langle v_z^2 \rangle_i) + \rho_i \frac{\partial \phi_{total}}{\partial z} = 0 \tag{3.3}$$

where $< v_z^2 >_i$ is the mean square velocity of the i^{th} disk component. Equation (3.3) constitutes two equations, one each for the density of each of the two disk components. In order to obtain the vertical density distribution and hence the scale height of HI at each R, one needs to solve equation (3.1) and the set of two equations given by equation 3.3 jointly, which together constitute a set of three coupled differential equations in the variables ρ_i and ϕ_{total} in two dimensions R, z. Even if all the initial conditions are known, obtaining a rigorous solution of the above equations is going to be extremely complicated and computationally expensive. Thus we look for suitable approximations to simplify the problem.

3.2.2 Approximations

Combining equation (3.1) and (3.3) and assuming isothermal condition for each of the two disk components we get:

$$\langle v_z^2 \rangle_i \frac{\partial}{\partial z}\left[\frac{1}{\rho_i}\frac{\partial \rho_i}{\partial z}\right] = -4\pi G(\sum_{i=1}^{2}\rho_i + \rho_h) + \frac{1}{R}\frac{\partial}{\partial R}\left(R\frac{\partial \phi_{total}}{\partial R}\right) \tag{3.4}$$

Now, we replace the radial derivative term by its approximate value by utilising our knowledge of the shape of the observed rotation curve, which will effectively reduce the above equation to a one dimensional problem along the z direction, as follows:

$$\left(R\frac{\partial \phi_{total}}{\partial R}\right)_{R,z} = ({v_{rot}}^2)_{R,z} \tag{3.5}$$

where $(v_{rot})_{R,z}$ is the intrinsic rotational velocity at any R, z. However, we do not *a priori* know $(v_{rot})_{R,z}$ as a function of z at a given R. However, at each R, the observed rotation curve gives the intensity–weighted average of $(v_{rot})_{R,z}$ along the vertical direction. We approximate the value of $(v_{rot})_{R,z}$ at each z by the commonly used intensity–weighted average velocity, i.e., the rotational velocity given by the observed rotation curve. As a result of this approximation, equation (3.4) reduces to

$$\langle v_z^2 \rangle_i \frac{\partial}{\partial z}\left[\frac{1}{\rho_i}\frac{\partial \rho_i}{\partial z}\right] = -4\pi G(\sum_{i=1}^{2}\rho_i + \rho_h) + \frac{1}{R}\frac{\partial}{\partial R}({v_{rot}}^2(R))_{obs} \tag{3.6}$$

The last term on the r.h.s now becomes a function of R only, and can be easily determined from the gradient of the observed rotation curve. We note that the presence of the last term on the r.h.s dilutes the effect of the net local mass density as far as the downward gravitational pull is concerned. Simple calculations show that in the rising part of the rotation curve the value of the term is of the same order of magnitude, but entering with opposite sign, as that of the net local gravity which results in a more puffed–up gas distribution and hence a larger value for the gas scale height.

We further stress that in solving equation (3.6), we have used the dark matter core density (ρ_h) and the last term involving the gradient of the rotational velocity, both of which have been obtained from the observed rotation curve. While the latter has been determined

directly from the observed curve, ρ_h was estimated after subtracting the disk contribution to the rotational velocity based on the calculated mass model of the disk (see Section 3.4).

3.3 Numerical calculations

The two coupled, second–order, ordinary differential equations given by equation (3.6) are solved numerically using the Fourth order Runge–Kutta Method of integration in an iterative fashion (See Narayan & Jog 2002b, Banerjee & Jog 2007). Since each of the two equations is a second–order differential equation, we need to state the following two initial conditions at the mid–plane (i.e., $z = 0$) for each component for solving the equations:

$$\rho_i = (\rho_0)_i \qquad \frac{d\rho_i}{dz} = 0 \tag{3.7}$$

However, the modified mid–plane density $(\rho_0)_i$ for each component is not known *a priori*. Instead the net surface density $\Sigma_i(R)$, given by twice the area under the curve of $\rho_i(z)$ versus z, known observationally, is used as a secondary boundary condition. The required value of $(\rho_i)_0$ is then determined by trial and error, and eventually the $\rho_i(z)$ distribution is fixed.

3.4 Input Parameters

As mentioned above, we have to provide as inputs the surface density $\Sigma_i(R)$ and the vertical velocity dispersion $(\sigma_z)_i =< (v_z^2)_i >^{1/2}$ of each of the two components (stars and HI) in order to solve equation (3.6) at a given radius R, in addition to the observed rotation curve of the galaxy. Most of the input was taken from the compilation of THINGS (Walter et al. 2008) papers. The stellar surface densities $\Sigma_*(R)$ are taken from Leroy et al. (2008) for all dwarfs except NGC 2366 which is based on Oh et al. (2008). Since a direct measurement of the velocity dispersion of stars (σ_z^*) is not available, it is calculated (as described in Appendix B of Leroy et al. (2008) based on the scale length of the disk R_D and the surface density of the stars $\Sigma_*(R)$. This assumes a stellar disk in vertical hydrostatic equilibrium, neglecting gas gravity and thus slightly underestimates the stellar velocity dispersion. However, the

response of the gas to the net galactic potential is governed by the value of its own velocity dispersion (see equation (3.6)), and so a small change in the vertical density distribution of the stellar component can change the calculated gas scale heights but marginally. The exponential stellar disk scale lengths R_D are again from Leroy et al. (2008). We furthermore need the scale height of the stars (h_*) in order to calculate the volume density, $(\rho_0)_*$. We used $h_* = R_D/7.3$ and an average flattening ratio (Kregel, van der Kruit, & de Grijs 2002).

We derived the HI surface density $\Sigma_{\mathrm{HI}(R)}$ and adopted a constant velocity dispersion (σ_z^{HI}) based on maps from Walter et al. (2008). The resulting HI scale height depends strongly on the assumed value of the vertical velocity dispersion σ_z^{HI}, which lies between 7 – 9 $\mathrm{km\,s^{-1}}$. Our calculations show that a change in the value of the assumed HI velocity dispersion by 1 $\mathrm{km\,s^{-1}}$ (or approximately 10 percent) changes the HI scale height by 14–15 percent. Therefore, the accuracy of the determined HI scale height depends on the accuracy with which σ_z^{HI} can be determined. Tamburro et al. (2009), using the same THINGS data, published a more complete analysis of the velocity dispersions. Most galaxies show a gradual fall in HI velocity dispersion with radius, $\sim$ a few km $\mathrm{s^{-1}}$ per unit of $\mathrm{R_{25}}$. In addition to assuming a constant value, we use a smoothly falling velocity dispersion to model those two galaxies of our sample, Ho II and IC 2574, for which this more complete velocity dispersion information is available (Tamburro et al. 2009).

The dark matter central core densities ρ_0 and core radii R_c are taken from de Blok et al. (2008) except for Ho II where we used values from Bureau & Carignan (2002). These are determined from the observed rotation curves assuming rotational equilibrium, and a dark matter distribution modelled as a pseudo–isothermal halo. The observed rotation curves are taken from de Blok et al. (2008) for DDO 154 and NGC 2366, from Oh et al. (2008) for IC 2574 and from Bureau & Carignan (2002) for Ho II. Key parameters used as input are listed in Table 3.1. We note here that de Blok et al. (2008) estimated the disk contribution to the rotation curve by employing mass models for the stellar and the gaseous disks. This was subtracted from the observed rotation curve to obtain the contribution of the dark matter halo from which its core density and core radius are derived. The mass model of the disk is well constrained and allows for small variations in its parameters only that in turn may

result in small changes in the deduced halo parameters; the effect on the gas scale height will be minimal.

The essence of the radial mass distribution of the galaxy is effectively captured in the rotation curves. Dwarf galaxies in general have a rising rotation curve, i.e., the rotation velocity of these low-luminosity galaxies increases steadily with radius as far as 3–4 R_D (Salucci et al. 2007), unlike spiral galaxies which sport flat rotation curves. We further note that in our previous work, we had modelled the observed gas scale height data to obtain the best–fit halo parameters, as was done for the Galaxy (Narayan et al. 2005), M31 (Banerjee & Jog 2008) and UGC 7321 (Banerjee, Matthews & Jog 2010). Here the inverse approach is used, namely the observed rotation curve data is modelled to obtain the dark matter halo parameters and then the resulting HI vertical scale height distribution is derived. This approach is valid as long as the halo profile can be approximated by a pseudo–isothermal sphere.

3.5 Results and Discussion

We present in the top four panels of Figure 3.1 the resulting HI scale height versus radius for DDO 154, Ho II, IC 2574 and NGC 2366, assuming for each galaxy the constant HI velocity dispersion as given in Table 3.1. For each galaxy, the scale height calculations were done twice: first by neglecting the radial term in the Poisson equation, mimicking the approach used for spiral galaxies (Narayan & Jog 2002b, Banerjee & Jog 2007), and a second time including the radial term. The two results differ from each other by about 10–20 percent, indicating that the exact shape of the rotation curve only enters as a small, systematic correction. As mentioned above, the effect of the radial term is to somewhat counteract net local gravity, resulting in a larger value for the gas scale height.

The individual data points follow, with some dispersion, a smooth increase with growing radius. Most of this dispersion is due to radial variations in the input parameters and associated uncertainties, such as when calculating the derivative of the rotation curve. The combined effect of these uncertainties is of the order of 100 pc.

TABLE 3.1: Input parameters of the different galaxies.

Galaxy	$\Sigma_*(0)$	R_D	R_{25}	$\sigma_z^{\rm HI}$	ρ_0	R_c
	$M_\odot\,pc^{-2}$	kpc	kpc	$km\,s^{-1}$	$M_\odot\,pc^{-3}$	kpc
DDO 154	5.7	0.8	1.22	8	0.028	1.34
Ho II	27.8	1.2	3.26	i) 7	0.009	10.0
				ii)14. - 0.91R if R $<$ 3.3		
				9.9 - 0.76(R - 3.3) otherwise		
IC 2574	24.6	2.1	7.53	i) 7	0.004	7.23
				ii)10.8 if R $<$ 6.4		
				10.8 - 0.95(R - 6.44) otherwise		
NGC 2366	10.5	0.5	2.18	9	0.035	1.36

A parameter which has a more substantial influence on the result is the velocity dispersion, and its dependence on radius. The two bottom panels of Figure 3.1 show for two of the galaxies, Ho II and IC 2574, the effect of using a gradually declining velocity dispersion rather than a constant value. The rapid increase in HI scale height for IC 2574 becomes less pronounced as a result of the higher velocity dispersion near the centre, increasing the gas scale height there by about a factor of two, and a lower velocity dispersion near the last measured point, resulting in a relative increase across the gas disk of about a factor of two, rather than a factor of three earlier. The effect is even more pronounced for Ho II where we find an almost constant, but thick HI disk throughout. This exercise illustrates the extent to which the resulting scale heights depend on accurate determinations of the velocity dispersion.

In the remainder of this paper, we will use for all galaxies the theoretical solution to the gas scale height while taking the radial term in the Poisson equation into account. In the case of Ho II and IC 2574 we take the solution for the gradually decreasing velocity dispersion of the gas. Figure 3.2 then shows a pair of plots comparing the HI scale height distribution as a function of normalised radius.

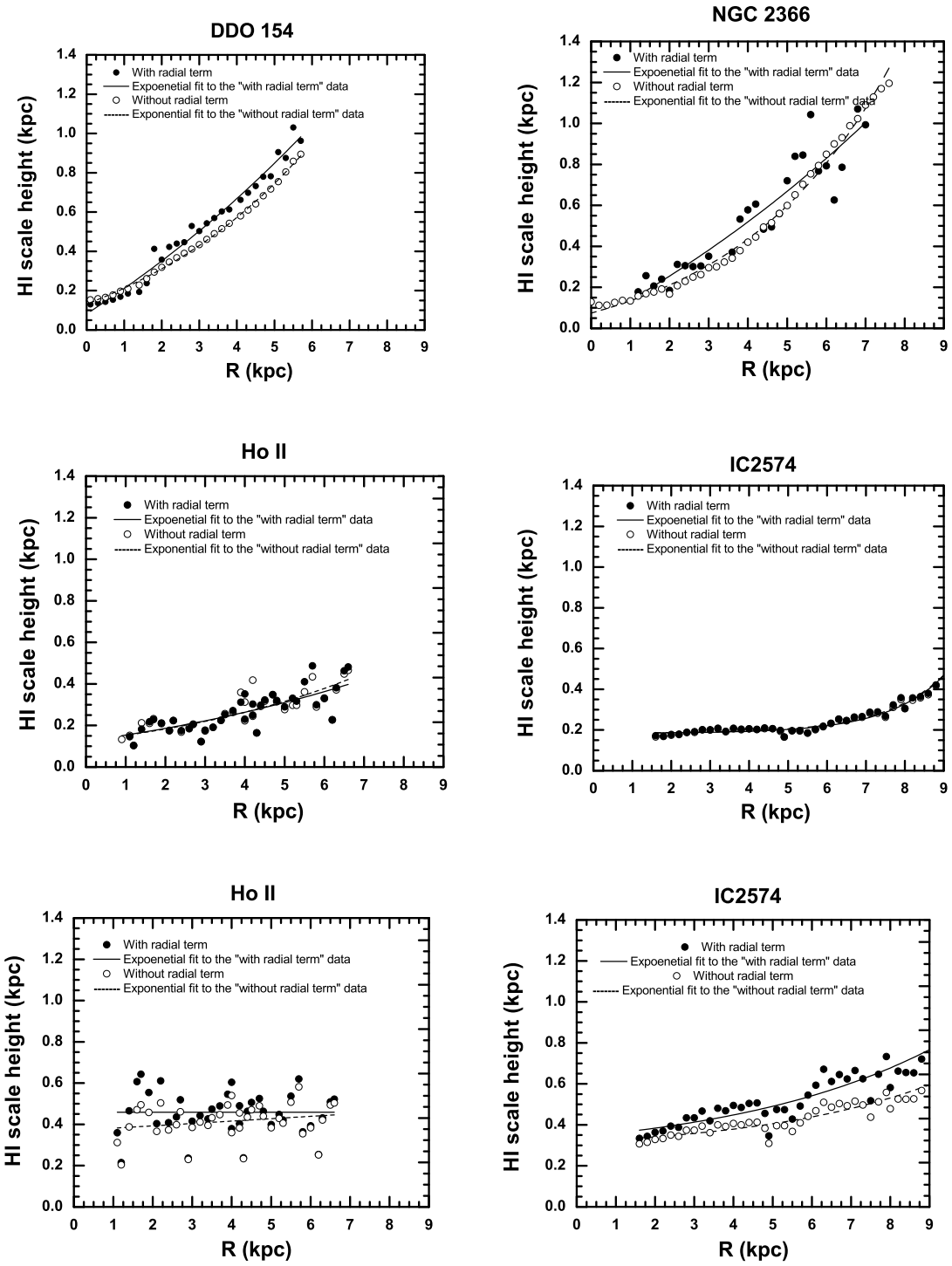

FIGURE 3.1: HI scale height (HWHM) versus R for the four galaxies analysed here, with and without taking into account the effect of the radial term in the Poisson equation (see legend in each of the panels). The drawn lines are exponential fits to the calculated scale heights. The top four panels show our calculations, assuming for each galaxy a constant velocity dispersion as a function of radius. As explained in the text, the inclusion of the radial term in the Poisson equation which takes care of the rising rotation curve, results in a slightly larger scale height in general. The two bottom panels show the inferred HI scale height for Ho II and IC 2574 when using a gradually decreasing velocity dispersion instead (see text for details).

TABLE 3.2: R_{max} (denoting the outermost extent of the HI disk) and R_{sd} (the radius where the disk surface density falls to 4 $M_\odot\,pc^{-2}$) for the different galaxies

Galaxy	R_{max}*	R_{sd}
	kpc	kpc
DDO 154	6.8	3.3
Ho II	6.8	6.2
IC 2574	9.3	9.3
NGC 2366	6.8	5.0

*The R_{max} values have been taken from Bagetakos et al. (2011).

We use two normalisations, the first one by maximum radial extent of the HI disk, $R_{\rm max}$ (taken from Bagetakos et al. 2011). We also normalise by $R_{\rm sd}$, which corresponds to the radius where the mass surface density drops below $4\,M_\odot\,pc^{-2}$. The $R_{\rm max}$ and the $R_{\rm sd}$ values for the different galaxies have been listed in Table 3.2.

We note that, with the exception of Ho II which has a thick gas disk throughout, the dwarfs all show HI flaring. The rate of flaring is highest in NGC 2366 and DDO 154 which can be ascribed to these two galaxies having a more centrally concentrated dark matter halo than the other two systems.

Figure 3.3 presents a collection of plots of the logarithm of the scale height versus radius, showing a near exponential behaviour, i.e. a linear slope, in each case. The curves for DDO 154 and IC 2574 display a break, necessitating two different slopes across two radial regimes, i.e., the gas scale height increases exponentially with radius with different scale lengths across the two regimes. It is interesting to compare this figure with Figure 3.4 which shows the disk surface density of gas and stars combined versus radius. Knees in the graphs of DDO 154 and IC 2574 occur at the same radius as the breaks in the exponential curves in Fig 3.3, confirming that the gas scale height depends strongly on the radial disk surface density distribution.

This should make us pause for a moment as in the adopted radial surface density distribution distribution we have ignored any contribution by molecular gas. In the introduction

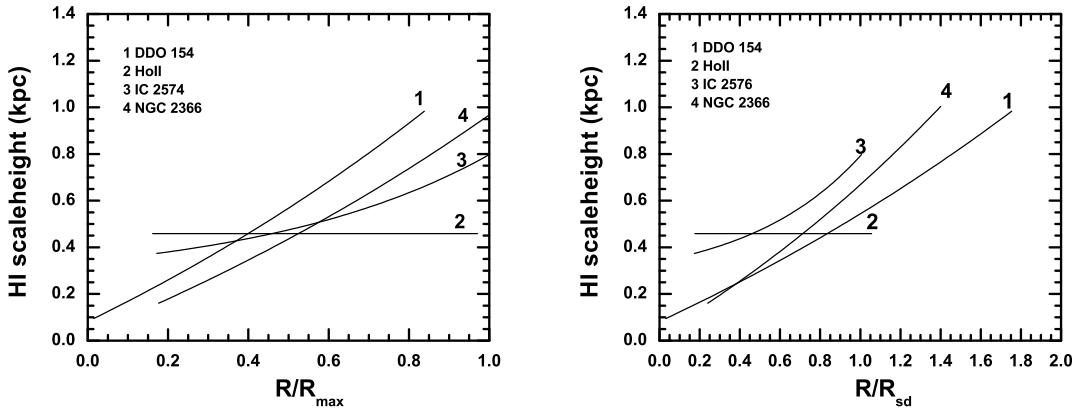

FIGURE 3.2: Plots showing the HI scale height (HWHM) versus normalised radius ($R/R_{\rm max}$ left–hand panel; $R/R_{\rm sd}$ right–hand panel) for the galaxies, taking into account the effect of the radial term in the Poisson equation and for Ho II and IC 2574 using the radially decreasing velocity dispersion for the gas. Normalisation by $R_{\rm max}$ is with respect to the outermost extent of the HI disk (from Bagetakos et al. 2011), whereas normalisation by $R_{\rm sd}$ is the radius where the mass surface density of gas plus stars reaches 4 $\rm M_{\odot}\,pc^{-2}$. For clarity, rather than the individual radial values, the exponential fits to the analytical solution are shown.

we mentioned that dIrr galaxies are deficient in CO which is used as a proxy to trace molecular gas. In fact, in galaxies with metallicities below $[12 + \log {\rm O/H}] < 7.5$ no CO emission has been detected (Taylor et al. 1998). We also mentioned in the introduction that a lack of CO does not necessarily imply a lack of molecular gas. If present, this molecular gas likely follows the stellar light distribution (Young et al. 1995, Bigiel et al. 2008, Leroy et al. 2009). Its effects on the flaring HI beyond the stellar disks of the dwarfs will therefore be negligible. In the inner parts the molecular gas, if present, will contribute to the mass density, effectively reducing the scale height locally.

Despite some modest potential adjustment at small radii due to a likely contribution of molecular gas to the mass density, and the inherent uncertainty in the measured parameters used as input to our analytical model, the main conclusion from this work is our confirmation of the flaring of HI in dwarf galaxies. We also confirm the prediction by Brinks et al. (2002) that the scale height in dwarfs is larger in absolute measure than in spiral galaxies. In dIrrs, we find scale heights from 200–400 pc in the inner regions to 600-1000 pc out to the last measured point.

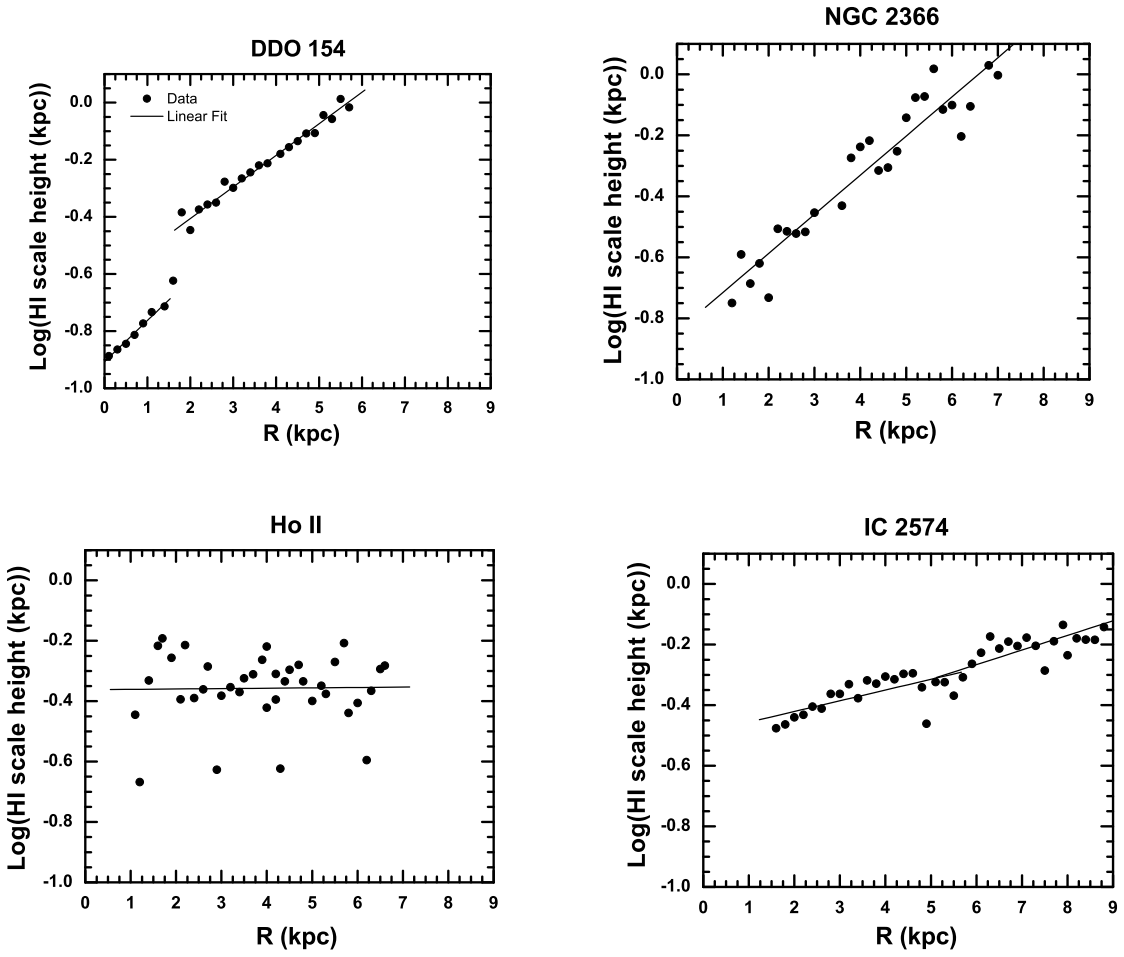

FIGURE 3.3: Plots of logarithm of the HI scale height versus radius, showing the scale height increases exponentially with radius for all the galaxies, but in some objects with a different scale length over different radial ranges (DDO 154, and to a lesser extent IC 2574).

Measuring the HI scale height in dwarf galaxies directly is fraught with difficulties, even in the relatively ideal case of an edge–on dIrr. The projected HI distribution on the sky is a combination of a flaring gas layer seen edge–on and a possible warp. It becomes a non–trivial task to extract the intrinsic gas density and scale height distribution (Olling 1995, 1996; Warmels 1988; Roychowdhury et al. 2010). In the case of more face–on dwarfs, a break in the spectral correlation function can be used to infer the scale height of the gas (Elmegreen, Kim & Staveley-Smith 2001,Padoan et al. 2001) but although this has been shown to work in principle in the LMC, this method requires high spatial resolution, high

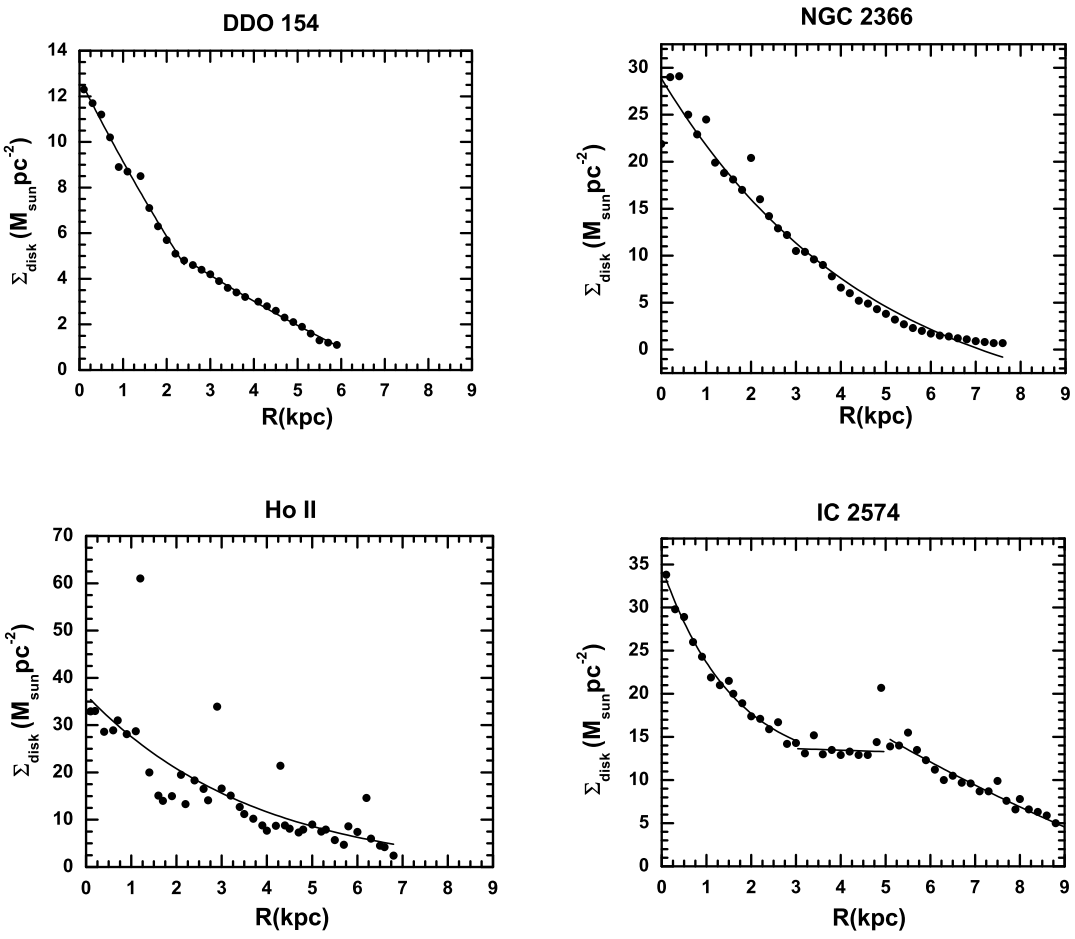

FIGURE 3.4: Plots of the disk surface density (stars plus gas) versus radius for all galaxies. Comparison with Figure 3.3 confirms that for each galaxy, disk surface density plays a major role in regulating the gas scale height distribution.

sensitivity data which is beyond what can routinely be obtained with current instruments.

As an independent check on our results, we compared the derived radial distribution of the HI scale height with the size distribution of type 3 HI holes, i.e., roughly spherical cavities in the HI layer created by the combined effects of stellar winds and supernovae in young stellar associations (See for details Bagetakos et al. 2011). These structures are expanding and eventually their radius can exceed the thickness of the layer they find themselves in, at which moment they would be classified as a type 2 or type 1 hole, a type 1 hole corresponding to a complete blow–out. The maximum size of the type 3 holes encountered is therefore a

lower limit on the local thickness of the gas layer. A comparison of the size distribution of HI holes in the four sample galaxies reveals that of the 20 type 3 holes all of them have radii that are in agreement with them being still fully contained within the gas layer. We note that if we were to adopt for Ho II and IC 2574 the models with constant velocity dispersion, 2 out of 8 holes would exceed the thickness of the gas layer in Ho II and 1 out of 5 in IC 2574, lending confidence to our approach and choice of input parameters.

In addition to the uncertainties in the input parameters and how they propagate, we made a couple of assumptions that should be mentioned here. In our approach, the stellar scale height is assumed to be constant in order to obtain the vertical dispersion (Sect. 3.4); the latter is used as input parameter in our model. Conversely, if the observed values for the stellar dispersion were known, we could obtain the resulting stellar scale height distribution *ab initio*. For spiral galaxies, the stellar scale height is shown to flare by a factor of 2–3 within the optical radius (Narayan & Jog 2002a) as was also shown observationally by de Grijs et al. (1997).

Also, the error incurred in replacing $(v_{rot})_{R,z}$ at each z by $(v_{rot})_{obs}$, which is higher in general, as per the approximations made in Sect. 3.2.2, results in a slight overestimation of the scale height. However, the error can not be more than a few percent as the effect of including the radial term itself is found to be less than ten percent and observations have shown that $(v_{rot})_{obs}$ R,z varies by ten percent or so along z (Kamphuis 1993).

In our analysis we assumed a pseudo–isothermal halo. In principle, if the HI scale height can be determined reliably in an independent manner, our method could be expanded to include as free parameter the flattening of the dark matter halo.

Finally, in Figure 3.5 we show a composite plot for the radial distribution of the mid–plane gas volume density for the four galaxies based on the exponential fits to the relations in Fig. 3.1. For reference, a volume density of $0.01\,\mathrm{M}_\odot\,\mathrm{pc}^{-3}$ corresponds to $0.4\,\mathrm{H–atom\,cm}^{-3}$. The flaring of gas results in a lower mid–plane density. It would be interesting to investigate if this decrease in volume density explains the low star formation efficiency, a topic that will be dealt with as part of the LITTLE THINGS project (See for a description of LITTLE THINGS, Hunter et al. 2011).

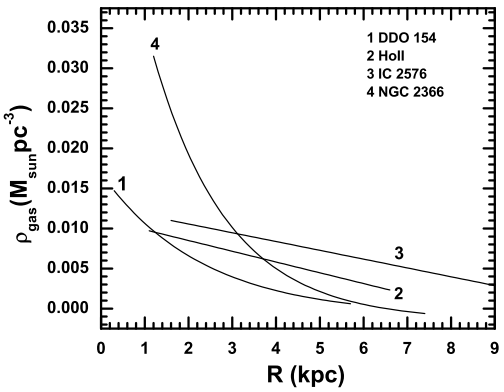

FIGURE 3.5: A composite plot depicting the radial distribution of the mid–plane gas volume density for all galaxies.

3.6 Conclusions

In this paper we derive the HI scale height as a function of radius for a group of four dwarf galaxies. We use a two–component model of gravitationally–coupled stars and gas in the force field of a dark matter halo to obtain the HI scale height. We extended our earlier analysis by explicitly addressing the issue of the rising rotation curve of dwarf galaxies. Our approach gives more realistic results than earlier models in which the self–gravity of the gas was ignored. This is especially relevant for dwarf galaxies where stars and gas dominate the disk gravity, roughly at par with each other. We find that Ho II has a thick HI disk throughout; the other three dwarf galaxies studied in this paper show flaring HI as a function of radius. Moreover, the overall HI scale height of dwarfs is larger than in spiral galaxies. This is due to a combination of a lower mass density in dwarf disks as a function of radius for the same velocity dispersion as encountered in larger spiral galaxies. The flaring of HI in the outer galaxy (beyond $R = 3 - 4R_D$) is mainly controlled by the dark matter halo contribution to the net potential of the galaxy. The derived gas scale height is in agreement with the size distribution of type 3 HI holes, i.e., roughly spherical, expanding cavities resulting from the energy deposited by rapidly evolving young stars. This type of holes is still contained within the gas layer and hence represents a lower limit to the gas scale height.

References

Ashman K. M., 1992, PASP, 104, 1109

Bagetakos, I., Brinks, E., Walter, F., de Blok, W. J. G., Usero, A., Leroy, A. K., Rich, J. W., Kennicutt, R. C., Jr. 2011, AJ, 141, 23

Banerjee, A., & Jog, C. J. 2007, ApJ, 662, 335

Banerjee, A., & Jog, C. J. 2008, ApJ, 685, 254

Banerjee, A., Matthews, L. D., & Jog, C. J. 2010, New A, 15, 89

Bigiel F., Leroy A., Walter F., Brinks E., de Blok W. J. G., Madore B., Thornley M. D., 2008, AJ, 136, 2846

Bolatto A. D., Leroy A. K., Rosolowsky E., Walter F., Blitz L., 2008, ApJ, 686, 948

Braun, R. 1991, ApJ, 372, 54

Brinks E., Burton W. B., 1984, A&A, 141, 195

Brinks E., Walter F., Ott J., 2002, in "Disks of Galaxies: Kinematics, Dynamics & Perturbations", ASP Conf Ser Vol.275, Astron. Soc. Pac., San Francisco, pg.57

Bureau, M., & Carignan, C. 2002, AJ, 123, 1316

Carignan C., Freeman K. C., 1988, ApJ, 332, L33

de Blok, W. J. G., Walter, F., Brinks, E., Trachternach, C., Oh, S.–H., & Kennicutt, R. C. 2008, AJ, 136, 2648

de Grijs, R., Peletier, R. F., & van der Kruit, P. C. 1997, A&A, 327, 966

de Zeeuw, T., & Pfenniger, D. 1988, MNRAS, 235, 949

Elmegreen B. G., Kim S., Staveley-Smith L., 2001, ApJ, 548, 749

Fraternali F., Binney J. J., 2008, MNRAS, 386, 935

Henderson A. P., Jackson P. D., Kerr F. J., 1982, ApJ, 263, 116

Hunter, D. A., Brinks, E. & the LITTLE THINGS team. 2011, Ap&SS (in press)

Kalberla P. M. W., Kerp J., 2009, ARA&A, 47, 27

Kamphuis, J.J, PhD Thesis, University of Groningen

Kregel, M., van der Kruit, P. C., & de Grijs, R. 2002, MNRAS, 334, 646

Leroy, A. K., Walter, F., Brinks, E., Bigiel, F., de Blok, W. J. G., Madore, B., & Thornley, M. D. 2008, AJ, 136, 2782

Leroy A. K., et al., 2009, ApJ, 702, 352

Levine, E. S., Blitz, L., & Heiles, C. 2006, ApJ, 643, 881

Marasco A., Fraternali F., 2011, A&A, 525, A134

Mateo M. L., 1998, ARA&A, 36, 435

Narayan, C. A., & Jog, C. J. 2002a, A&A, 390, L35

Narayan, C. A., & Jog, C. J. 2002b, A&A, 394, 89

Narayan, C. A., Saha, K., & Jog, C. J. 2005, A&A, 440, 523

Oh, S.–H., de Blok, W. J. G., Walter, F., Brinks, E., Kennicutt, R. C. 2008, AJ, 136, 2761

Oh, S.–H., de Blok, W. J. G., Brinks, E., Walter, F., Kennicutt, R. C., Jr. 2010, astro–ph/1011.0899

Olling R. P., 1995, AJ, 110, 591

Olling R. P., 1996, AJ, 112, 481

Padoan P., Kim S., Goodman A., Staveley-Smith L., 2001, ApJ, 555, L33

Rohlfs, K. 1977, Lectures on Density Wave theory (Berlin:Springer–Verlag)

Roychowdhury, S., Chengalur, J.N., Begum, A., Karachentsev, I. D. 2010, MNRAS, 404, L60

Salucci, P., Lapi, A., Tonini, C., Gentile, G., Yegorova, I., Klein, U. 2007, MNRAS, 378, 41

Sancisi, R., & Allen, R.J. 1979, A&A, 74, 73

Sicking, F. J. 1997, PhD Thesis, Groningen

Tacconi L. J., Young J. S., 1987, ApJ, 322, 681

Tamburro, D., Rix, H.–W., Leroy, A. K., Mac Low, M.–M., Walter, F., Kennicutt, R. C., Brinks, E., de Blok, W. J. G. 2009, AJ, 137, 4424

Taylor C. L., Kobulnicky H. A., Skillman E. D., 1998, AJ, 116, 2746

van der Kruit P. C., 1988, A&A, 192, 117

Walter, F., Brinks, E., de Blok, W. J. G., Bigiel, F.,Kennicutt, R. C., Thornley, M. D., & Leroy, A. 2008, AJ, 136, 2563

Warmels R. H., 1988, A&AS, 72, 427

Wilson C. D., 1995, ApJ, 448, L97

Wouterloot, J. G. A., Brand, J., Burton, W. B., & Kwee, K. K. 1990, A&A, 230, 21

Young J. S., et al., 1995, ApJS, 98, 219

4

The flattened dark matter halo of M31 as deduced from the observed HI scale heights [3]

Abstract

In this paper, we use the outer-galactic HI scale height data as well as the observed rotation curve as constraints to determine the halo density distribution of the Andromeda galaxy (M31). We model the galaxy as a gravitationally-coupled system of stars and gas, responding to the external force-field of a known Hernquist bulge and the dark matter halo, the density profile of the latter being characterized by four free parameters. The parameter space of the halo is optimized so as to match the observed HI thickness distribution as well as the rotation curve on an equal footing, unlike the previous studies of M31 which were

[3] Banerjee & Jog 2008, ApJ, 685, 254

based on rotation curves alone. We show that an oblate halo, with an isothermal density profile, provides the best fit to the observed data. This gives a central density of 0.011 $M_\odot$ pc^{-3}, a core radius of 21 kpc, and an axis ratio of 0.4. The main result from this work is the flattened dark matter halo for M31, which is required to match the outer galactic HI scale height data. Interestingly, such flattened halos lie at the most oblate end of the distribution of halo shapes found in recent cosmological simulations.

4.1 Introduction

It is well-known that the dark matter halo plays an important role in the dynamics of galaxies, especially in the outer regions (Binney & Tremaine 1987). Since a galactic disk is rotationally supported, the rotation curve serves as a useful tracer of the gravitational potential in the plane of the galaxy. The observed rotation curve is routinely used to deduce the mass distribution in a galaxy and hence its dark matter content (e.g., Begeman 1987, Kent 1986, 1987, Geehan et al. 2006). The thickness of the gas layer, on the other hand, depends on the vertical gravitational force and traces the potential perpendicular to the mid-plane (e.g., Narayan & Jog 2002 a). In this work, we use the rotation curve as well as the radial distribution of the thickness of the HI gas layer in the outer galaxy to study the shape and density profile of the dark matter halo in M31. In a disk plus bulge plus halo model of an external galaxy, the disk and the bulge can be mostly studied observationally. Therefore, the rotation curve and the vertical HI scale height data effectively complement each other to determine the dark matter halo distribution of a galaxy uniquely.

In the past, the idea of studying the dark matter halo properties by using the outer galactic HI flaring data has been used to explore the halos of NGC 4244 (Olling 1996), NGC 891 (Becquaert & Combes 1997), and the Galaxy (Olling & Merrifield 2000, 2001). However, the HI scale height distribution was mainly used to constrain the oblateness of the halo, and not its other parameters such as the power-law index. In some cases, the gas gravity and even the stellar gravity was ignored (Becquaert & Combes 1997) in determining the net galactic potential, and hence the gas scale height distribution.

These issues were taken care of in determining the Galactic halo parameters by Narayan et al (2005). Using the gravitationally-coupled, 3-component Galactic disk model (Narayan & Jog 2002 b), various density profiles of the halo were investigated, and an attempt was made to obtain the halo parameters, which provided the best fit (in the least square sense) to the observed HI scale height distribution. Finally, conformity with the shape of the observed rotation curve was used to remove the degeneracies in the best-fit values obtained by the first constraint. Also, unlike some of the previous models, the self-gravity of the gas was included in the analysis. From their study Narayan et al. (2005) concluded that a spherical halo, with a density falling off more rapidly than an isothermal halo, provides the best fit to the available data. This study was based on the HI scale height data then available up to 24 kpc from Wouterloot et al. (1990). Kalberla et al. (2007) have confirmed this by using their recent extended HI scale height data up to 40 kpc, and have also included a dark matter ring which they claim is needed to explain the observed HI scale height distribution in the Galaxy.

In this paper, we apply the above approach to investigate the dark matter halo properties of the Andromeda galaxy (M31 or NGC 224). Here we use both the rotation curve and the HI scale height data as rigorous constraints simultaneously and scan the entire parameter space systematically so as to obtain the best-fit halo parameters. In addition to the various density profiles, we also try to fit various shapes of the halo which was not done by Narayan et al. (2005). Earlier studies on M31 (Widrow et al. 2003, Widrow & Dubinski 2005, Geehan et al. 2006, Seigar et al. 2006, Tamm et al. 2007) were mostly aimed at developing a complete mass model (disk plus bulge plus halo), based on comparisons made with the available structural and kinematical data (surface brightness profiles, bulge-velocity dispersion relations, rotation curves), which assumed a spherical-shaped halo. On the other hand, we have studied the dark matter halo profile, and show it to be flattened.

In Section 4.2, we describe our model, and in Section 4.3 discuss the numerical calculations involved, and the input parameters used. In Section 4.4, we present the results and analysis of the numerical results; followed by the discussion, and conclusions in Sections 4.5 and 4.6 respectively.

4.2 Details of the model

4.2.1 Gravitationally coupled, 3-component, galactic disk model

A galaxy is modelled as a thick stellar disk, coplanar with the interstellar medium of atomic and molecular hydrogen gas, all the three components being gravitationally coupled to each other, and embedded in the dark matter halo (Narayan & Jog 2002 b). The bulge and the dark matter halo are taken to be rigid and non-responsive, and act as external forces on the 3-component disk system. Also, it is assumed that the components are in hydrostatic equilibrium in the vertical direction. Therefore, the density distribution of each component will be jointly determined by the Poisson equation, and the corresponding equation for pressure equilibrium perpendicular to the mid-plane.

The Poisson equation for an axisymmetric galactic system in terms of the galactic cylindrical co-ordinates (R, ϕ, z) is given by

$$\frac{\partial^2 \Phi_{total}}{\partial z^2} + \frac{1}{R}\frac{\partial}{\partial R}\left(R\frac{\partial \Phi_{total}}{\partial R}\right) = 4\pi G(\sum_{i=1}^{3}\rho_i + \rho_b + \rho_h) \tag{4.1}$$

where ρ_i with i = 1 to 3 denotes the mass density for each disk component. ρ_h and ρ_b denote the same for the halo and the bulge respectively. Φ_{total} denotes the net potential due to the disk, halo and the bulge. For a flat or gently-falling rotation curve, the radial term can be neglected as its contribution to the determination of the HI scale height is less than 10 percent as noted by earlier calculations (Narayan et al. 2005). So, the above equation reduces to

$$\frac{\partial^2 \Phi_{total}}{\partial z^2} = 4\pi G(\sum_{i=1}^{3}\rho_i + \rho_b + \rho_h) \tag{4.2}$$

The equation for hydrostatic equilibrium in the z direction is given by (Rohlfs 1977)

$$\frac{\partial}{\partial z}(\rho_i\langle(v_z^2)_i\rangle) + \rho_i\frac{\partial \Phi_{total}}{\partial z} = 0 \tag{4.3}$$

where $\langle(v_z^2)_i\rangle$ is the mean square random velocity along the z direction for the component

i. We further assume each component to be isothermal for simplicity, so that the velocity term is constant with z.

Eliminating Φ_{total} between eq. (4.2) and eq. (4.3), and assuming an isothermal case, we get

$$\langle (v_z^2)_i \rangle \frac{\partial}{\partial z} \left[\frac{1}{\rho_i} \frac{\partial \rho_i}{\partial z} \right] = -4\pi G (\sum_{i=1}^{3} \rho_i + \rho_b + \rho_h) \tag{4.4}$$

which represents a set of three coupled, second-order differential equations, one for each component of the disk. From the above equation, it is evident that though there is a common gravitational potential, the response of each component will be different due to the difference in their random velocity dispersions.

4.2.2 Bulge

We model the bulge of M31 as a spherically symmetric mass distribution represented by a Hernquist profile (Hernquist 1990), where M_b is the total mass of the bulge, and r_b is its core radius. The mass profile and density corresponding to this distribution are given by

$$M_{bulge}(R) = \frac{M_b R^2}{(r_b + R)^2} \tag{4.5}$$

and

$$\rho_{bulge}(R) = \left(\frac{M_b}{2\pi r_b^3} \right) \frac{1}{(R/r_b)(1 + R/r_b)^3} \tag{4.6}$$

respectively. Since M31 is an Sb type galaxy, the bulge contribution is important, and plays a role in determining the rotation curve even in regions outside the bulge.

4.2.3 Dark Matter Halo

We use the four-parameter dark matter halo model (de Zeeuw & Pfenniger 1988; Becquaert & Combes 1997) with the density profile given by

$$\rho(R,z) = \frac{\rho_0}{\left[1+\frac{m^2}{{R_c}^2}\right]^p} \tag{4.7}$$

where $m^2{=}R^2 + (z^2/q^2)$, ρ_0 is the central core density of the halo, R_c is the core radius, p is the density index, and q is the vertical-to-planar axis ratio of the halo (spherical: $q = 1$; oblate: $q < 1$; prolate: $q > 1$).

4.3 Numerical Calculations

4.3.1 Solution of equations

For a given bulge and halo density profile, the equation to be solved to obtain the vertical density distribution at any radius for any component (stars, HI & H_2) is given by eq.(4.4), which simplifies to:

$$\frac{d^2\rho_i}{dz^2} = \frac{\rho_i}{\langle({v_z}^2)_i\rangle} \times [-4\pi G(\rho_s + \rho_{HI} + \rho_{H_2} + \rho_b + \rho_h)] + \frac{1}{\rho_i}\left(\frac{d\rho_i}{dz}\right)^2 \tag{4.8}$$

This represents three coupled, second-order, ordinary differential equations in ρ_s, ρ_{HI} and ρ_{H_2} which denote the mass densities for stars, HI and H_2 respectively. This problem is solved in an iterative fashion, as an initial value problem, using fourth order, Runge-Kutta method of integration, with the following two initial conditions at the mid-plane i.e z = 0 for each component:

$$\rho_i = (\rho_0)_i, \qquad \frac{d\rho_i}{dz} = 0 \tag{4.9}$$

However, the modified mid-plane density $(\rho_0)_i$ for each component is not known a priori. Instead the net surface density $\Sigma_i(R)$, given by twice the area under curve of $\rho_i(z)$ versus z, is used as the second boundary condition, since this is known observationally. Hence the required value of $(\rho_i)_0$ can be determined by trial and error method, which eventually fixes the $\rho_i(z)$ distribution. We find that four iterations are adequate to give convergence with an

accuracy to the second decimal point. For a three-component disk, the vertical distribution is steeper than a sech^2 close to the mid-plane (Banerjee & Jog 2007) but at large z values it is close to a sech^2 distribution. Here we use the HWHM (half width at half maximum) of the resulting model vertical distribution to define the scale height as was done in Narayan & Jog (2002 a, b).

4.3.2 Input Parameters for M31

The model described so far is general, now we apply it to M31. For that, we require the surface density and the vertical velocity dispersion for each component to solve the coupled set of equations at each radius. The observed values are used for the gas, whereas for the bulge and the stellar component the values derived from the mass-model are used except for the vertical dispersion velocity of the stars.

The radial distribution of the HI surface density is taken from Sofue & Kato (1981), while the surface density for the H_2 gas, being an order of magnitude smaller and confined to the inner region (Koper 1993), was taken to be zero. The vertical dispersion velocity of the HI gas, $(v_z)_{\rm HI}$, is taken to be 8 km s^{-1}, as given by the observations of a large sample of about 200 external galaxies (Lewis 1984).

For the stars, we assume an exponential disk with a central surface density of 460 M$_\odot$ pc^{-2}, and an exponential disk scale length, R$_d$ of 5.4 kpc after Geehan et al. (2006). The disk scale length matches with the R-band scale length of Widrow et al. (2003), whereas Koper (1993) gives a value of 5.1 kpc. Also, the maximum disk mass of 8×10^{10} M$_\odot$ predicted by the Widrow et al. (2003) model sets the central disk surface density value to 440 M$_\odot$ pc^{-2} for $R_d = 5.4$ kpc. So the difference between the values used in our work with other values in the literature is of the order of a few percent.

The bulge is taken to have a Hernquist profile as described earlier, with a total mass M_b of 3.3×10^{10} M$_\odot$ and core radius r_b of 0.61 kpc, as given by the same model (Geehan et al. 2006). Kerins et al. (2001) give a mass M_b of 4×10^{10} M$_\odot$, whereas Widrow et al. (2003) give a mass of 2.5×10^{10} M$_\odot$. As expected, the bulge becomes progressively less important as we move radially outward in the galaxy, and so is not important in the determination of

the rotation curve or the HI scale height in the outer parts, which is our region of interest. However, it does affect the determination of the rotation curve in the intermediate range, hence the bulge has to be included for a correct treatment of the problem.

The stellar radial velocity dispersion is assumed to fall off exponentially with a scale length of 2 $\times$ R_d as is observed in the Galaxy (Lewis & Freeman 1989), for M31 this gives a value of 10.8 kpc. Also, the ratio of the vertical to the radial stellar velocity dispersion is taken to be 0.5 at all radii, equal to its observed value in the solar neighbourhood (Binney & Merrifield 1998). Based on these, the central value of 126 km s^{-1} for the radial dispersion is deduced from the observed value at 2 R_d for M31 by Tamm et al. (2007).

4.4 Results & analysis

4.4.1 Halo density profiles: The 3-D Grid

We scan the allowed values for the entire parameter space for the dark matter halo, to obtain the best fits to the data for the rotation curve and the HI scale heights in the outer parts of M31.

We vary the halo density index p between 1, 1.5 and 2. Here p = 1 corresponds to the isothermal and $p = 1.5$ to the NFW (Navarro et al. 1996) halo density profile at large radii. These two profiles are routinely used in galactic mass modelling and other studies. Narayan et al.(2005) found that a steeper-than NFW profile ($p = 2$) best conforms with the HI scale height data in the outer regions of our Galaxy, suggesting the evidence of finite-sized halos. So, we study each of the above three cases individually. For each value of p, a realistic range of ρ_0 and R_c for the spherical case is chosen to form a grid of $\{\rho_0, R_c\}$ pairs. ρ_0 is varied between 0.001 - 0.15 $M_\odot$ pc^{-3} in steps of 0.002 $M_\odot$ pc^{-3}, and R_c is varied between 1 - 35 kpc in steps of 0.5 kpc. At first, we use a spherical halo for simplicity. Although it gives the correct rotation curve, it fails to match the outer galactic HI scale height data within the error bars. Figure 4.1 shows that the outer galactic HI scale height distribution obtained by using the best-fit values for a spherical isothermal halo (p=1) flares far above the observed data, giving a poor fit. The same is found to be true for the other density profiles ($p = 1.5$

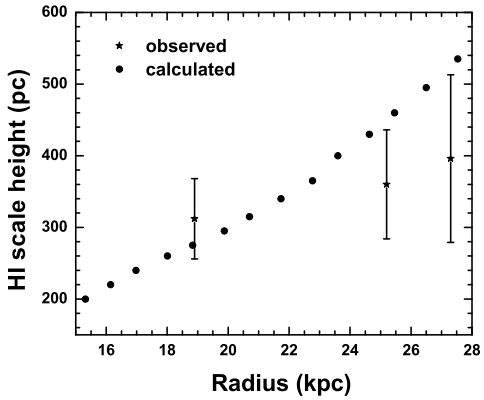

FIGURE 4.1: Plot of the HI scale height (in pc) with the galactocentric radius (in kpc) for the best-fit case for the spherical shape ($q = 1$) halo for the density law p=1 (isothermal). Clearly, the model curve rises way above the observed distribution in the outer galaxy which is the region of interest. Thus a spherical halo is ruled out.

and 2) as well.

This naturally called for the use of an oblate (flattened) halo. This is because the mid-plane surface density increases with the flattening of the halo, thus resulting in a higher vertical constraining force. The effect, as expected, is exactly the opposite in case of a prolate halo. The latter would therefore give an even poorer fit than the spherical case, and hence is not tried here. Therefore, in addition to the above parameters, the axis ratio q is varied as well between 0.1 and 0.9 in steps of 0.1. This gives a total of 47250 grid points to be scanned for each value of p. We first thoroughly scan this grid to locate the region of minimum χ^2.

In retrospect, Narayan et al. (2005) had pinned the rotation curve at a single point only (i.e the solar point with R = 8.5 kpc) using the local Oort constants A and B, for which the values are available for the Galaxy. This effectively fixed the rotation curve locally, with respect to shape as well. Also, the global trends exhibited by the observed curve was used as the final criterion to choose the best fit density index ($p = 2$). Here, on the other hand, we apply a more rigorous treatment by pinning the rotation curve at all the observed points. This, in fact, was imperative since the Oort A and B constants for M31 are not known.

4.4.2 The rotation curve constraint

For each of the above grid points, we evaluate the galactic rotation curve using our (disk plus bulge plus halo) model as follows. For an exponential disk, the rotation velocity $v_{disk}(R)$ is given by (Binney & Tremaine 1987)

$$v^2_{disk}(R) = 4\pi G\Sigma_0 R_d y^2[I_0(y)K_0(y) - I_1(y)K_1(y)] \tag{4.10}$$

where Σ_0 is the disk central surface density, R_d the disk scale length and y = R/2R$_d$, R being the galactocentric radius. I_n and K_n (where n=0 and 1) are the modified Bessel functions of the first and second kind respectively. The above relation is for an infinitesimally thin disk which we use here for simplicity. For a thick disk, a separate result has to be used (as given in Becquaert & Combes 1997) , which we check gives a value within $< 1\%$ of the value given by eq.(4.10), hence we are justified in using the above simpler form.

For the spherical bulge, rotation velocity $v_{bulge}(R)$ is given by

$$v^2_{bulge}(R) = \frac{GM_{bulge}(R)}{R} \tag{4.11}$$

where M$_{bulge}(R)$, the mass enclosed within a sphere of radius R for a Hernquist bulge, is given by the r.h.s. of equation (4.5).

For an oblate halo of axis ratio q and density index p, the circular speed v_{halo} is obtained by differentiating the expression for the potential from Sackett & Sparke (1990), and Becquaert & Combes (1997) to be:

$$v^2_{halo}(R) = 4\pi G\rho_0 q \int_0^{1/q} \frac{R^2x^2[1 + \frac{R^2x^2}{R_c^2(1+\epsilon^2x^2)}]^{-p}}{(1+\epsilon^2x^2)^2} dx \tag{4.12}$$

where $\epsilon = (1 - q^2)^{1/2}$. We obtain the value of the integral numerically in each case. So, the total rotation velocity $v(R)$ at any galactic radius R is given by adding the contributions for the three components in quadrature as:

$$v^2(R) = v^2_{disk}(R) + v^2_{bulge}(R) + v^2_{halo}(R) \tag{4.13}$$

Next we performed the χ^2 analysis of the calculated distributions with respect to the observed one for each of the $p = 1$, 1.5 and 2 cases. The galactic rotation curve for M31 is given by Widrow et al. (2003), and Carignan et al. (2006). We choose the rotation curve from Widrow et al. (2003) for our analysis following Geehan et al (2006) for reasons of internal consistency as we have used the bulge and the stellar parameters from their mass model. We find that the calculated rotation curves do not depend significantly on the shape of the halo, i.e., q. Also, all the three density indices ($p = 1$, 1.5 and 2) give reasonably good fit to the observed rotation curve, in that they lie well within the error bars of the observed curve in the radial range of 2-30 kpc. However, in terms of χ^2 analysis, p = 1 (the isothermal case) is the most favoured.

4.4.3 The HI scale height constraint

Now, for each of the above three cases ($p = 1$, 1.5, 2), we considered only those grid points for HI scale height determination, whose χ^2 values were less than 11, which is the total number of data points in the observed rotation curve. Elementary statistics suggests that a model distribution can be taken to be a reasonably good fit if its χ^2 value with respect to the observed distribution is of the order of the number of data points in the observed distribution (Bevington 1969). Also, for these given set of grid points, we have checked that the rotation curve lies well within the error bars in the region of interest i.e the outer galactic region. For $p = 1$, there were 3684 such grid points, 4910 for $p = 1.5$ and 5799 for $p = 2$.

For the set of grid points chosen above, we calculated the HI scale height in the outer galactic region, i.e, beyond three disk scale lengths (R = 16.2 kpc) following the analysis done for the Galaxy case (Narayan et al 2005), and obtained the χ^2 with respect to the observed scale height data (Braun 1991). The dark matter halo is expected to be more important in the outer parts and hence the scale height values in this range are used as a constraint to obtain the halo parameters.

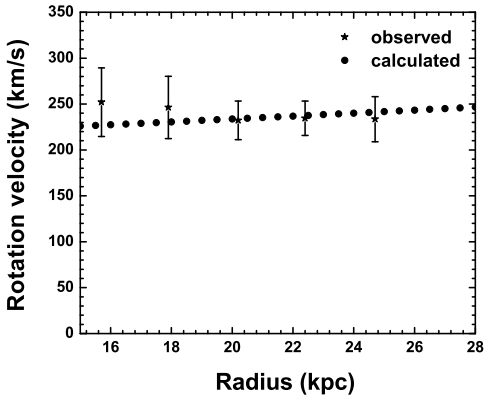

FIGURE 4.2: Plot of the rotation velocity (in km s^{-1}) versus radius (in kpc) for the best-fit case of an isothermal halo of oblate shape with an axis ratio $q = 0.4$. Our model rotation curve matches well with the observed data (Widrow et al. 2003) within the error bars.

4.4.4 Resulting Best-fit halo parameters

We find that a flattened, isothermal halo (p=1, $q = 0.4$) with a small central density (0.011 $M_\odot$ pc^{-3}), and a core radius of 21 kpc provides the best fit to both the observed rotation curve and the HI scale height data. The other density profiles ($p = 1.5$, and 2) give higher values for the χ^2 minimum and hence are not favoured, however, the dependence on the power-law index p is weak. Interestingly these also give $q = 0.4$ as the preferred shape and the same central density but with a higher core radius of 27 kpc and 34 kpc respectively.

In Fig.4.2, we compare our best fit rotation curve with the observed one in the outer regions although the fit was done over the entire radial range of 2-30 kpc (Section 4.4.2).

Similarly, Fig.4.3 depicts the best-fit scale height distribution in the outer disk region.

In Fig. 4.4, we compare the resulting scale height distributions for the various values of $q = 0.2$ - 1 in steps 0.2, obtained using the best-fit values for ρ_0 and R_c in each case. It shows that although the χ^2 analysis selects $q = 0.4$ to be the best fit, a range of q values between 0.4 - 0.6 gives fits to the observed data within the error bars - but the departure of the calculated distribution from the real data points increases with increasing q.

This is further illustrated in Figure 4.5, where we plot the χ^2 value for the best-fit case for each axis ratio vs. the axis ratio, q. The χ^2 shows a clear minimum at q =0.4 which is

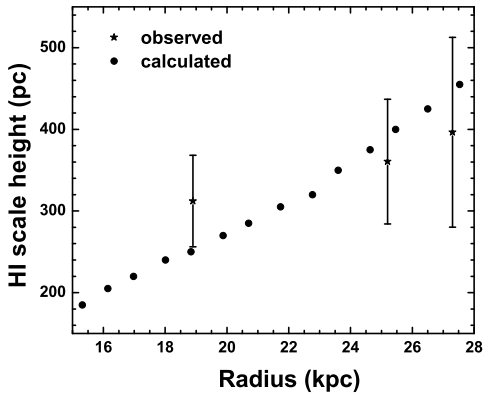

FIGURE 4.3: Plot of HI scale height (in pc) versus the radius (in kpc) for the best-fit case of an isothermal halo of oblate shape with an axis ratio $q = 0.4$. The flattened halo of our best-fit model predicts a HI scale height distribution that agrees well with observations (Braun 1991) within the error-bars.

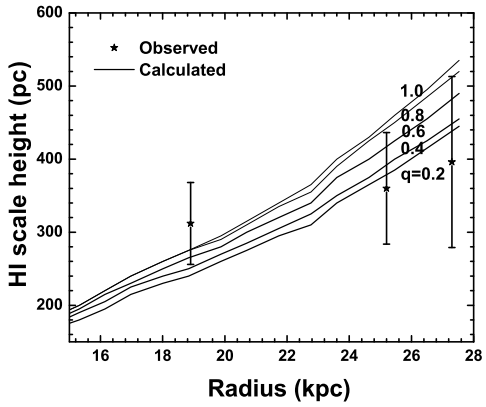

FIGURE 4.4: Plot of the HI scale height (in pc) versus radius (in kpc) for an isothermal density profile and for different values of flattening: $q = 0.2$, 0.4, 0.6 , 0.8 and 1, for the best-fit values of ρ_0 and R_c in each case. This shows that a range of values between $q = 0.4$ - 0.6 gives fits to the observed data within the error bars, but the χ^2 analysis identifies $q = 0.4$ as the best-fit case.

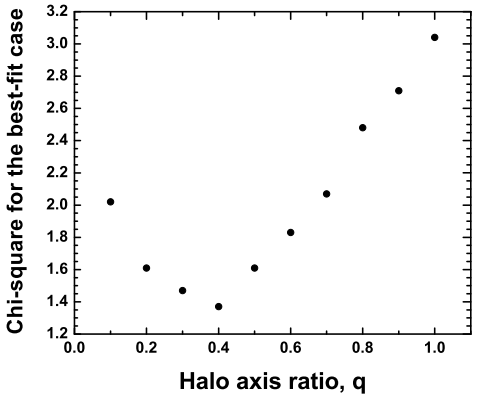

FIGURE 4.5: Plot of χ^2 for the best-fit case for a given axis ratio versus the axis ratio, q, of the dark matter halo. The χ^2 shows a clear minimum at q =0.4 which is thus the axis ratio that best explains the observations. Note that a flattened halo ($q = 0.4$) is clearly distinguished from and preferred over the spherical case ($q = 1$)

thus the axis ratio that best explains the observations. In particular, a flattened halo ($q = 0.4$) is clearly distinguished from and preferred over the spherical case ($q = 1$).

Interestingly, such flattened halos lie at the most oblate end of the distribution of halo shapes obtained in recent Λ CDM cosmological simulations (e.g., Bailin & Steinmetz 2005, see their Fig. 2; Bett et al. (2007), see their Fig. 13)- the axis ratio q used in the present paper is equal to the ratio of the semi-major axes c/a in these papers. Thus, either M31 is an unusual galaxy, or the simulations need to include additional physics such as the effect of baryons that could affect the shape of the halo. Further, a moderate variation in HI gas dispersion results in a less flattened halo as shown in Section 4.5.3.

4.5 Discussion

1. HI Scale height data in outer disk: The HI scale hight constraint as applied in this paper is ideally suited for application to gas-rich, late-type spiral galaxies with an extended HI disk. In order to be useful as a constraint, the HI scale height data should be available beyond 3 - 4 R_d and even farther out in the galaxy. This is where the disk gravitational force begins to drop out and the dark matter halo takes over. We note that obtaining the HI scale

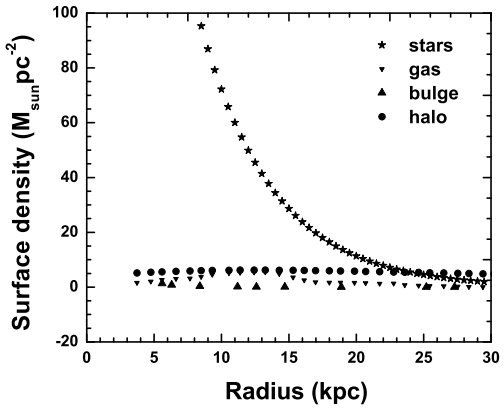

FIGURE 4.6: Plot of stellar, gaseous, bulge and halo surface densities within the HI scale height in units of $M_\odot$ pc^{-2} versus radius in kpc. It shows that the stellar surface density is comparable to the halo surface density up to $\sim$ 25 kpc, and only beyond this the halo starts to dominate the disk surface density as we go outward in the galaxy

height data is an observationally challenging task (Sancisi & Allen 1979), and therein lies the main difficulty in using this method. As far as our work is concerned, the observational data (Braun 1991) gives only three data points beyond R = $3R_d$. We consider the region only beyond R = $3R_d$ following the Galaxy case (Narayan et al. 2005). Also, the irregularity or the scatter in the observed data in the inner region suggests the presence of a bar or spiral arm or some unknown structure, and is therefore excluded from the analysis.

In Fig.4.6 we illustrate the above point by plotting the halo surface density within the HI scale height, as well as the corresponding values for the bulge, stars, and HI gas versus the radius. For using the HI scale height constraint, the vertical force close to the galactic mid-plane is needed, this is why the surface density of the halo within the HI scale height is included. This figure shows that the halo surface density just begins to take over the stellar density at the point beyond which we do not have any observed data. Availability of more data points in the outer parts, with lower error-bars, is thus clearly desirable and would yield a tighter constraint on the halo shape and the density profile.

2. Simultaneous constraints: The calculated rotation curve does not depend on the shape of the halo (q). All the q values give equally good fits to the observed data. Surprisingly, the χ^2 minima for the rotation curve and the HI scale height data, taken separately, lie on

different regions of the grid. The best-fit to the rotation curve alone gives high values of the central density and small values of core radius. The best-fit to the scale height data, on the other hand, gives a lower central density and a larger core radius. Geehan et al. (2006) obtained a best-fit ρ_0 of 0.033 $M_\odot$ pc^{-3} (somewhat higher than the value we get) and R_c of 8.2 kpc , probably because they had used the rotation curve as the only constraint. We, on the other hand, have used two complementary constraints; the planar one involving the rotation curve, and the vertical one involving the HI scale height. This allows us to uniquely determine the physical parameters of the halo, and the determination of the true minimum in the grid spanning all the parameters for the dark matter halo.

We find that the observed HI scale height increases linearly with radius and does not flare, and this can be explained if the halo is flattened and consequently implies a smaller central density, while keeping the same mass within a radius to explain the observed rotation curve.

3. Dependence on the HI velocity dispersion: The calculation of the HI scale height is crucially dependent on the chosen value of the vertical velocity dispersion of HI. We do not have any observationally measured value for the gas dispersion for M31. Here we have assumed it to be constant at 8 km s^{-1} at all radii, as is observed for about 200 galaxies (Lewis 1984). If at all, the observed dispersion falls off with radius very gradually in the outer galaxy (Kamphuis 1993, Narayan et al. 2005). Repeating the whole analysis for a slightly smaller value of $(v_z)_{\rm HI}$ = 7 km s^{-1}, we find the best fit ρ_0 and R_c to be 0.007 $M_\odot$ pc^{-3} and 19.5 kpc respectively with q = 0.8-0.9, implying a less oblate halo, but with larger χ^2 values, than obtained for the best-fit case with 8 km s^{-1} in Section 4.4. Physically this trend can be explained as follows: in this case the pressure support is smaller hence the gravitational force required to balance it has to be smaller to match the same observed data, hence a less flattened halo is expected.

We also tried a case with a small radial fall-off in the HI dispersion from 8 to 7 km s^{-1} in the outer disk between 18-27 kpc. This variation is assumed ad-hoc, but it allows us to explore the effect of such a gradient on the halo shape deduced. In this case again the best-fit is obtained for a less oblate halo of q = 0.5-0.6 (compared to the q = 0.4 obtained for

a constant dispersion of 8 km s^{-1}, Section 4.4). Here χ^2 values are lower but show a shallow minimum for the dependence on the halo shape q. This is because, in this case, the observed fairly flat scale height distribution is sought to be mainly explained by a radial variation in the gas dispersion. While this gives lower χ^2 values as expected, it also has weak dependence on the halo shape, which is therefore not constrained well.

It is interesting that a small radial gradient in gas dispersion results in a rounder halo ($q \sim 0.6$) which is more typical of the halo shapes seen in the cosmological simulations (Bailin & Steinmetz 2005, Bett et al. 2007). This shows how crucial the value of the gas velocity is in this model, in determining the flattening of the halo, which has possible implications for the galaxy formation scenarios. This highlights the necessity of accurate measurement of gas dispersion in galaxies.

4. Comparison with the Milky Way Galaxy: The ratio of the total mass in the halo to the total mass in the disk (in stars and gas) within a certain radius is an important physical quantity, since it tells one how significant the halo is at a certain radius. For the best-fit value for p=1 and q=0.4, we calculate the halo mass as a function of the radius by integrating the halo density profile as given in equation (4.7). The disk mass in the two components is as observed (Section 4.3.2). It is now known that M31 has an extended disk up to 40 kpc with a similar disk scale length in the inner and outer regions (Ibata et al. 2005). We find that the fraction of the total mass in a dark matter halo is 83 % within R= 30 kpc or about 5 R_d, and is 89 % within R= 40 kpc or about 7 R_d. In comparison, for the Galaxy, using the isothermal halo model for the Galaxy and the stellar disk model as given by Mera et al. (1998) and the observed values of HI and H_2 gas (Scoville & Sanders 1987), we obtain the corresponding ratio of the halo mass the total mass to be 80 % within 5 R_d (=16 kpc) , and 84 % within 7 R_d (= 22 kpc). These are remarkably similar in the two galaxies.

On the other hand, the scale height distribution is different in the two galaxies: it is nearly flat increasing linearly for M31 whereas it flares in the outer Galaxy. To explain this, an isothermal, flattened, oblate-shaped halo is needed for M31 as shown here, whereas using a similar approach it was shown that a spherical halo with density falling faster than an isothermal is needed to explain the data for the Galaxy (Narayan et al. 2005). Thus, the

dark matter halo shapes and density profiles do not appear to be universal even in large spiral galaxies.

4.6 Conclusions

We have used both the observed rotation curve and the outer galactic HI scale height data to constrain the dark matter halo profile of M31. We have systematically explored various shapes and power-law indices for the density distributions for the halo to fit the observed data. Our galactic disk model consists of coupled stars and HI gas, where the gas-gravity is taken into account on an equal footing with the stellar gravity. We find that an oblate isothermal halo with a central density of 0.011 $M_\odot$ pc^{-3}, a core radius of 21 kpc best fits the observations. The axis ratio for the best-fit results is 0.4. This is in a sharp contrast to the spherical halo used to model M31 in the literature so far. The rotation curve constraint alone is usually used which determines the mass within a radius but cannot uniquely determine the shape of the halo. The present work highlights the fact that using the two simultaneous and complementary constraints of rotation curve and the HI scale height data in the outer galactic region, allows one to identify the shape as well as the density distribution of the dark matter halo in spiral galaxies.

We stress that the availability of more data points for the HI scale heights in the outer galaxy beyond 5-6 disk scale lengths, and an accurate determination of the HI gas velocity dispersion, would provide a tighter constraint for the shape and the density profile of the dark matter halo. In fact, having such data for other galaxies would allow the above method to be applied to a systematic study of the dark matter halo properties in different galaxies.

References

Bailin, J., & Steinmetz, M. 2005, ApJ, 627, 647

Banerjee, A., & Jog, C.J. 2007, ApJ, 662, 335

Becquaert, J. F., & Combes, F. 1997, A&A, 325, 41

Begeman, K. 1987, Ph.D. thesis, University of Groningen.

Bett, P., Eke, V., Frenk, C.S., Jenkins, A., Helly, J., & Navarro, J. 2007, MNRAS, 376, 215

Bevington, P.R. 1969, Data Reduction and Error Analysis for the Physical Sciences. McGraw-Hill, New York

Binney, J., Merrifield, M., 1998, Galactic Astronomy. Princeton Univ. Press, Princeton, NJ

Binney, J., Tremaine, S., 1987, Galactic Dynamics. Princeton Univ. Press, Princeton, NJ

Braun, R. 1991, ApJ, 372, 54

Carignan, C., Chemin, L., Huchtmeier, W. K., & Lockman, F. J. 2006, ApJ, 641L, 109

de Zeeuw, T., & Pfenniger, D. 1988, MNRAS, 235, 949

Geehan, J. J., Fardal, M. A., Babul, A., & Guhathakurta, P. 2006, MNRAS, 366, 996

Hernquist, L. 1990, ApJ, 356, 359

Ibata, R., Chapman, S., Ferguson, A. M. N., Lewis, G., Irwin, M., & Tanvir, N. 2005, ApJ, 634, 287

Kalberla, P. M. W., Dedes, L., Kerp, J., & Haud, U. 2007, A&A, 469, 511

Kamphuis, J.J. 1993, Ph.D. thesis, University of Groningen

Kent, S.M. 1986, AJ, 91, 1301

Kent, S.M. 1987, AJ, 93, 816

Kerins, E., Carr, B.J., Evans, N.W., Hewett, P., Lastennet, E., Le Du, Y., Melchoir, A.-L., Smartt, S.J., & Valls-Gaband, JD. 2001, MNRAS, 323, 13

Koper, E. 1993, Interestellar medium in M31 and other nearby galaxies, Ph.D. thesis, State University of Leiden.

Lewis, B. M. 1984, ApJ, 285, 453

Lewis, J.R., & Freeman, K. C. 1989, AJ, 97, 139

Mera, D., Chabrier, G. , Schaeffer, R. 1998, A & A, 330, 953

Narayan, C.A., & Jog, C.J., 2002 a, A & A, 390, L35

Narayan, C.A., & Jog, C.J., 2002 b, A & A, 394, 89

Narayan, C. A., Saha, K., & Jog, C. J. 2005, A&A, 440, 523

Navarro, J. F., Frenk, C. S., & White, S. D. M. 1996, ApJ, 462, 563

Olling, R. P. 1996, AJ, 112, 457

Olling, R. P., & Merrifield, M. R. 2000, MNRAS, 311, 361

Olling, R. P., & Merrifield, M. R. 2001, MNRAS, 326, 164

Rohlfs, K. 1977, Lectures on Density Wave Theory. Springer-Verlag, Berlin

Sackett, P. D., & Sparke, L. S. 1990, ApJ, 361, 408

Sancisi, R., & Allen, R.J. 1979, A & A, 74, 73

Scoville, N.Z., & Sanders, D.B. 1987, in Interestellar Processes, eds. H.A. Thronson & D.J. Hollenbach Dordrecht, Reidel.

Seigar, M. S., Barth, A. J., & Bullock, J. S. 2006, astro-ph/0612228

Sofue, Y., & Kato, T. 1981, PASJ, 33, 449

Tamm, A., Tempel, E., & Tenjes, P. 2007, arxiv:0707.4375v1

Widrow, L. M., Perrett, K. M., & Suyu, S. H. 2003, ApJ, 588, 311

Widrow, L. M., & Dubinski, J. 2005, ApJ, 631, 838

Wouterloot, J.G.A., Brand, J., Burton, W.B., & Kwee, K.K. 1990, A & A, 230, 21

5

Dark matter dominance at all radii in the superthin galaxy UGC 7321 [4]

Abstract

We model the shape and density profile of the dark matter halo of the low surface brightness, superthin galaxy UGC 7321, using the observed rotation curve and the H I scale height data as simultaneous constraints. We treat the galaxy as a gravitationally coupled system of stars and gas, responding to the gravitational potential of the dark matter halo. An isothermal halo of spherical shape with a core density in the range of 0.039 - 0.057 $M_{\odot}$ pc^{-3} and a core radius between 2.5 - 2.9 kpc, gives the best fit to the observations for a range of realistic gas parameters assumed. We find that the best-fit core radius is only slightly higher than

[4] Banerjee et al. 2010, NewA, 15, 89

the stellar disk scale length (2.1 kpc), unlike the case of the high surface brightness galaxies where the halo core radius is typically 3-4 times the disk scale length of the stars. Thus our model shows that the dark matter halo dominates the dynamics of the low surface brightness, superthin galaxy UGC 7321 at all radii, including the inner parts of the galaxy.

5.1 Introduction

Since spiral galaxies are rotationally supported systems, disk rotation curves generally serve as valuable tracers of the gravitational potential in the galactic plane. Through traditional mass-modelling, the observed curve is routinely used to infer the mass distribution of galaxies and hence their dark matter contents (e.g. Begeman 1987; Kent 1987; Geehan et al. 2006). In contrast, the thickness of the gas layer depends on the vertical gravitational force and thus traces the potential perpendicular to the plane e.g.,(Narayan & Jog 2002a).

Recently, the rotation curve and the outer galactic H I flaring data have been used together to probe the dark matter halos of a few galaxies. The rotation curve mainly determines the mass enclosed within a given radius, and therefore the power-law index of the density profile of the halo. The flaring curve, on the other hand, determines its shape uniquely. So, both the constraints have to be used on an equal footing to correctly determine the parameters of the dark matter halo of any galaxy.

The H I scale height data coupled with the rotation curve has been used to study the dark matter halos of NGC 4244 (Olling 1996) , NGC 891 (Becquaert & Combes 1997) and the Galaxy (Olling & Merrifield 2000, 2001) in the past. Narayan et al. (2005) studied the Galactic dark matter halo by rigorously incorporating the self-gravity of the gas into their model for the Galaxy unlike some of the previous studies given in the literature. They concluded that a steeper-than-isothermal, spherical halo best fits the observations, the scale height data at that time being available up to galactocentric distances of 24 kpc. These results were confirmed by Kalberla et al. (2007), who, however, included a dark matter ring in their model to explain their extended H I scale height data available till 40 kpc. In our previous work (Banerjee & Jog 2008), we studied the dark matter halo of M31, where we

developed a model similar to the Galaxy (Narayan et al. 2005) . However, in addition, we included the bulge into the model, and also varied the shape of the halo as a free parameter, unlike the Galaxy case. Further, we fitted the rotation curve over the entire radial range instead of pinning it at a single point like the Galaxy case. We scanned the four dimensional grid of the four free parameters characterizing the halo, in a systematic manner, and found that an isothermal halo of an oblate shape of axis ratio $q = 0.4$ gives the best fit to the available data.

In this paper, we apply for the first time a similar approach to study the dark matter halo properties of a low surface brightness (LSB) "superthin" galaxy: UGC 7321. UGC 7321 is a bulgeless, pure disk galaxy of Hubble Type Sd, and has a highly flattened stellar disk with a planar-to-vertical axis ratio of 10.3. A few of its key properties are summarized in Table 5.1. The galaxy has an extended H I disk, and the scale height data are available up to 6-7 disk scale lengths (Matthews & Wood 2003). So it is highly suitable for the application of the above method to probe its dark matter halo properties.

Based on traditional mass-modelling which only uses the observed rotation curve as the constraint, it has been found that the late-type, low surface brightness galaxies are generally dark matter dominated, often within the inner portions of their stellar discs (de Blok & McGaugh 1997) . In the case of UGC 7321, other lines of evidence have already suggested that it, too, is a highly dark matter-dominated galaxy. It has large ratios of its dynamical mass to its H I mass and blue luminosity, ($M_{\rm dyn}/M_{\rm HI} = 31$ and $M_{\rm dyn}/L_B = 29$, respectively; (cf. Roberts & Haynes 1994) , and an extraordinarily small stellar disk scale height ($\sim$150 *pc* for a distance of 10 Mpc based on an exponential fit; Matthews 2000). These properties suggest the need for a massive dark halo to stabilize the disk against vertical bending instabilities (Zasov et al. 1991) .

UGC 7321 is devoid of a central bulge component (Matthews et al. 1999) and its molecular gas content appears to be dynamically insignificant (Matthews & Gao 2001; Matthews & Wood 2001). We, therefore, model the galaxy as a gravitationally coupled, two-component system of stars and atomic hydrogen gas with the dark matter halo acting as a source of external force to this system. We use a four-parameter density profile for the dark matter

TABLE 5.1: UGC 7321 Parameters: *(All quantities are taken from Matthews et al. (1999) and Uson & Matthews (2003) which assume d = 10 Mpc)*

Parameters	Value
A_{opt}(kpc)	16.3 [a]
$L_B(\mathrm{L}_\odot)$	1.0×10^9 [b]
$M_{\mathrm{H\,I}}(\mathrm{M}_\odot)$	1.1×10^9 [c]
h_R(kpc)	2.1 [d]
z_0(pc)	150 [e]
$\mu_{B,i}(0)$(mag arcsec^{-2})	23.5 [f]
v_{rot}(kms^{-1})	105
Star formation rate ($\mathrm{M}_\odot$ per year for massive stars $\geq 5\mathrm{M}_\odot$)	~ 0.02

[a]Linear diameter at limiting observed B-band isophote of 25.5 mag arcsec^{-2}
[b]Blue luminosity
[c]H I mass
[d]disk scale length measured from R-band image
[e]stellar scale height obtained from an exponential fit
[f]Deprojected (face-on) central disk surface brightness in the B band, corrected for internal and Galactic extinction

halo (de Zeeuw & Pfenniger 1988; Bequaert & Combes 1997): the core density, the core radius, the power-law density index and the axis ratio of the halo being the four free parameters characterizing it. We methodically vary the four parameters within their respective feasible ranges, and try to obtain an optimum fit to both the observed rotation curve and the vertical scale height data at the same time. As we shall see, this method predicts a spherical, isothermal halo with a core density of about 0.039- 0.057 $\mathrm{M}_\odot$ pc^{-3} and core radius of 2.5 - 2.9 kpc for this galaxy.

The layout of the present paper is as follows. We briefly discuss the model in section 5.2, and in section 5.3 the method of solving the equations and the input parameters used is discussed. In section 5.4, we present the results, followed by the discussion and conclusions in sections 5.5 and 5.6, respectively.

5.2 Description of the model used

5.2.1 Gravitationally coupled, two-component, galactic disk model

The galaxy is modelled as a gravitationally-coupled, two-component system of stars and atomic hydrogen gas embedded in the dark matter halo, which exerts an external force on the system while remaining rigid and non-responsive itself. This is a simplified version of the Galaxy case (Narayan & Jog 2002b) , where a gravitationally-coupled, three-component system of stars, atomic and molecular hydrogen was considered. Here, the two components, present in the form of discs, are assumed to be axisymmetric and coplanar with each other for the sake of simplicity. Also, it is assumed that the components are in a hydrostatic equilibrium in the vertical direction. Therefore, the density distribution of each component will be jointly determined by the Poisson equation, and the corresponding equation for pressure equilibrium perpendicular to the mid-plane.

In terms of the galactic cylindrical co-ordinates (R, ϕ, z), the Poisson equation for an azimuthally symmetric system is given by

$$\frac{\partial^2 \Phi_{total}}{\partial z^2} + \frac{1}{R}\frac{\partial}{\partial R}\left(R\frac{\partial \Phi_{total}}{\partial R}\right) = 4\pi G(\sum_{i=1}^{2}\rho_i + \rho_h) \tag{5.1}$$

where ρ_i with i = 1 to 2 denotes the mass density for each disk component while ρ_h denotes the mass density of the halo. Φ_{total} denotes the total potential due to the disk and the halo. For a nearly constant rotation curve as is the case here, the radial term can be neglected as its contribution to the determination of the H I scale height is less than ten percent as was noted by earlier calculations Narayan et al. (2005). So, the above equation reduces to

$$\frac{\partial^2 \Phi_{total}}{\partial z^2} = 4\pi G(\sum_{i=1}^{2}\rho_i + \rho_h) \tag{5.2}$$

The equation for hydrostatic equilibrium in the z direction is given by Rohlfs (1977)

$$\frac{\partial}{\partial z}(\rho_i\langle(v_z^2)_i\rangle) + \rho_i\frac{\partial \Phi_{total}}{\partial z} = 0 \tag{5.3}$$

where $\langle(v_z^2)_i\rangle$ is the mean square random velocity along the z direction for the i^{th} component. Further we assume that each component is isothermal i.e., the random velocity v_z remains constant with z.

Combining eq. (5.2) and eq. (5.3), we get

$$\langle(v_z^2)_i\rangle \frac{\partial}{\partial z}\left[\frac{1}{\rho_i}\frac{\partial \rho_i}{\partial z}\right] = -4\pi G(\sum_{i=1}^{2}\rho_i + \rho_h) \tag{5.4}$$

This represents a set of two coupled, second-order, ordinary differential equations which needs to be solved to obtain the vertical density distribution of each of the two components. Although the net gravitational potential acting on each component is the same, the response will be different due to the different velocity dispersions of the two components.

5.2.2 Dark Matter Halo

We use the four-parameter dark matter halo model (de Zeeuw & Pfenniger 1988; Bequaert & Combes 1997) with the density profile given by

$$\rho(R,z) = \frac{\rho_0}{\left[1+\frac{m^2}{{R_c}^2}\right]^p} \tag{5.5}$$

where $m^2{=}R^2 + (z^2/q^2)$, ρ_0 is the central core density of the halo, R_c is the core radius, p is the power-law density index, and q is the vertical-to-planar axis ratio of the halo (spherical: $q = 1$; oblate: $q < 1$; prolate: $q > 1$).

5.3 Numerical Solution of the Equations & Input Parameters

5.3.1 Solution of equations

For a given halo density profile, eq. (5.4) is solved in an iterative fashion, as an initial value problem, using the fourth-order, Runge-Kutta method of integration, with the following two

initial conditions at the mid-plane (i.e., $z = 0$) for each component:

$$\rho_i = (\rho_0)_i, \qquad \frac{d\rho_i}{dz} = 0 \tag{5.6}$$

As the modified mid-plane density $(\rho_0)_i$ for each component is not known a priori, the net surface density $\Sigma_i(R)$, given by twice the area under the curve of $\rho_i(z)$ versus z, is used as the secondary boundary condition, as this quantity is known from observations (see section 5.3.2). The required value of $(\rho_i)_0$ is thus determined by a trial and error method, which gives the required $\rho_i(z)$ distribution after four iterations with an accuracy to the second decimal place. Existing theoretical models suggest a sech^2 profile for an isothermal density distribution. But for a three-component disk, the vertical distribution is shown to be steeper than a sech^2 function close to the mid-plane (Banerjee & Jog 2007).However, at large z values, it is close to a sech^2 distribution. Hence we use the half-width-at-half-maximum of the resulting model vertical distribution to define the scale height as was done in Narayan & Jog (2002a,b).

5.3.2 Input Parameters

We require the vertical velocity dispersion and the surface density of each of the two galactic disk components to solve the coupled set of equations at a given radius. The central stellar surface density is derived directly from the optical surface photometry (Matthews et al. 1999) by assuming a reasonable stellar mass-to-light ratio. The deprojected B-band central surface brightness of UGC 7321 (corrected for extinction) translates to a central luminosity density of 26.4 $\mathrm{M}_\odot$ pc^{-2}. Using the $B - R$ color of the central regions ($\sim$1.2; Matthews et al. (1999)) and the "formation epoch: bursts" models from Bell & de Jong (2001) predicts $(M/L)_\star = 1.9$, which we adopt here. (Other models by Bell & de Jong give values of $(M/L)_\star$ ranging from 1.7 to 2.1). This in turn yields a central stellar surface density of 50.2 $\mathrm{M}_\odot$ pc^{-2} for UGC 7321.

The stellar velocity dispersion of this galaxy has been indirectly estimated to be 14.3 kms^{-1} at the centre of the galaxy ($R = 0$) (Matthews 2000). This is very close to the value

of the central (vertical) stellar velocity dispersion (16 kms^{-1}) for the dwarf spiral galaxy UGC 4325 measured by Swaters (1999), and to the value (20 kms^{-1}) estimated analytically for the superthin galaxy IC 5249 by van der Kruit et al. (2001). We assume the central value of velocity dispersion to fall off exponentially with radius with a scale length of 2 R_d (which is equal to 4.2 kpc for UGC 7321) as is seen in the Galaxy (Lewis & Freeman 1989). Uson & Matthews (2003) give the deprojected H I surface density for UGC 7321 as a function of radius. The velocity dispersion of H I is obtained from the Gaussian fits to the edges of position-velocity cuts on the observed data. This gives a value between 7-9 kms^{-1}. The data are consistent to the typical value of the H I dispersion in other galaxies (See section 5.5.2 for a detailed discussion).

The molecular hydrogen gas, H_2, has not been taken into account, as it appears to be dynamically insignificant compared to the other components of the disk. Matthews & Gao (2001) detected a weak CO signal from the central ∼2.7 kpc of UGC 7321, which translates to a total molecular hydrogen mass of $H_2 \approx 2.3 \times 10^7$ $M_\odot$ (although this value is uncertain by at least a factor of 2-3 as a result of uncertainties in optical depth effects and the appropriate value of the CO-to-H_2 conversion factor). This corresponds to a mean H_2 surface density of $\Sigma_{H2} \approx 1$ $M_\odot$ in the inner galaxy, which agrees fairly well with independent estimates from the dust models of Matthews & Wood (2001) and from a study of the distribution of dark clouds from *Hubble Space Telescope* images (J. S. Gallagher & L. D. Matthews, unpublished). Therefore, the presence of H_2 has been ignored in subsequent calculations.

5.4 Results and analysis

We perform an exhaustive scanning of the grid of parameters characterizing the dark matter density profile to obtain an optimum fit to both the observed rotation curve and the scale height data. To start with, we consider a spherical halo ($q = 1$) for simplicity.

We vary the remaining three free parameters characterizing the density profile of the halo (see eq. (5.5)) within their respective feasible ranges (as summarized in Table 5.2), and obtain the contribution of the halo to the rotation curve for each such grid point in this three-dimensional grid. The power-law density index p is allowed to take the values 1, 1.5

TABLE 5.2: 3D grid of dark halo parameters scanned

Parameter	*Range*	*Resolution*
$\rho_0(\mathrm{M}_\odot\ \mathrm{pc}^{-3})$	$0.0001 - 0.1$	0.0001
	$0.001 - 0.5$	0.001
R_c(kpc)	$1.5 - 12$	0.1
p	$1 - 2$	0.5

and 2 successively. Here, a value of $p = 1$ corresponds to the standard isothermal case used routinely for simplicity and also because it corresponds to the flat rotation curve. The value of $p = 1.5$ refers to the NFW profile Navarro et al. (1996) at large radii, whereas $p = 2$ gives an even steeper dark-matter halo profile, as was found for the Galaxy case Narayan et al. (2005). For each value of p, the core density ρ_0 and the core radius R_c are varied as given in Table 5.2 to ensure an exhaustive scanning for the dark matter halo parameters since we have little prior knowledge of the plausible values these parameters can take in a superthin galaxy.

5.4.1 The rotation curve constraint

The total rotational velocity at each radius is obtained by adding the contribution from the stars, the gas and halo in quadrature as

$$v^2(R) = v^2_{star}(R) + v^2_{gas}(R) + v^2_{halo}(R) \tag{5.7}$$

Here the way to obtain the different terms is discussed below. This result is matched with the observed rotational velocity at all radii.

The deprojected gas surface density versus radius data for UGC 7321 (Uson & Matthews 2003) can be modelled as one which remains constant at 5 $\mathrm{M}_\odot\ \mathrm{pc}^{-2}$ at galactocentric radii less than 4 kpc, and which then falls off exponentially with a scale length of 2.8 kpc. The gas surface density does not include a correction for He. For this radial distribution, we

calculated the contribution of the gas to the rotation curve (using eq. (2-158) & (2-160) of Binney & Tremaine (1987)), and found it to be negligible compared to that of the stellar component. However, it was included in the calculations for the sake of completeness.

The rotational velocity at any radius R for a thin exponential stellar disk is given by Binney & Tremaine (1987)

$$v^2_{star}(R) = 4\pi G\Sigma_0 R_d y^2[I_0(y)K_0(y) - I_1(y)K_1(y)] \tag{5.8}$$

where Σ_0 is the disk central surface density, R_d the disk scale length and $y = R/2R_d$, R being the galactocentric radius. The functions I_n and K_n (where n=0 and 1) are the modified Bessel functions of the first and second kind, respectively.

For the spherical halo, the rotational velocity, $v_{halo}(R)$, is given by

$$v^2_{halo}(R) = \frac{GM_{halo}(R)}{R} \tag{5.9}$$

where $M_{halo}(R)$, the mass enclosed within a sphere of radius R for a the given halo density profile, and is obtained from the density as given by the right-hand side of eq. (5.5).

For an oblate halo of axis ratio q and density index p, the circular speed $v_{halo}(R)$ is obtained by differentiating the expression for the potential from Sackett & Sparke (1990), and Becquaert & Combes (1997) to be:

$$v^2_{halo}(R) = 4\pi G\rho_0 q \int_0^{1/q} \frac{R^2x^2[1 + \frac{R^2x^2}{R_c^2(1+\epsilon^2x^2)}]^{-p}}{(1+\epsilon^2x^2)^2} dx \tag{5.10}$$

where $\epsilon = (1 - q^2)^{1/2}$. We obtain the value of the integral numerically in each case.

Thus upon obtaining the rotation curve corresponding to each grid point, we perform the χ^2 analysis comparing computed to the observed H I rotation curve. The observed rotation curve is taken from Uson & Matthews (2003) and has 30 data points with very small error-bars (typically a few percent of the observed velocity amplitudes even after accounting for systematic uncertainties). It was derived by implicitly assuming a constant (Gaussian) H I

velocity dispersion of 7 kms^{-1}. Ideally, we should have considered only those grid points which give χ^2 values of the order of 30 (i.e., the number of data points) as those giving appreciably good fits to the observed curve Bevington (1969). But we relax this criterion and choose a larger range of grid points around the minimum i.e grid points which give χ^2 values less than 300 for applying the next constraint i.e the vertical H I scale height data. This allows us to impose the simultaneous constraints (planar + vertical) on our model. (See section 5.4.3 for a discussion). So finally we get 36 grid points for $p = 1$, 80 for $p = 1.5$ and 69 for $p = 2$ case. As we shall see later, the final set of best-fit parameters obtained give reasonably good fits to both the observed rotation curve and the scale height data.

5.4.2 The H I scale height constraint

For each value of p, we obtain the H I scale height distribution beyond 3 disk scale lengths, for each of the grid points filtered out by the first constraint as discussed in the previous section. Next we perform the χ^2 analysis of our model H I scale height versus radius curves with respect to the observed one and try to fit our model to the observed data only beyond 3 disk scale lengths in keeping with the earlier studies in the literature (Narayan et al. 2005; Banerjee & Jog 2008). For M31, the surface-density and therefore the vertical gravitational force due to the dark matter halo exceeds that of the disk only in the outer regions (See Fig.6 of Banerjee & Jog 2008). As the disk dynamics in this region are controlled by the halo alone, the above method helps us in studying the effect of the halo on the scale height distribution, decoupled from that of the other components. For the case of UGC 7321, at first we take the gas velocity dispersion to be equal to 7 kms^{-1} . However it fails to give a good fit to the observed data. Next we try both 8 kms^{-1} and 9 kms^{-1} successively, but choose the latter for subsequent calculations as it gives much better fit to the observed data as compared to the 8 kms^{-1} case.

For the choice of $v_z = 9$ kms^{-1}, the best-fit core density is 0.041 M$_\odot$ pc^{-3} and a core radius is 2.9 kpc, as indicated by the smallest χ^2 value. The small value of the best-fit halo core radius thus obtained indicates that the halo becomes important already at small radii. This suggests that the fitting of the theoretical curve with the observed one should not be

restricted only to regions beyond 3 R_d for an LSB galaxy like UGC 7321 as the halo is already important at small radii. Hence, we next fit the scale height data over entire radial range (i.e., 2-12 kpc) with the same constant v_z value of 9 kms^{-1}. The best-fit values change by less than a few percent compared to the above case where the fit was done only beyond 3 R_d. The best-fit core density now becomes 0.039 M$_\odot$pc^{-3} whereas the best-fit core radius continues to be 2.9 kpc.

Since the disagreement of the observed rotation curve with the predicted one is mostly in the inner galaxy, we check if the fit can be improved by reducing the central value of the stellar surface density by twenty percent or so, keeping the v_z value constant at 9 kms^{-1}. This is reasonable as there are uncertainties of at least that order in evaluating both the M/L ratio and the deprojected surface brightness of the stellar disk. However, this variation fails to improve the results significantly.

We then take a cue from the nature of the mismatch of our model curve with the observed one, which clearly shows the need to use a higher value of gas velocity dispersion in the inner parts, while a slightly lower value is required in the outer regions. Also, the nature of the mismatch rules out an oblate halo as a possible choice as that will lower the scale heights throughout the entire radial range, thus making the fits worse in the inner regions. To account for this, we then repeat the whole procedure by imposing a small gradient in the gas velocity dispersion by letting it vary linearly between 9.5 kms^{-1} at $R = 7$ kpc and 8 kms^{-1} at $R = 12.6$ kpc. Although such a variation is ad-hoc, the observational constraints on this value are weak enough to allow for a small variation with galactocentric radius, with 9.5 kms^{-1} approaching the upper limit allowed by the data. Using the same gradient in the inner regions, we get a gas velocity dispersion of 10.8 kms^{-1} at $R = 2$ kpc. We may note here that a similar gradient in the H I velocity dispersion was obtained in the case of the Galaxy (Narayan & Jog 2002b) and led to a better fit to the observed scale height in the inner Galaxy (See section 5.5 for a detailed discussion). A fit to the whole range of observations (2 - 12 kpc) gives an isothermal halo of spherical shape with a core density of 0.043 M$_\odot$ pc^{-3} and a core radius of 2.6 kpc best fits the observations. These values are only slightly different (within 10 percent) from the values obtained with a constant velocity of 9

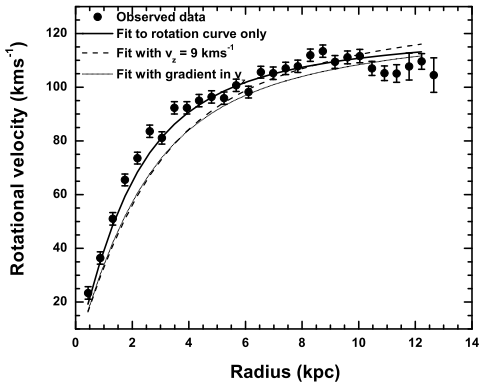

FIGURE 5.1: Plot of the rotational velocity (in kms^{-1}) versus radius (in kpc) for the best fit case of a spherical isothermal halo and a constant gas velocity dispersion of $v_z = 9$ kms^{-1} (dashed line) and for the case of v_z falling slightly with radius (dotted line) superimposed on the best fit to the rotation curve alone. Overall, the model rotation curves follow the trend of the observed data.

kms^{-1}.

In Fig.5.1, we give our best-fit for the case of constant $v_z = 9$ kms^{-1}, and the case with a v_z slightly falling with radius as compared to the fit to the rotation curve alone, superimposed on the observed one. Our model curves follow the trend of the observed data well throughout the entire radial range.

In Fig.5.2, we compare the best-fit scale height distributions for the above two cases with the observed one. Clearly, the case with a gradient in gas velocity dispersion gives a remarkably better fit (χ^2 value 2.8), although as far as χ^2 values are concerned, the case of constant $v_z = 9$ kms^{-1} cannot be ruled out altogether (χ^2 value 14.7) (This is because basic statistics suggests that the fit to the model is considered to be reasonably good if the χ^2 value is of the order of the number of data points in the fit as discussed earlier at the end of section 5.4.1. Here the total number of data points in the H I scale height data is 11.)

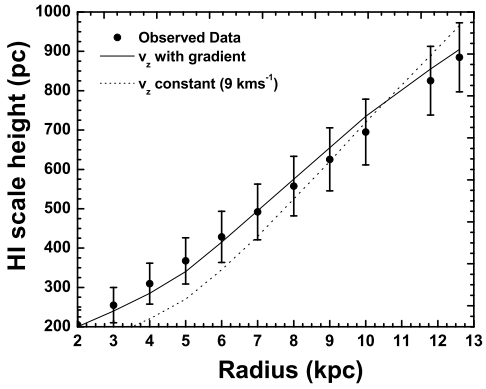

FIGURE 5.2: Plot of H I scale height (in pc) versus radius (in kpc) for the best-fit case of a spherical isothermal halo with constant gas velocity dispersion ($v_z = 9$ kms^{-1}; dotted line) and for v_z declining slowly with radius (solid line). In this case, the model curves have been fitted over the entire radial range. The model with constant v_z predicts an H I scale height distribution that does not reproduce the observed values in the inner regions of the galaxy ($R < 7$ kpc). Assuming a slight gradient in v_z clearly gives a better fit

5.4.3 Quality of individual fits as a result of imposing two simultaneous constraints

We reiterate the fact that our method is aimed at obtaining an optimum fit to both the observational constraints, namely the rotation curve and the HI scale height data. This evidently results in a compromise in the quality of individual fits to either of the observed curves (See Fig.5.1 & 5.2). Traditional mass modelling techniques resort to the rotation curve constraint alone, and therefore the fit is much better. However imposing two simultaneous constraints on the theoretical model gives a more realistic picture than the case in which best-fit is sought to a single constraint alone. It is noteworthy that even when the fit is sought to the rotation curve alone, the best-fit R_c continues to be of the order of R_D which is the main result of this work. However the ρ_0 value obtained is different in the two cases.

5.5 Discussion

The dark halo properties and overall stability of superthin galaxies like UGC 7321 are of considerable interest in the context of galaxy formation and evolution. In particular, such galaxies seem to pose a significant challenge to hierarchical models of galaxy formation, whereby galaxies are built-up through violent mergers of subgalactic clumps since such mergers may result in significant disk heating and trigger instabilities (e.g., D'Onghia & Burkert 2004, Eliche-Moral et al. 2006, Kormendy & Fisher 2005). While theorists have predicted that the thinnest galaxy disks must require massive dark halos for stabilization (Zasov et al. 1991; Gerritsen & de Blok 1999), little information has been available on the dark halo properties of individual superthin galaxies until now.

UGC 7321 is the first superthin galaxy for which both a detailed rotation curve and the gas layer thickness were derived Uson & Matthews (2003). This has allowed us to use both these constraints simultaneously to characterize its dark halo properties, as well as to obtain new insight into the stability of its disk against star formation. Our best-fit halo core density and the core radius are consistent, with deviations of a few percent, with the dark matter fundamental plane correlations (Kormendy & Freeman 2004), which depict the systematic properties of the dark matter halo in late-type and dwarf spheroidal galaxies. Below we comment further on the implications of several of our key findings.

5.5.1 The small core radius of the dark matter halo

The core radii of the dark matter halos of massive high surface brightness galaxies studied so far are usually found to be comparable to their optical size, or equivalently, 3-4 times larger than the exponential stellar disk length Gentile et al. (2004). The Galaxy has a core radius of 8-9.5 kpc which is equal $3R_d$ (Narayan et al. 2005) while M31 has a core radius equal to 21 kpc which is almost equal to $4R_d$ (Banerjee & Jog 2008). For UGC 7321, we find a very small core radius of 2.5-2.9 kpc, which is just slightly greater than its disk scale length ($R_d = 2.1$ kpc). This shows that the dark matter becomes important at small radii consistent with previous mass-modelling of LSB spirals, based on other techniques (de Blok & McGaugh 1997; de Blok et al. 2001). This is illustrated in another way in Fig.5.3, which

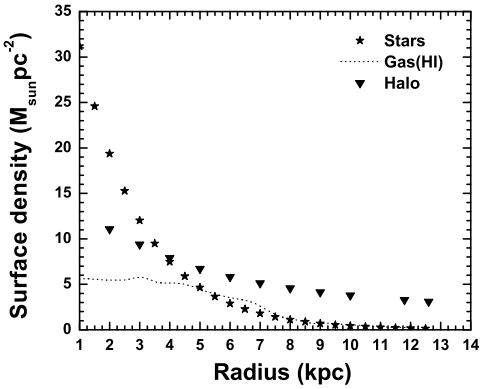

FIGURE 5.3: Plot comparing the surface-density (in $M_\odot$ pc^{-2}) of the stars, gas and the dark-matter halo as a function of radius (in kpc). It clearly shows that the gravitational potential of the halo dominates over that of the disk as early as two disk scale lengths (r = 4 kpc)

gives a comparative plot of the surface-density of the stars, gas and the halo with radius in this galaxy. The halo surface density was calculated within the total gas scale height as was done for M31 (Banerjee & Jog 2008). It clearly shows that the surface-density and hence the gravitational potential of the halo becomes comparable to that of the disk already at R = $2R_d$. This behaviour is quite different from that of a high surface density galaxy like M31 (cf Fig.6, Banerjee & Jog 2008), where the halo contribution starts to dominate at much larger radii ($5R_d$). Our results support the idea that superthin disks like UGC 7321 are among the most dark matter-dominated of disk galaxies.

5.5.2 Dependence on gas parameters

Gradient in gas velocity dispersion As noted earlier, if we impose a constant velocity dispersion, we require a value of 9 kms^{-1} to get a reasonably good fit to the observed scale height data, while an even better fit requires a velocity gradient implying even larger dispersion in the inner region (Fig.5.2). In the earlier work for the Galaxy (Narayan et al. 2005), a slope of -0.8 kms^{-1} kpc^{-1} for the gas velocity dispersion was obtained for the inner Galaxy between 2-12 kpc (pinned at 8 kms^{-1} at 8.5 kpc) as it gave the best-fit to the nearly constant H I scale heights. Oort (1962) had tried the same idea but had needed a higher gradient of -2

kms^{-1} kpc^{-1} since he did not include the gas gravity and therefore needed a larger variation to account for the constant H I scale height in the inner Galaxy. Narayan et al. (2005) tried to constrain the halo properties using the outer galaxy H I data, where they had used gas velocity gradient of -0.2 kms^{-1} kpc^{-1}. This is similar to the value we have for UGC 7321. This was based on the fact that some galaxies show a falling velocity dispersion which then saturates to 7 kms^{-1} (See Narayan et al. 2005 for a discussion). Recently, Petric & Rupen (2007) have measured the H I velocity dispersion across the disk of the face-on galaxy NGC 1058. The authors find the H I velocity dispersion to have a fairly complex distribution, but nonetheless show a clear fall-off with radius (see Fig.8 of their paper). Using this figure, one can estimate a gradient of roughly -0.1 kms$^{-1}kpc^{-1}$ in the outer disk, which is consistent with values observed for other galaxies. A similar fall-off has also been seen in NGC 6946 (Boomsma et al. 2008) as well as in several other galaxies (Bottema et al. 1986; Dickey et al. 1990; Kamphius 1993). So this gives some observational support to our assumption.

Superposition of two HI phases

A more realistic case would be to treat the HI as consisting of two phases or components, characterized by a warm (v_z = 11 kms^{-1}) and a cold medium (v_z= 7 kms^{-1}) respectively. These values match the range seen in the above fits and represent the two phases as observed in the Galaxy (Kulkarni & Heiles 1988). However,observationally the fraction of mass in these two phases as a function of radius is not known. Assuming that this fraction is constant with radius, we let its value vary as a free parameter.

The best-fit χ^2 in this case is 13.7 as compared to 2.8 for the case with a velocity gradient treated earlier. Although we do not get as good a fit as was obtained in the case where there is a gradient in the velocity, the best-fit core radius R_c still comes out to be 2.5 kpc which is again of the order of R_D. That the dark matter dominates at small radii therefore still remains a robust result irrespective of the input gas parameters used. The best-fit case gives the fraction of HI in the cold medium to be 0.2.

We had taken this ratio to be constant for simplicity. Interestingly, this assumption

is justified by the recent detailed study by Dickey et al. (2009) involving absorption and emission spectra in 21 cm in the outer Galaxy. They use this to map the distribution of the cold and warm phases of the HI medium, and surprisingly find this ratio to be a robust quantity in the radial range of R_{sun} to 3 R_{sun}. They find this ratio is $\sim 0.15 - 0.2$, which agrees well with the best-fit ratio 0.2 that we obtain. It is interesting that this ratio obtained by two different techniques is similar in the two galaxies.

The case with a gradient with a higher velocity dispersion within the optical radius gives the lowest χ^2 value (Fig.5.2), which we adopt as our best case. We note that this choice is not inconsistent with the constant phase ratio measured by Dickey et al. (2009) which was for the outer Galaxy.

High value of the gas velocity dispersion

The high gas velocity dispersion required to get an improved fit to the scale height data is surprising given the superthin nature of the galaxy, whose small stellar scale height implies that it is among the dynamically coldest of galactic disks (e.g., Matthews 2000).

The origin of this high gas velocity is beyond the scope of this paper. However, independent of its origin, this high value of the gas velocity dispersion can partly explain why star formation is inefficient in UGC 7321. This is because, to first order, a higher gas dispersion will tend to suppress star formation since Toomre Q criterion ($Q < 1$) is less likely to be satisfied, hence the disk is less likely to be unstable to star formation.

5.6 Conclusions

We have modelled the LSB superthin galaxy UGC 7321 as a gravitationally-coupled system of stars and H I gas, responding to the gravitational potential of the dark-matter halo, and used the observed rotation curve and the H I vertical scale heights as simultaneous constraints to determine the dark halo parameters. We find that the best-fit gives a spherical, isothermal halo with a central density in the range of 0.039-0.057 $M_\odot$ pc^{-3} and core radius of 2.5-2.9 kpc. The value of the best-fit core density is comparable to values obtained for HSB galaxies. The core radius is comparable to that of the disk scale length unlike HSB galaxies studied by this method, implying the importance of the dark-matter halo at small

radii in UGC 7321. Thus we find that UGC 7321 is dark matter dominated at all radii, and the results of our analysis support the idea that the thinnest of the galaxies are the most dark matter dominated.

Acknowledgement

We thank Prof. John Kormendy and also the anonymous referee for their insightful comments which have helped to improve the paper.

References

Banerjee, A., & Jog, C.J. 2007, ApJ, 662, 335

Banerjee, A., & Jog, C.J. 2008, ApJ, 685, 284

Becquaert, J.F., & Combes, F. 1997, A&A, 325, 41

Begeman, K. 1987, Ph.D. thesis, University of Groningen.

Bell, E.F., & de Jong, R.S. 2001, ApJ, 550, 212

Bevington, P.R. 1969, Data Reduction and Error Analysis for the Physical Sciences, McGraw-Hill, New York

Binney, J.,& Tremaine, S., 1987, Galactic Dynamics. Princeton Univ. Press, Princeton, NJ

Boomsma, R., Oosterloo, T. A., Fraternali, F., van der Hulst, J. M., & Sancisi, R. 2008, A & A, 490, 555

Bottema, R., Shostak, G. S., & van der Kruit P. C. 1986, A&A, 167, 34

de Blok, W. J. G. & McGaugh, S. S. 1997, MNRAS, 290, 533

de Blok, W. J. G., McGaugh, S. S., & Rubin, V. C. 2001, AJ, 122, 2396

de Zeeuw, T., & Pfenniger, D. 1988, MNRAS, 235, 949

D'Onghia, E. & Burkert, A. 2004, ApJ, 612, 13

Dickey, J. M., Hansen, M. M., & Helou, G. 1990, ApJ, 352, 522

Dickey, J. M., Strasser, S., Gaensler, B. M., Haverkorn, M., Kavars, D., McClure-Griffiths, N. M., Stil, J., & Taylor, A. R. 2009, ApJ, 693, 1250

Eliche-Moral, M. C., Balcells, M., Aguerri, J. A. L., & González-Garía, A. C. 2006, A&A,

457, 91

Geehan, J. J., Fardal, M. A., Babul, A., & Guhathakurta, P. 2006, MNRAS, 366, 996

Gentile, G., Salucci, P., Klein, U., Vergani, D., & Kalberla, P. 2004, MNRAS, 351, 903

Gerritsen, J. P. E. & de Blok, W. J. G. 1999, A&A, 342, 655

Kalberla, P. M. W., Dedes, L., Kerp, J., & Haud, U. 2007, A&A, 469, 511

Kamphuis, J. 1993, PhD dissertation, University of Groningen

Kent, S.M. 1987, AJ, 93, 816

Kormendy, J. & Fisher, D. B. 2005, RevMexAA, 23, 101

Kormendy, J., Freeman, K.C., 2004, IAU Symposium 220, Dark Matter in Galaxies, ed. Ryder et al., ASP, 377.

Kulkarni, S.R., & Heiles, C. 1988, in "Galactic and extragalactic radio astronomy", 2nd edition, eds. Verschuur,G.L. and K.I. Kellerman (New York : Springer Verlag), pg. 95

Lewis, J.R., & Freeman, K. C. 1989, AJ, 97, 139

Matthews, L. D. 2000, AJ, 120, 1764

Matthews, L.D., & Gao, Y. 2001, ApJ, 549, L191

Matthews, L. D., Gallagher III, J. S., & van Driel, W. 1999, AJ, 118, 2781

Matthews, L. D. & Wood, K., 2001, ApJ, 548, 150

Matthews, L. D., & Wood, K., 2003, ApJ, 593, 721

Narayan, C.A., & Jog, C.J., 2002a, A & A, 390, L35

Narayan, C.A., & Jog, C.J., 2002b, A & A, 394, 89

Narayan, C. A., Saha, K., & Jog, C. J. 2005, A&A, 440, 523

Navarro, J. F., Frenk, C. S., & White, S. D. M. 1996, ApJ, 462, 563

Olling, R. P. 1996, AJ, 112, 457

Olling, R. P., & Merrifield, M. R. 2000, MNRAS, 311, 361

Olling, R. P., & Merrifield, M. R. 2001, MNRAS, 326, 164

Oort, J. H. 1962, in The Distribution and Motion of Interstellar Matter in Galaxies, IAU Symp. 15, ed. L. Woltjer (New York: Benjamin), 3

Petric, A. O., & Rupen. M. P. 2007, AJ, 134, 1954

Roberts, M. S. & Haynes, M. P. 1994, ARA&A, 32, 115

Rohlfs, K. 1977, Lecture Notes on Density Wave Theory. Springer-Verlag, Berlin

Sackett, P. D., & Sparke, L. S. 1990, ApJ, 361, 408

Swaters, R. A. 1999, PhD thesis, Univ. of Groningen

Uson, J. M., & Matthews, L. D. 2003, AJ, 125, 2455

van der Kruit, P.C., Jiménez-Vicente, J., Kregel, M., & Freeman, K. C. 2001, A&A, 379, 374

Zasov, A. V., Makarov, D. I., & Mikailhova, E. A. 1991, Soviet Aston. Lett., 17, 374

Clarification to the referee's comments

Question: Fig 5.2 Uson & Matthews (2003) mention that the disk is warped and flared but do not give scaleheight data for UGC 7321. Where does the used data come from? Have the scale height data been corrected for resolution effects? If not, the larger scale height seen at the centre (to model which is assumed that the velocity dispersion increases towards the centre) may be attributable to the resolution effects and not a change in velocity dispersion. Matthews & Wood (ApJ, 593, 721, 2003) find evidence for a thick gas layer even after accounting for warping and flaring. They attribute this to a galactic fountain. What effect does it have on the model presented in the paper?

Answer: The quantitative characterization of the H I scale height was made in Matthews & Wood (2003). The analytic form that was used to parametrize the change in H I scale height as a function of radius in the data was quoted in that paper (See their Eqn. (1)). Because of the proximity of UGC7321 and the good resolution of the data, the layer is largely resolved. Furthermore, instrumental resolution was taken into account in the analysis. Therefore the larger scale height seen at the centre (to model which is assumed that the velocity dispersion increases towards the centre) can not be attributed to the resolution effects. While it is true that the evidence for an HI halo was found in that work, it was also seen that one could not match the data without also including both a warp and flaring. That mass contribution of the HI halo gas is negligible, and the gas scale height parameters we used in this work were for the "main" H I disk, not the halo material. So the HI halo would not have had any effect on the modeling in our paper.

Question 2: §3.1, Page 47, paragraph starting "The vertical stellar distribution has been studied observationally (see for a review van der Kruit 1988)..." This entire discussion is really centered on spiral galaxies and not dwarfs. Since all the other discussion is about dwarfs, at the very least it should be made clear that the discussion is for a different class of galaxies. Similarly the discussion in the last paragraph of this section is regarding large spirals and not dwarfs.

Answer: I agree.

6

Progressively More Prolate Dark Matter Halo in the Outer Galaxy as Traced by Flaring H I Gas[5]

Abstract

A galactic disk in a spiral galaxy is generally believed to be embedded in an extended dark matter halo, which dominates its dynamics in the outer parts. However, the shape of the halo is not clearly understood. Here we show that the dark matter halo in the Milky Way Galaxy is prolate in shape. Further, it is increasingly more prolate at larger radii, with the

[5]Banerjee & Jog 2011, ApJ, 732, L8

vertical-to-planar axis ratio monotonically increasing to 2.0 at 24 kpc. This is obtained by modeling the observed steeply flaring atomic hydrogen gas layer in the outer Galactic disk, where the gas is supported by pressure against the net gravitational field of the disk and the halo. The resulting prolate-shaped halo can explain several long-standing puzzles in galactic dynamics, for example, it permits long-lived warps thus explaining their ubiquitous nature.

6.1 Introduction

Spiral galaxies are observed to have extended, nearly-flat rotation curves which indicate the existence of a dark matter halo. In fact, the radial distribution of the dark matter halo of a spiral galaxy is deduced from its observed rotation curve (Rubin 1983, Binney & Tremaine 1987). However, the shape of the halo is not well-understood although it is expected to play a significant role in galaxy dynamics and evolution (Ryden 1990, Bekki & Freeman 2002). Different observational tracers such as tidal streams or thickness of the interstellar gas layer so far have given only the average halo shape, which in most cases, is found to be either oblate or spherical. In general, this is also the shape assumed in theoretical studies for simplicity.

The vertical thickness of the interstellar gas provides an additional constraint, since it allows one to trace the force normal to the plane and hence the shape of the dark matter halo on the galactic scale. But this approach has been applied only to a handful of cases so far (Becquaert & Combes 1997, Olling & Merrifield 2001, Narayan et al. 2005, Banerjee & Jog 2008, Banerjee et al. 2010, O'Brien et al. 2010). The vertical thickness of the HI gas is observed to increase sharply with radius in the outer Galaxy, which cannot be explained by a dark matter spheroid of constant shape (Narayan et al. 2005), instead this requires a halo shape varying with radius (Kalberla et al. 2007).

In this Letter, we model the observed steeply flaring HI gas to constrain the shape of the halo, and show that the halo in the outer Galaxy is prolate. Further, the axis ratio varies with radius such that the halo is progressively more prolate in the outer parts with a maximum vertical-to-planar axis ratio of 2.0 at around 8 disk scale lengths. In Section 6.2 we describe the formulation of the problem, the results are presented in Section 6.3. Section

6.4 contains a discussion of related points, and Section 6.5 summarizes our conclusions.

6.2 Formulation of the Problem

6.2.1 Model for Disk Vertical Structure

We have employed the multi-component model of the stars and gas of the galactic disk, in the field of the dark matter halo developed by Narayan et al. (2005). For simplicity, each disk component is assumed to be isothermal.

The Poisson equation for an axisymmetric galactic system in terms of the galactic cylindrical co-ordinates (R, ϕ, z) is given by

$$\frac{\partial^2 \Phi_{total}}{\partial z^2} = 4\pi G(\sum_{i=1}^{3} \rho_i + \rho_h) \tag{6.1}$$

where ρ_i with i = 1 to 3 denotes the mass density for each disk component, namely stars, HI and H_2, and ρ_h denotes the same for the halo. Here Φ_{total} denotes the net potential due to the disk and the halo. For a flat or a gently-falling rotation curve, the radial term can be neglected as its contribution to the determination of the HI scale height is less than 10 percent as noted by earlier calculations (Narayan et al. 2005).

The equation for hydrostatic equilibrium in the z direction is given by (Rohlfs 1977)

$$\frac{\partial}{\partial z}(\rho_i \langle (v_z^2)_i \rangle) + \rho_i \frac{\partial \Phi_{total}}{\partial z} = 0 \tag{6.2}$$

where $< (v_z^2)_i >$ is the mean square random velocity along the z direction for the component i. We further assume each component to be isothermal for simplicity, so that the velocity dispersion is constant with z.

Eliminating Φ_{total} between eq. (6.1) and eq. (6.2), and assuming an isothermal case, we get

$$\langle (v_z^2)_i \rangle \frac{\partial}{\partial z}\left[\frac{1}{\rho_i}\frac{\partial \rho_i}{\partial z}\right] = -4\pi G(\sum_{i=1}^{3} \rho_i + \rho_h) \tag{6.3}$$

which represents a set of three coupled, second-order differential equations, one for each component of the disk. These are solved together to obtain the vertical density distribution of each disk component. This problem is solved in an iterative fashion, as an initial value problem, using the fourth order, Runge-Kutta method of integration. The two boundary conditions at the mid-plane i.e $z = 0$ for each component are:

$$\rho_i = (\rho_0)_i, \qquad \frac{d\rho_i}{dz} = 0 \tag{6.4}$$

However, the modified mid-plane density $(\rho_0)_i$ for each component is not known a priori. Instead the net surface density $\Sigma_i(R)$, given by twice the area under curve of $\rho_i(z)$ versus z, is used as the second boundary condition, since this is known from observations. The HWHM (half width at half maximum) of the resulting model vertical distribution is used to define the vertical scale height.

Our earlier study of the Galaxy based on this approach (Narayan et al. 2005), where a constant shape of the halo was used, showed that the observed flaring HI scale height distribution in the outer Galaxy can be explained by a spherical halo with the density falling faster than an isothermal case. This model, however, gave a total mass at the lower end of mass-range obtained by other techniques such as motions of satellites (Sackett 1999), which therefore questions its validity.

6.2.2 Construction of the Dark Matter Halo Profile

Here we propose and try an alternative viable idea, namely, a prolate halo with a shape varying with radius. A prolate spheroid by definition has the vertical-to-planar axis ratio greater than 1, and it can be thought of as obtained by rotating an ellipse about its major axis. While a prolate halo fares better than a spherical halo of the same mass in explaining the flaring HI distribution, a single shape cannot explain the scale height data in the outer Galaxy over a large range of radii R = 9-24 kpc (Narayan et al. 2005, Kalberla et al. 2007). A halo that is progressively more prolate with radius is indicated to explain the observed steep flaring.

At any R, an isodensity contour for a spheroid is defined by a constant "m" where $m^2 = R'^2 + z'^2/{q_R}^2$; R' and z' are the co-ordinates of the points on the contour and q_R denotes the vertical-to-planar axis ratio of the spheroid at R. Here R is the intercept on the mid-plane, that is, at $z = 0$. The mass of a shell bounded by two surfaces m and $m + dm$ is a constant independent of the shape of the spheroid q_R (see eq. 2.74 of Binney & Tremaine 1987), and this gives the following condition:

$$q_R\, \rho_R(q_R) \;=\; \rho_R(q = 1) \tag{6.5}$$

where $\rho_R(q_R)$ is the density along a prolate isodensity contour through R, and $\rho_R(q = 1)$ is the density along the corresponding spherical contour with radius R. Thus if the original spherical shell were instead taken to be a prolate spheroidal shell by construction, its density will be lower by a factor q_R. Thus the vertical force near the mid-plane, a crucial determinant of the HI scale height, will be lower and this could qualitatively explain the HI flaring that is observed.

6.2.3 Solution of Equations for a Prolate Halo

We start with the Galactic mass model obtained by fitting the observed rotation curve (Mera et al. 1998) which gives the pseudo-isothermal spherical halo density distribution at a radius r to be:

$$\rho(r) = \frac{\rho_0}{1 + \frac{r^2}{{r_c}^2}} \tag{6.6}$$

where $\rho_0 = 0.035$ $\mathrm{M_\odot}$ $\mathrm{pc^{-3}}$ and $r_c = 5$ kpc are respectively the best-fit central density and the core radius for the halo. This determines the mass within a spherical shell at each $r = R$. If the shape were taken as prolate instead, the density will change as per eq. (6.5) while the mass in the shell remains constant. One can ensure that the fit to the rotation curve still remains valid with deviation of only a few percent since the rotation velocity has a weak dependence on the shape of the halo mass distribution (Sackett & Sparke 1990). In contrast, a small change in the halo shape of a given mass can have a striking effect on the vertical scale height. We exploit this idea to constrain the variation in the halo shape, q_R , with the

radius R. In a sense, each shell acts independently. We model q_R as a simple second-order polynomial in R i.e $q_R = 1. + \alpha_1(R-9) + \alpha_2(R-9)^2$ over a range R = 9 - 24 kpc. Here α_1, α_2 are free parameters. Combining this trial q_R with eq. (6.5) and (6.6) gives the halo density, ρ_h, which is used as an input parameter in solving eq. (6.3).

The main aim of this paper is to investigate whether a prolate halo explains the observed HI flaring within the purview of the above mass model. We next calculate the HI scale height versus radius theoretically by solving eq. (6.3) numerically with the procedure as outlined in Section 6.2.1. The input parameters such as the stellar surface density, and stellar and gas velocity dispersions are taken to be the same as in our earlier work on the Galaxy (Narayan et al. 2005). The surface densities of HI and H_2 are taken from observations (Wouterloot et al. 1990). The resulting HI scale height values obtained by solving eq. (6.3) for different trial are q_R values are fit to the observed data (Wouterloot et al.1990) over the range R = 9-24 kpc. The halo is taken to be spherical at R = 9 kpc. Since the error bars on the data are not available (Wouterloot et al. 1990), therefore we assume error bars of 5% and obtain the best-fit values of the parameters α_1,α_2 using the method of least squares. These are: α_1 = 0.020 and α_2 = 0.003 and the range α_1 = 0.010 - 0.080 and α_2 = 0.001 - 0.004 gives reasonably good fit as well (Bevington 1969).

6.3 Results

The plot of the resulting vertical scale height versus R, and the comparison with the observational data which were corrected for the Galactic warp (Wouterloot et al. 1990), is shown in Figure 6.1. The corresponding best-fit q_R increases from a value of 1 corresponding to a spherical halo at R = 9 kpc to a prolate halo with q_R = 2.0 at R = 24 kpc. We stress that the q_R value denoting the halo shape as obtained here is a local property, and our approach has allowed us to obtain a radial variation in it. In contrast, studies involving tidal streams (Ibata et al. 2001, Law & Majewski 2010) and other observational tracers assumed the halo shape to be constant, and found it to be typically spherical or oblate ($q_R < 1$) (Sackett 1999). There are a few exceptions involving studies of microlensing (Holder & Widrow 1996) and stellar streams (Helmi 2004) which yield a prolate halo, but again with a global, constant

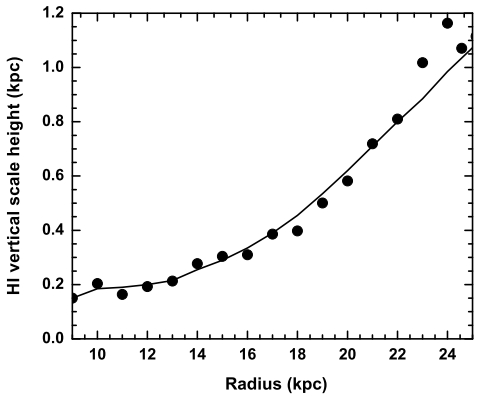

FIGURE 6.1: The calculated vertical scale height for the atomic hydrogen gas, HI, (solid line) and the observational values (Wouterloot et al. 1990) (filled circles) versus Galactocentric radius R. The theoretical curve is the best-fit case, and corresponds to a dark matter halo which is progressively more prolate with radius. In the radial range studied, the halo is found to be most prolate with the vertical-to-planar axis ratio, $q_R = 2.0$ at $R = 24$ kpc.

shape $q_R < 1.5$ within $R = 60$ kpc.

Figure 6.2 gives the isodensity contours (on the R-z plane) denoting this increasingly prolate halo in the outer Galaxy, and the inset shows the resulting q_R versus R. We emphasize that our study traces the halo shape variation over a large radial distance upto 24 kpc, that is 8 disk scale lengths (with the disk scale length being 3.2 kpc as in the Mera et al. (1998) model) or twice the optical radius of the Galaxy. Surprisingly, a prolate halo with a maximum $q_R = 2.0$ at $R = 24$ kpc is sufficient to explain the steep rise in the gas thickness by a factor of 6 seen over a radial range of 9-24 kpc. This is because the density in a prolate shell at a given R is inversely proportional to q_R (see eq. 6.5), while the vertical force due to gravity and hence the resulting scale height depends in a nonlinear way on the density near the midplane (Banerjee & Jog 2007). Thus a small decrease in the midplane density is sufficient to explain the observed sharp increase in scale heights.

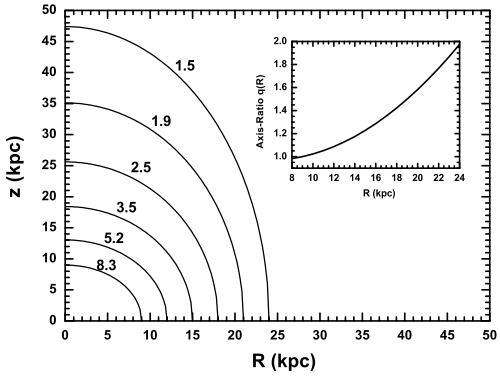

FIGURE 6.2: The resulting best-fit prolate-shaped isodensity contours of the dark matter halo on the R-z plane, with vertical-to-planar axis ratio increasing with radius as depicted in the inset. This clearly brings out the increasingly prolate geometry of the halo shape. The densities of the successive contours moving radially outwards are 8.3, 5.2, 3.5, 2.5, 1.9, and 1.5 in units of 10^{-3} $M_{\odot}$ pc^{-3}.

6.4 Discussion

1. Dependence on gas velocity dispersion: The value of gas dispersion plays a crucial role in these calculations, but it is not easy to measure and depends on the fraction of HI in the different phases. In the outer Galaxy the ratio of the 21 cm emission and absorption is shown to be remarkably constant upto R=25 kpc which implies a constant ratio of the warm and cold phases of HI (Dickey et al. 2009). However, the pressure support for the gas is mainly from non-thermal or turbulent motions which dominate the thermal velocity dispersion, and Dickey et al. (2009) do not give the non-thermal velocitites. Hence here we use the measured dispersion at the solar location of 9 kms^{-1} (Malhotra 1995). This is expected to decrease at larger radii and saturate to 7 kms^{-1} (see Narayan et al. 2005). These values were used as input parameters in our calculations. These values are in good agreement with the radial variation seen in external galaxies (Kamphuis 1993, Tamburro et al. 2009).

2. Mass of the prolate dark matter halo: In this paper we start with the screened isothermal mass model of the Galaxy as given by Mera et al. (1998), which has a mass of 10^{12} $M_{\odot}$ within $R < 100$ kpc. Due to the construction adopted in this paper, the mass

in each shell is conserved as an initially spherical shell is stretched into a prolate shell (eq. [6.5]). Thus the total mass of the halo is conserved. Hence the total mass of the prolate halo in our model is the same as in the Mera et al. mass model. We note that in our model we have only dealt with the region of $R < 24$ kpc.

This total mass is in a good agreement with the value obtained using different observational tracers such as motions of satellites, and high velocity stars (Sackett 1999, also see Gnedin et al. 2010, McMillan 2011 for more recent estimates). Thus the current model overcomes the problem with the earlier model (Narayan et al. 2005) which gave a total halo mass within 100 kpc that was three times smaller than the above value. Recall that this was the motivation for trying the variation in the halo shape with radius (Section 6.2). Thus our model explains the observed HI scale heights and also gives a total mass in agreement with typical values in the literature.

3. Asymmetry in gas scale heights: The scale height distribution is known to be asymmetric in the two halves of the Galaxy (Levine et al. 2006, Kalberla et al. 2007) being higher by a factor of about two in the northern galactic hemisphere than in the south. We have only modeled the northern data (Wouterloot et al. 1990) here for simplicity to check if our proposed model of a prolate dark matter halo with a radially-dependent shape could explain the steeply increasing HI scale height data. To model the southern region, we would need the observed HI surface density values as input parameters. Levine et al. (2006) measure the HI scale height for both north and south, but only the net value of the gas surface density, averaged over the north and south is given.

Recently, Kalberla & Kerp (2010) have given observed HI surface density values separately for the north and south. Applying our model to the southern data alone, we find that the best-fit q_R values are significantly lower. A prolate halo with a radially-increasing axis ratio is still preferred over an oblate or spherical case, but with smaller values of $\alpha_1 = 0.009$ and $\alpha_2 = 0.0$ (compared to 0.02 and 0.003 respectively for the northern data, Section 6.2.3). These give a maximum axis ratio of 1.14 at R=24 kpc as compared to $q_R = 2.0$ obtained for the north. This low value of q_R is sufficient to explain the data in the south, since the scale heights are lower and the rate of flaring beyond 18 kpc is much less steep in the south than

in the north. Thus the dark matter halo of the Galaxy has a prolate shape but its value is different in the two hemispheres, being more prolate in the north. A more realistic future treatment should consider simultaneous modeling of north and south HI scale height data.

There is a limitation in applying this model farther out in the plane since the gas dispersion values are not well-known. With this caveat in mind, if we model the data the range $9 - 40$ kpc (Kalberla & Kerp 2010) by extrapolating the above input parameters, the best fit gives a maximum $q_R = 4.5$ at $R = 40$ kpc. We have not modeled the inner Galaxy ($R <$ 9 kpc) here, since the halo contribution is shown to be small in this region (Narayan & Jog 2002), hence the scale heights cannot be used to constrain the halo shape.

4. Comparison with shapes from cosmological simulations: Interestingly, the prolate-shaped dark matter halo obtained here by modeling the HI vertical scale height data agrees well with the general trends seen in cosmological simulations. The latter give a range of halo shapes with a preference for a prolate shape (Bailin & Steinmetz 2005, Bett et al. 2007) but with a lower vertical-to-planar axis ratio. However, these are measured at scales of about 100 kpc (Bailin & Steinmetz 2005) which are much larger than that of a galactic disk, hence the quantitative comparison is not meaningful. The predictions of our model can be checked and confirmed by the signatures of other local tracers in future observational studies such as GAIA.

5. Dynamical implications of a prolate halo: A prolate-shaped dark matter halo as obtained here has important implications for many classic problems in galactic dynamics. For example, a prolate halo would cause a lower differential precession and hence can support long-lasting warps (Ideta et al. 2000), this can explain why warps are commonly seen. Second, a prolate halo can naturally explain (Helmi 2004) the fact that the satellites are seen to be limited to the polar plane normal to the galactic plane, as observed in many galaxies, known as the Holmberg effect. The dynamical implications of a prolate halo, in particular one which is increasingly more prolate with radius, deserve a detailed study.

6.5 Conclusions

By modeling the flaring HI gas distribution, we have shown that the shape of the dark matter halo is prolate in the outer Galaxy over a radial range of $R = 9 - 24$ kpc, where it can have possible observable dynamical consequences. We treat the halo as a set of spheroidal shells which have progressively more prolate shapes with increasing radii. Thus, we obtain the local shape of the halo and show that the maximum vertical-to-planar axis ratio is 2.0 at $R = 24$ kpc. These results are in contrast with most of the earlier work involving various observational tracers, which gave either a spherical or a flattened, oblate halo with a constant shape. However, our results agree with the trends from cosmological simulations which tend to favor a prolate halo. A prolate halo, in particular one which is increasingly more prolate at larger radii, has important implications for galaxy dynamics and evolution, which need to be studied further.

References

Bailin, J. & Steinmetz, M. 2005, ApJ, 627, 647

Banerjee, A. & Jog, C.J. 2007, ApJ, 662, 335

Banerjee, A. & Jog, C.J. 2008, ApJ, 685, 254

Banerjee, A., Matthews, L.D. & Jog, C.J. 2010, NewA, 15, 89

Becquaert, J. F. & Combes, F. 1997, A&A, 325, 41

Bekki, K. & Freeman, K. C. 2002, ApJ, 574, L21

Bett, P., Eke, V., Frenk, C.S., Jenkins, A., Helly, J. & Navarro, J. 2007, MNRAS, 376, 215

Bevington, P.R. 1969 Data Reduction and Error Analysis for Physical Sciences. (New York: McGraw Hill Book Company)

Binney, J. & Tremaine, S. 1987, Galactic Dynamics. (Princeton: Princeton Univ. Press)

Dickey, J. M., Strasser, S., Gaensler, B. M., Haverkorn, M., Kavars, D., McClure-Griffiths, N. M., Stil, J., & Taylor, A. R. 2009, ApJ, 693, 1250

Gnedin, O.Y., Brown,W.R., Geller, M.J., & Kenynon, S.J. 2010, ApJ, 720, L108

Helmi, A. 2004, ApJ, 610, L97

Holder, G. P. & Widrow, L. M. 1996, ApJ, 473, 828

Ibata, R., Lewis, G. F., Irwin, M., Totten, E. & Quinn, T. 2001, ApJ, 551, 294

Ideta, M., Hozumi, S., Tsuchiya, T. & Takizawa, M. 2000, MNRAS, 311, 733

Kalberla, P.M.W., & Kerp, J. 2010, ARAA, 47, 27

Kalberla, P.M.W., Dedes, L., Kerp, J. & Haud, U. 2007, A&A, 469, 511

Kamphuis, J.J. 1993, Ph.D. thesis, University of Groningen

Law, D. R. & Majewski, S. R., 2010, ApJ, 714, 229

Levine, E. S., Blitz, L. & Heiles, C. 2006, ApJ, 643, 881

Malhotra, S. 1995, ApJ, 448, 138

McMillan, P.J., 2011, MNRAS, In press. (arXiv: 1102.4340)

Mera, D., Chabrier, G. & Schaeffer, R. 1998, A&A, 330, 953

Narayan, C. A. & Jog, C.J. 2002, A&A, 394, 89

Narayan, C.A., Saha, K. & Jog, C.J. 2005, A&A, 440, 523

O'Brien, J.C., Freeman, K.C., & van der Kruit, P.C. 2010, A & A, 515, A63

Olling, R. & Merrifield, M.R. 2001, MNRAS, 326, 164

Rohlfs, K. 1977, Lectures on Density Wave theory (Berlin:SpringerVerlag)

Rubin, V. 1983, Science, 220, 1339

Ryden, B.S. 1990, MNRAS, 244, 341

Sackett, P.D. & Sparke, L.S. 1990, ApJ, 361, 408

Sackett, P.D. 1999, in ASP conference series vol. 182, Galaxy Dynamics: The shape of dark matter halos, eds. D. Merritt, J.A. Sellwood, M. Valluri., (ASP, San Fransisco, 1999), 393

Tamburro, D., Rix, H.-W., Leroy, A. K., Mac Low, M.-M., Walter, F., Kennicutt, R. C., Brinks, E. & de Blok, W. J. G. 2009, AJ, 137, 4424

Wouterloot, J.G.A., Brand, J., Burton, W. B. & Kwee, K. K. 1990, A&A, 230, 21

7

Summary, Discussion & Future Work

Summary

This thesis aims at the dynamical study of the vertical structure of the galactic disks in spiral galaxies and their dark matter halos with a twofold objective on end.

In the first part, it investigates the effect of the inclusion of gas gravity on the vertical structure of the stars and gas. The motivation of this study lies in the fact that the gas is a low dispersion component and therefore resides closer to the galactic mid-plane compared to the stars. It is therefore expected that it should strongly regulate the disk dynamics near the mid-plane. However the gas gravity is generally ignored in the dynamical modeling of the galaxy as it constitutes a very low mass fraction of the disk. Our results demonstrate

the importance of the inclusion of gas gravity in the dynamical model of a galaxy.

This thesis has conclusively shown that the self-gravity of the gas plays a crucial role in determining the vertical structure of stars even in ordinary spirals like the Milky Way. In these galaxies, the gas gravity has been neglected in the past as the mass fraction in the gas is an order of magnitude smaller than that in the stars. Numerical calculations carried out in this thesis give a strong evidence of the steepening effect of the gas-gravity on the vertical density distribution of stars. The resultant vertical density distribution is found to be steeper than the sech^2 function that is expected for an isothermal disk of self-gravitating stars. In fact, in the last few decades, astronomical observations have indicated a steeper-than-sech^2 vertical density profile for the stars near the mid-plane of the galaxy. Therefore, our model explains these observed phenomena, and highlights the necessity to include the self-gravity of the gas in the theoretical model of a galaxy.

The inclusion of the gas gravity therefore becomes essential in the case of dwarf irregular galaxies which are rich in gas, with stars and gas contributing to the disk dynamics on an equal footing. The dwarf galaxies mimic the primeval galaxy population and therefore it is necessary to know the gas scale height in these galaxies to study star-formation activities and other related phenomena in the early aeons of time. However, it is not possible to determine the gas scale height in these irregular galaxies directly due to limitations of astronomical observations. Our model of gravitationally-coupled stars and gas in the force field of a dark matter halo can be used to predict the vertical density distribution of stars and gas for large spirals with flat rotation curves. Here we have devised a new technique to take care of the rising rotation curves of dwarf galaxies.

The second part of the thesis concerns probing the density distribution of the dark matter halos of spiral galaxies using both the observed rotation curve and the HI thickness data.

Dark matter halos on galactic scales continues to be a very active field of research. This

is because the Lambda-CDM model, the brainchild of modern cosmology, in spite of being immensely successful on cosmological scales, is mired by serious anomalies on the scales of galaxies. Although cosmological simulations and observational tracers indicate a range of possible shapes for galactic dark matter halos, generally a spherical shape is still adhered to while developing a theoretical model of the galaxy. However it is necessary to be careful in choosing the halo shape as it plays a crucial role in galaxy formation and evolution, and regulates myriad disk dynamical features like the longevity of galactic warps and the sustenance of spiral arms, to name a few.

Traditionally, the rotation curve of the galaxy is used to determine its dark matter halo properties. However, we note that the rotational velocity is a function of the radial component of the galactic potential, which is weakly dependent on the shape of the halo. The vertical thickness of the HI gas, on the other hand, is a function of the vertical component of the galactic potential which is strongly dependent on the shape of the halo. Hence, the thickness of the H I gas layer can be used to probe the vertical component of the galactic potential, and hence the shape of the halo. In this thesis, the dual constraints of both the rotation curve and the H I vertical thickness have been used to obtain the dark matter halo density distribution.

Constraining a spheroidal dark matter halo characterized by four free parameters using the dual constraints of the rotation curve and the H I scale height data, can prove to be computationally expensive if the code is not duly optimized. The 4-D grid constitutes about 50,000 grid points, and for each such grid point one has to obtain the rotation curve and the H I vertical scale height as a function of radius. Calculating the H I vertical scale height at each galactocentric radius involves the numerical solution of three coupled, second order, ordinary differential equations. Also, two initial conditions are required to solve for each of the three, coupled second order differential equations. The numerical code was carefully optimized such that the entire set of calculations is performed within an hour or two.

Using the above methodology, we study the dark matter halos of the Andromeda (or M31) which is the largest neighbouring spiral galaxy of the Milky Way. We also study the superthin, low surface brightness galaxy UGC 7321 and lastly our own Galaxy. Following is the summary of our results:

For **Andromeda (or M31)**, we find a highly flattened isothermal dark matter halo with the vertical-to-horizontal axis ratio equal to 0.4, which interestingly lies at the most oblate end of the halo shapes found in cosmological simulations. This indicates that either M31 is a unusual galaxy, or the simulations need to include additional physics, such as the effect of the baryonic disk, that can affect the shape of the halo.

For **UGC 7321**, we find a spherical isothermal halo, with a core radius almost equal to the disk scale length. This reveals that the dark matter dominates the dynamics of this galaxy at all radii, including the inner parts of the galaxy. This is unlike the case for the large spiral galaxies, where the core radius is typically about 3-4 disk scale lengths. Interestingly, the best-fit halo central density and the core radius are consistent, with deviations of a few percent, with the dark matter fundamental plane correlations, which depict the systematic properties of the dark matter halo in late-type and dwarf spheroidal galaxies.

For **Milky Way**, we find a prolate halo in the outer galaxy, with the vertical-to-planar axis ratio monotonically increasing to 2.0 at 24 kpc, or 8 radial disk scale lengths. The resulting prolate-shaped halo can explain several long-standing puzzles in galactic dynamics, for example, it permits long-lived warps thus explaining their ubiquitous nature.

Discussion

Coherence of the results in the context of galaxy formation: The fact that different galaxies show markedly different shapes of the dark matter halo may look surprising at first. However cosmological (dark matter only) simulations have indicated a range of shapes for the galactic dark matter halos from prolate to spherical to oblate, with the prolate shape being the most favoured one (Bailin & Steinmetz 2005, Bett et al. 2007). Therefore observing differently-shaped dark matter halos for different galaxies is not a surprising result. Also attempts have been made to characterize the halo shapes as a function of various properties

of the halo like its mass and redshift. In particular, less massive halos are found to be more spherical. Also, halos of a given mass get flatter with increasing redshift (Mo, van de Bosch & White 2010). Simulations also suggest that the shape of the halo is tightly correlated with its merger history, with halos that assembled earlier being more spherical. It is found that prolate halos form via mergers with low angular momentum, oblate halos from those with high angular momentum, and triaxial halos result from multiple mergers with varying degrees of angular momentum (Moore et al. 2004). The situation is even more complex in a more realistic cosmological hydrodynamic simulation, which takes into account the back-effect of the baryonic disk on the dark matter halo. When baryons cool and accumulate in the centers of their dark matter halo, they make the halo more spherical (Kazantidis et al. 2004). Therefore it is evident that the galactic dark matter halo shape is the outcome of the complex interplay of various contributing factors and a simple explanation is not always easy to offer.

The assumption of an ellipsoidal dark matter halo: Cosmological N-body simulation studies have shown that, to a good approximation, halo equidensity surfaces can be described by ellipsoids (Mo, van de Bosch & White 2010). So the assumption made in this thesis about the spheroidal halo shape is not ad-hoc. It is true that the vertical HI thickness data is sensitive to the mass distribution near the midplane. Therefore constraining the global shape of the halo based on HI thickness only would have been erroneous. However we have used the rotation curve constraint as well. The rotational velocity at any radius depends on the total mass enclosed within that radius (and not only to the mass distribution near the midplane), and also weakly on the shape of the halo. Therefore our conclusion about the global shape of the halo is robust.

Cold molecular gas as dark matter in spiral galaxies: In some theoretical studies, the dark matter in spiral galaxies has been proposed to be in the form of cold gas, in molecular form and rotationally supported known as the dark gas (Pfenniger et al. 1994, Combes & Pfenniger 1997). In fact, recent studies by the Planck team have indicated the presence of molecular gas or "dark gas" that do not follow the CO emission (Ade et al. 2011). However, till now, there has been no evidence for such a component to be universal in galaxies. Further

such a form of dark matter would make the galactic disk highly unstable (Revaz et al. 2009).

Future Work

1. **Imprint of Gas Gravity on the Thick Disk:** The novel idea highlighting the significance of gas gravity has deep implications and prompts further research and investigations. The strong effect of the gas gravity on the vertical density profile of the stellar disk indicates that it should also bear its imprint on the Milky Way thick disk, as the epoch of its formation 10^9 years ago is marked by a value of gas fraction, almost an order of magnitude higher than its present day value. Interestingly, the findings of the upcoming Gaia mission can harnessed to verify this theoretical prediction.

2. **Role of Gas Gravity on Superthin galaxies:** Superthin galaxies are dark matter dominated galaxies where stars and gas dominate the disk mass on an equal footing. These are characterized by a very small value of the stellar disk scale height and therefore are referred to as superthins. The constraining effect of the gas component possibly holds the clue as to the reason behind the absence of thick disks in superthin galaxies, which are marked by a high fraction of gas. Therefore it is worth investigating this issue as a future problem.

3. **Cosmological Origin of Dark Matter Halo Shapes:** Our studies have indicated that the shape of the dark matter halo of a galaxy is not universal even within the same class of galaxies. Andromeda (or M31) and the Milky way are both ordinary spirals with comparable disk mass. However it is found that there is a stark difference in their shapes. While M31 is has a highly oblate dark matter halo, the Milky Way has a substantially prolate halo with the vertical-to-horizontal axis ratio increasing with radius. UGC 7321, on the other hand, has a spherical halo. This is surprising and calls for further investigations into the origin of the shapes of dark matter halos. In fact, cosmology predicts a range of halo shapes but the physical origin behind them is not clearly understood. Therefore, we intend to probe the origin of dark matter halo shapes in the cosmological simulation data sets. This will clarify the role played by

galaxy formation and evolution processes in moulding the shape of the dark matter halo.

4. **Redshift versus Dark Matter Halo Shapes:** The back-effect of the baryons (stars plus gas) is one of the most plausible factors that can affect the shape of the dark matter halo in an isolated field galaxy on galactic scales. In fact, recent theoretical studies have indicated the flattening effect of the disk on the dark matter halo. The strong effect of the gas gravity on the vertical density profile of the stellar disk indicates that it should also bear its imprint on its dark matter halo, especially at high redshifts marked by a higher value of gas fraction. Therefore, as a future project, it will be interesting to study the dependence of dark matter halo shape on redshift and disk mass in data of galaxy simulations including baryons.

References

Ade, P. A. R. et al. 2011, arxiv:1101.2029

Bailin, J., & Steinmetz, M. 2005, ApJ, 627, 647

Bett, P., Eke, V., Frenk, C. S., Jenkins, A., Helly, J., & Navarro, J. 2007, MNRAS, 376, 215

Combes, F. & Pfenniger, D. 1997, A&A, 327, 453

Kazantzidis, S., Kravtsov, A. V., Zentner, A. R., Allgood, B., Nagai, D. & Moore, B. 2004, ApJ, 611L, 73

Mo, van de Bosch & White 2010, Galaxy Formation and Evolution (Cambridge: Cambridge Univ. Press)

Moore, B., Kazantzidis, S., Diemand, J. & Stadel, J. 2004, MNRAS, 354, 522

Pfenniger, D., Combes, F. & Martinet, L. 1994, A&A, 285, 79

Revaz, Y. ,Pfenniger, D. ,Combes, F. & Bournaud, F. 2009, A&A, 501, 171